Carbon Nanotubes based Elastomer Composites-An Approach towards Multifunctional Materials

Deepalekshmi Ponnamma[a], Kishor Kumar Sadasivuni[b,*], Yves Grohens[c], Qipeng Guo[d], Sabu Thomas[a,b] *

[a]School of Chemical Sciences, Mahatma Gandhi University, P D Hills P O, Kerala, India 686560

[b]Centre for Nanoscience & Nanotechnology, Mahatma Gandhi University, P D Hills P O, Kerala, India 686560

[c]LIMATB laboratory, Université de Bretagne Sud, rue St Maudé, 56100 Lorient, France.

[d]Institute for Frontier Materials, Deakin University, Locked Bag 2000, Geelong, Victoria 3220, Australia.

* Corresponding Authors

Tel- +91-8281301696, E-mail- kishor_kumars@yahoo.com (Kishor Kumar Sadasivuni)

Tel- +91-9447223452, +91-481- 2730003, E mail- sabupolymer@yahoo.com (Sabu Thomas)

Abstract

The current study focuses on giving a basic understanding of the tubular graphene sheets or Carbon Nanotubes (CNTs) and points towards its role in fabricating elastomer composites. Since the properties and the performance of the CNT reinforced elastomer composites predominantly depend on the rate of dispersion of fillers in the matrix, the physical and chemical interaction of polymer chains with the nanotubes, crosslinking chemistry of the rubbers and the orientation of the tubes within the matrix, here, a thorough study of these topics is carried out. For this, various techniques of composite manufacturing such as pulverization, heterocoagulation, freeze drying etc. are discussed by emphasizing the dispersion and alignment of CNTs in the elastomers. The importance of functionalization technique as well as the confinement effect of nanotubes in elastomer media is derived. In a word, this article is aimed exclusively at addressing the prevailing problems related to the CNT dispersion in various rubber matrices, the solutions to produce advanced high-performance elastomeric composites and various fields of applications of such composites, especially electronics. Special attention has also been given to the non linear visco elasticity effects of elastomers such as Payne effect, Mullin's effect and hysterisis in regulating the composite properties. Moreover, the current challenges and opportunities for efficiently translating the extra ordinary electrical properties of CNTs to rubbery matrices are also dealt with.

Contents

Acknowledgement

Appendix

References

1. Introduction

Carbon Nanotubes (CNTs) are long cylindrical graphene sheets with or without hemifullerene end caps and composed of covalently bonded carbon atoms. They are found to be more reactive than graphene because of the presence of misaligned unhybridized p-orbitals of carbon atoms in them. Since their discovery in 1990's by Iijima [1], a lot of investigations on the fabrication of functional nanotube composites have come out. This is mainly because of their extremely high Young's modulus [2], electrical and thermal conductivity [3], flexibility [4], bending strength, aspect ratio (300-1000), and chemical inertness. Their mechanical properties, in together with relatively low density [5], make CNTs ideal candidates for weight-efficient structures and so they are considered to be the ultimate reinforcements in elastomer composites. These extremely light weight materials are much stronger

when compared to steel and better conductors compared to copper. Their high tensile strength (150-180GPa) and tensile modulus (640 GPa-1TPa) make CNTs the unique fillers in the nano world. Their one dimensional structure allows metallic nanotubes to transport electrons through the entire tube without scattering. This transport behavior and CNT's large phonon mean free path length are responsible for their high electrical and thermal conductivity [6]. All these superior properties of CNTs offer great opportunities towards the synthesis of new composites. High performance light weight structural materials made of CNT/elastomer composites used in space exploration is one example among the tremendous possibilities of CNT composites [7].

Even a single nanotube is hundred times stronger and six times lighter than steel with excellent conductivity. This means a group of CNTs can make wonders, provided it should be uniformly distributed. Thus the future of CNT's application lays mainly in the fabrication of technologically important materials ranging from reinforced composites to electrical sensors [8]. But, the large number of applications of CNT composites as in electronics, optics and bio medical fields has been limited to a certain extent by a few factors. The low level of dispersion of CNTs in polar liquids arising from the tendency of CNTs to aggregate because of the hydrophobic-hydrophobic interactions existing in them is one important aspect to be considered in this scenario. The uneven distribution of fillers in elastomer matrix definitely causes the composite properties to decrease since it affects the filler uniformity in each phase and the physical/chemical interaction between the filler and the polymer [9-10]. In order to effectively transfer the stress from one phase to the other, strong bonding between fillers and polymer chains are necessary. Hence the effective dispersion and the long term stability of CNTs in matrix is the most significant, yet challenging part in composite fabrication [11]. In short, the difficulty in dispersing CNTs homogeneously throughout the matrix without destroying their integrity (highly polarisable smooth sided nature of CNTs cause for its bundling

tendency), provided a good interfacial interaction with the elastomer matrix is achieved and their inconsistency (all known preparation methods give mixtures of nanotube chiralities, diameters and lengths along with different amount of impurities and structural defects) are considered to be the disadvantages with this filler [12]. But the tremendous advantages make these points silent. The research works on CNTs goes on increasing worldwide. Fig. 1 illustrates the observed distribution of productivity of CNTs among the continents [13].

Elastomers are characterized by low electrical ($<10^{-11}$ S/m) and thermal conductivities (≈ 0.2 W/m K). But the incorporation of nanoscale conducting fillers like nanotubes, graphene, graphite nanoplatelets etc. improves their electrical conductivity significantly up to 10 S/m [14]. Due to the very high aspect ratio and specific surface area of CNTs the modulus and the tensile strength of elastomers dramatically increase to great extents even at less concentration. The modified CNTs reinforced elastomer composites are reported for having high tensile modulus (over the native elastomer) without much reduction in their strain-at-break [15] values. Recent efforts to use CNTs as filler material in elastomers have shown promising results in increasing the electrical conductivity, mechanical stiffness and strength [16]. The applicability of fluorocarbon foamed elastomers/CNT composites in making electromagnetic interference (EMI) shielding material is reported [17]. This material is also useful for electromagnetic static discharge. Thus the growing area of nanotube chemistry is to be well explored for future applications. This review tries to bring out the amazing properties of CNTs and its elastomer composites in detail by giving special emphasis to the application side. Before proceeding towards the composite part, let us discuss about the properties of CNTs in detail.

2.Carbon nanotubes-A brief history

2.1. *Types*

There are mainly two types of CNTs- Single Walled Carbon Nanotubes (SWCNTs) and Multi Walled Carbon Nanotubes (MWCNTs); however various nanotube related structures do exist and are reported. Fig. 2a shows a few structural forms of CNTs.

SWCNTs result when one layer of graphene is wrapped into the form of a cylinder. These tubes have diameter of about 1.2-1.4 nm which may vary due to strain and different mode of wrappings. Both the side walls and the end caps of SWCNTs have different physical and chemical properties. As radius of the tube decreases, the partial sp^3 character of carbon atoms increases and thus leads to more reactivity. SWCNTs can be named by a chiral vector denotation (n, m) which describes how to roll up a graphene layer to make CNTs in an infinite graphene sheet (n and m denote unit vectors along two different directions in the graphene crystal lattice) [18-19]. Depending upon these chiral vectors, SWCNTs show difference in their properties such as optical activity, mechanical strength and electrical conductivity. Based on the chirality, CNTs can be again classified as given in Fig. 2b. When n=m, it is called armchair form, when n-m=0, it is zigzag and all the others, chiral (Table 1). Also for zig zag, n is a multiple of 3 whereas for chiral, n-m is a multiple of 3. The nanotubes could be metallic (armchair CNTs) and semiconducting (n-m=3i). In the case of semi metallic/semiconductor, the band gap can vary from 0-2eV [18].

The structure of MWCNTs is demonstrated by two models - Russian doll model (structure explained as concentric graphene layers) and the parchment model (a single graphene sheet rolled around it). The interlayer distance is 3.4 A°especially in the case of armchair tubes. Whereas for zig zag tubes the distance is found to be 3.52 A° and in chiral tubes the situation is a little complicated. A special type of MWCNT called double walled CNT has more significance in its high resistance to

chemicals. It has a high flexural modulus than SWCNT due to the presence of an additional layer; and higher toughness than MWCNT due to its smaller size [12]. For both SWCNTs and MWCNTs the length varies from nm-cm. Special features known as elbow connections are common in MWCNTs compared to SWCNTs. This type of connection is formed between an armchair and a zig zag tube and it involves a pentagonal ring on the outer side and a heptagon on the inner side. These elbow connections and branching structures contribute towards the molecular scaffolding property of MWCNTs [12]. Also in MWCNT, it is possible for the inner nanotube core to slide within the outer shell without friction, thus improving its kinetic properties. CNTs show thermal conduction along the tube axis and also exhibit ballistic conduction (unimpeded flow of charge or energy carrying particles over high distances) [6]. However they are insulators laterally to the tube axis. This helps in tuning the properties. Table 2 gives a comparison in properties of CNTs with graphite [20].

In addition to SWCNTs and MWCNTs, several other forms of graphitic tubes also exist. For instance, nanotubes form 'torus', when bent in to a droughnut shape. It is proposed that ten elbow connections in a common plane can make a torus. But if the position of the lower pentagon heptagon pair is shifted by a single bond, the tube cannot form torus and on repetition of this shift, helical or coiled structures may form. Nanotori have very high values of magnetic moment [21] as well. Another structural form called 'nanobud' is the result of a combination of CNT and fullerene in which the fullerene balls are covalently bonded to the CNT surface. These materials behave as good field emitters and also the fullerene bud can prevent slippage of CNTs by anchoring on the matrix material in composites, thus improving the mechanical properties. Cup stacked CNTs having semi-conductor behavior are formed by stacking graphene micro layers [22]. Moreover the pyrolysis of hydrocarbons using a carbon arc plasma generator produces solid conical structures (nanocones) as well as disks [12].

Very recently nanotubes coalised in to fiber capable of transmitting an electric current about 1000 times than copper was reported from Rice University. These CNT fiber cables are flexible, strong and conductive and are suitable in lightweight power transmission systems like aerospace. This yet another structural feature of CNTs consists of trillions and trillions of tightly packed nanotubes, all aligned in the same direction [23]. Qiu et al. studied the influence of the structural changes on the electrical resistivity of the fiber upon organic liquid ingress in CNT fibers. The local regions of bundle network were broken up depending on the liquid environments and affect the electrical performance (resistance increased upon immersion and decreased with removal of liquids) thus testing its applicability in external insulating and sensing materials [24]. Though the invention by Rice researchers rocked in the excellent performance of nanotube fibers, the study of this material is not new. In a review article, the high specific strength, stiffness, electrical and thermal conductivity, and extreme flexibility of such fibers were discussed and of course their applications in structural reinforcement materials and thermal, atmospheric and biochemical sensors. This article examines almost all aspects and properties of CNT fibers and will be a good reference for the beginners in this field [25].

Among all the various types of nanotubes discussed, the most important ones that attracted much attention are SWCNTs and MWCNTs due to their high stability and ease of preparation. And therefore focus is given on their properties and composites in this review. As discussed, CNTs are the strongest and stiffest in terms of tensile structure and elastic modulus due to sp^2 bonds, but there are some points which they cannot satisfy. For instance, upon excessive strain, they usually undergo plastic deformation. The high aspect ratio and hollow structure of CNTs also result in buckling (a failure mode characterized for a structure when subjected to high compressive stress) when they are

compressed, because of this reason they are not considered to be strong upon compression. Moreover,

its mechanical and electronic properties vary remarkably depending on the tube radius and the type.

2.2. *Preparation and purification*

The three main types of preparation of nanotubes include arc discharge, laser ablation and chemical

vapour deposition (CVD). In arc discharge, an arc (generated by 100 amps current) causes the

consumption of the graphite anode inside a stainless steel vacuum chamber. Due to high temperature

carbon sublimes and CNTs get deposited on the cathode. Efficient cathode cooling produces high

quality CNTs since it avoids excessive sintering. Helium gas with high pressure in the chamber can

further enhance the yield [26]. During laser ablation, graphite is vaporized using a pulsed laser beam

which is produced by metal catalyst particles in a high temperature reactor chamber containing an inert

gas. As the vaporized carbon condenses, CNTs are collected at the cooler side of the reactor. This

method is quite similar to arc discharge and is significantly important in the case of SWCNTs; but

expensive [27]. The decomposition of gas phase molecules to reactive species and thereby inducing

the particle growth are the main aspects in CVD. A layer of metal catalyst particles (Ni, Co, Fe or a

combination) at high temperature act as the substrate. Two gases -processor gas (NH_3, N_2 or H_2) and a

carbon containing gas (acetylene, ethylene or methane) are passed in to the chamber where the latter

breaks and the molecular carbon deposits at the edge of the metal particles in the form of CNTs. The

surface area of the metal nanoparticles is usually increased by mixing them on another catalyst support

such as MgO or Al_2O_3 which can be later removed by acid treatment. CVD is the most convenient and

common method providing maximum yield [28-30]. In addition to these three methods, CNTs can be

synthesized by following other roots also. For instance, the pyrolysis of benzene in hydrogen

(especially for MWCNTs), electrochemical methods and catalytic decomposition etc. promote the

growth of nanotubes [12].

The various synthesis methods particularly CVD technique induces certain impurities in the obtained nanotubes out of which the most common being graphitic nanoparticles, amorphous carbon, fullerenes, polyaromatic hydrocarbons, etc. Catalyst particles like transition metals can also be present as impurity. Depending on the reactivity of impurities and the stability of CNT samples, the contaminants can be removed by chemical, physical or by combined methods. The chemical methods include oxidation or dehydrogenation (for removing carbon nanoparticles), acidic treatment (for removing metal catalyst) and other chemical reactions (for removing the catalyst support). Oxidation of CNTs using air or oxygen was the first method employed for CNT purification. This was quite successful in increasing the percentage of pure CNTs, since most of the amorphous carbon content oxidizes much faster than pure CNTs. Acid treatment purification was also used as a complementary method to oxidation. But this would cause defects in sidewalls as well as carboxylation at the ends and sidewalls of the tubes. In this situation, a combination of different liquid–phase oxidizing agents like $KMnO_4$, H_2O_2 or bromine water is practiced to yield a maximum of purified CNTs, with or without acids [31-33]. Usually ultrasonic treatment is done as an additional mixing process coupled with almost every technique because ultrasonic bath has the ability to release the impurities from CNTs which are originally stuck together.

Several new purification techniques are also found to be useful for getting high yield of CNTs without causing its structural degradation. Among these, purification using polymers is the most effective [34]. This method is based on the difference in van der Waals potential between CNT and its chemical environment. Due to van der Waals interactions, organic polymers form stable polymer-nanotube composite solutions causing the graphitic impurities to sediment. This CNT polymer interaction is the strongest for conjugated polymers since the binding force in them comes from both van der Waals and electrostatic interactions whereas in non conjugated polymers the former alone

plays the role. Both acidic and organic polymer treatment have been successfully utilized by Djordjević et al. [34] for purifying MWCNTs and proved separation method for purifying the nanotubes and nanoparticles in high yield. The method involves filtering a stable colloidal dispersion of the material in water/surfactant solution. Thus the nanotubes are extracted from the the the effectiveness of conjugated organic polymer. The organic polymer used was poly (m-phenylene vinylene-co-2, 5-dioctyloxy p-phenylene vinylene) (PmPV). Bonard et al. [35] demonstrated a liquid-phase suspension leaving the impure particles in the filtrate. As a second stage of purification, they practiced flocculation of the dispersion by size-selection. They could obtain 90 % yield without damaging the tube tips or tube walls. Zheng et al. [36] also designed a two-step purification process for the SWCNTs produced by CVD, which involves the acid treatment and oxidation in limited air. They could also formulate a growth mechanism for CNTs. According to this mechanism, the reason for the growth of nanotubes is the lower gas diffusion rate with more SWCNTs grown on the catalyst. This also explains why catalysts with high porosity like aerogel can greatly enhance the CNT yield.

The physical methods of purification of CNTs involve mechanical separation of different kind. This includes strong sonication of suspension of the impure material (Snooker effect) [37] and collection of magnetic particles with a permanent magnet, thus separating the purified CNTs. Combinations of physical and chemical methods can also be used for better yield.

2.3. Dispersion and modification

Once the nanotubes have been processed and purified to an acceptable level, the next stage in the production of a composite is to homogeneously disperse the tubes in the polymer matrix. The most important problem to be solved during composite manufacture is regarding the dispersion of fillers in the matrix. Dispersion involves separation and then stabilization of CNTs in a medium. In CNT composites, homogeneously dispersed CNTs in the polymer matrix reduce the possibility of CNT

entanglement which often causes significant undesirable changes in composite behavior [9-10, 38]. The nanotube aggregation within a polymer system would certainly have a negative impact on its stiffening ability [39]. So effective separation is required for overcoming; the existing inter-tube van der Waal attraction, which is anomalously strong in CNTs due to their high polarizability. Depending on the tube shape/sizes and the orientation of tubes with respect to each other, such an attraction can act within the range of a few nanometers [40].

Many applications of CNT composites require the preservation of neat and highly electronically active surface of CNTs (not covered by a surfactant). Also if the tubes are closely packed, an initial formation of a temporary (partial) exfoliation state is required in order to have better interaction with the polymer or the dispersant to adsorb on the surface [41]. Mechanical stirring/mixing and the common ultrasonication process are employed for this purpose; both providing the local shear stress that can break down the bundles. The large variation of existing tubes (differing in synthesis process, impurities, surface chemistry, etc.) and the different application requirements reveal that the suitability of a dispersion technique is system-dependent. The manufacturing techniques such as melt blending [42-45], in situ polymerization or polycondensation in the presence of nanotubes, [46-48] and solution mixing [49-50] are also useful in improving the dispersion of CNTs in a polymer matrix. Ultrasonication cannot produce thermodynamically stable CNT solutions in water and after sonication, CNTs individualize but still the reaggregation possibility to form bundles exists as this is their thermodynamically stable state. So true water soluble solutions are those solutions that entropically favor segregated CNTs where the reaggregation in a solvent is less favoured. Shear mixing is also effective in making homogeneous dispersion of nanotubes in the matrix. In situ polycondensation of monomers in the presence of nanofillers too is a promising approach for a more

homogeneous distribution, due to closer contact of polymer and filler during synthesis. Composite fibres with higher degree of orientation can be produced by melt spinning also [43-49].

In order to improve CNT dispersion, two methods are often used: formation of covalent bonds or the establishment of non-covalent interactions between the matrix and nanotube's surface [51]. Before proceeding to this another common practice of using ionic liquids is mentioned hereafter.

2.3.1. Effect of ionic liquids

Ionic liquids ensure better CNT/elastomer compatibility and recent studies reveal the importance of these materials in making effective CNT dispersions. The advantage of this lies in the hopelessness of any vigorous oxidation or damage to the nanotubes as in chemical treatment. Compared to the physical method of surfactant addition, these ionic liquids can act both as dispersing and reinforcing agent. Likozar et al. [52] studied the diffusing effect of ionic liquids in various functionalized MWCNT/elastomer composites. They noticed a 1.83 fold increase of elongation at break for the hydrogenated nitrile CNT/elastomer composite, in the presence of especially one ionic liquid, namely, 1-butyl-1-methylpyrrolidinium tetrafluoroborate, with only 7 wt% ionic liquid loading. At this level, they could stretch the sample up to 508% without any failure in mechanical properties. The use of ionic liquids additionally resulted in high tensile strength (21.4 MPa) at <7 wt % concentration as well. Using energy-dispersive X-ray spectrometric scanning electron microscope (SEM) and transmission electron microscope (TEM) they could notice a homogeneous distribution of ionic liquids within the polymer chains, especially when the diffusion of ionic liquid into composites took place for more than 48 hours. Subramaniam and coworkers [14, 53] prepared nicely distributed MWCNTs in chloroprene rubber (CR) with the help of the ionic imidazolium liquid. The interaction between the CNTs and the ionic liquid was physical (cation–π/π-π) in nature. In their successive work,

they were able to synthesize conductive CR composites at low concentration of CNTs [53]. The presence of filler-filler and rubber-filler interactions were also evidenced from the dependence of dynamic properties on the ionic liquid concentration. In subsequent studies the authors pointed out the thermal degradation of CR composites based on ionic liquid modified CNTs. The thermal stability is found to be enhanced for ionic liquid assisted system due to their better dispersion as well as interfacial interactions [54]. The composites showed three and four stages of degradation behaviour in nitrogen and air respectively. Even though the authors tried to explain flame retardancy of composites, they didn't observe a noticeable change in the heat release rate values. Using the principle of noncovalent π-π interaction, Liu et al. [55] also synthesized MWCNT/polyurethane (PU)-ionic liquid composites. With the help of Fourier transformation infra red (FTIR) spectroscopy and X ray photo electron spectroscopy (XPS) they described the bonding interaction between the ionic liquid and the CNT/PU composite. With less concentration of CNTs, they got excellent improvement in the mechanical properties because of ionic liquid assisted dispersion. The same group of Stöckelhuber et al. also gave a clear picture of these effects by dispersing MWCNTs in CR with the help of another ionic liquid, 1-butyl 3-methyl imidazolium bis(trifluoromethyl-sulphonyl)imide (BMI). They also found that the filler network re-arranges during the process of curing and leads to good conductivity. Filler dispersion kinetics is analysed based on the wetting of CNTs and BMI, and concluded the replacement of BMI cations with CR molecules on the tube surface. Thus the article provides information on filler dispersion kinetics and its dependence on conductivity [56]. Moreover the non-monotonic dependence of electrical conductivity of MWCNT/CR/imidazolium based ionic liquid on the applied compression/decompression force is also explored [57].

2.3.2. Covalent modification

Functionalization exfoliates the bundles of nanotubes prior to composite manufacturing, thus allowing uniform distribution of them in the matrix with enhanced tube-matrix interaction. The sidewalls as well as the end caps of the CNTs can be functionalized covalently or non-covalently. In covalent modification chemical processes generate functional groups on the end caps as well as on the sidewalls of nanotubes. These functional groups favour improved interfacial bonding between the CNTs and the matrix and correspondingly improve the mechanical capacities of the composites. Modification can also lead to the disintegration of large diameter CNT bundles in to smaller ones. The stability of functionalized CNTs in the suspended state can be attributed to the steric or electrostatic repulsion mechanism or both [58-60].

The technique of covalent functionalization increases CNT solubility in the matrix by causing exfoliation of the bundles. This leads to the dramatic increase in modulus of elastomers while retaining their elongation at break. The technique involves defect site creation on the surface of the nanotubes and functionalization from the defects, for e.g. creating a carboxyl functional group on the end caps of the nanotubes and forming acid derivatives from it by further steps. The common method of functionalization practiced is oxidation which allows the carboxyl and hydroxyl groups to be attached on the sidewalls as well as on the end caps. Table 3 illustrates the different methods of covalent sidewall functionalization of CNTs [61]. This describes the mode of reaction, the type of addend, degree of functionalization and the style of attachment of groups on CNTs. All the functionalization methods have a highly reactive intermediate which can attack the nanotubes [62]. Covalent functionalization can be confirmed by absorption and resonance Raman spectroscopy, FTIR spectroscopy etc. and the degree of functionalization can be obtained from thermo gravimetric analysis (TGA) and XPS. Morphological analysis gives an idea about the diameter of the tubes and atomic

force microscopy (AFM) helps to find out the length of the tubes and thus a clear picture about the disentanglement. But unfortunately, functionalization can cause a decrease in the optical, electrical and thermal properties of nanotube composites since many of these properties are π conjugation dependent [61].

Shanmugharaj et al. described the influence of acid/silane treatment on CNT surface due to oxidation/surface interaction and thereby leading to lattice distortions. They also demonstrated that the thermal stability of the composite was increased when silane modified CNTs were incorporated into NR. On comparison, NR composites filled with silane functionalized CNTs prepared by melt processing showed better enhancement for almost all properties than pure CNT/NR composites [63]. Functionalization can also be done during the purification process of CNTs by exposing them to strong oxidizing acids. The functional groups such as oxygenated and nitrogenated groups grafted on the CNT's surface induce electron donor–acceptor interactions with the unsaturated bonds in the elastomer matrix.

2.3.3 Non-covalent modification

Non-covalent functionalization such as wrapping CNTs with surfactants leads to CNT fluorescence based identification. This provides stability to the CNT suspension in specific solvents like water, depending on the nature and concentration of the dispersant, length of the CNTs and the possible inorganic salts present in the solution. Marsh et al. observed the wrapping of annealed CNTs with 1% SDS and charge doping increased their stability in suspension. Here the shorter CNTs formed more stable dispersions than longer CNTs of the same diameter [64]. Melt blending, solution mixing and coagulation methods are commonly employed to produce non-covalent modified CNT dispersions. Anand et al. [65] studied the influence of various surfactants on the properties of

SWCNT/natural rubber (NR) system. They used different surfactants sodium dodecyl benzene sulphonate (NaDDBS), sodium dodecyl sulphate (SDS), polyvinyl alcohol (PVA), isooctyl phenoxy polyethoxy ethanol (Triton X-100) and sodium benzoate. NaDDBS was found to be the most effective among all the others due to the presence of aryl groups and comparatively longer alkyl chain. However strong interaction and bonding are known to be desirable for load sharing between CNTs and the matrices to be reinforced [65]. Touer et al. [15] made stable suspensions of SDS wrapped SWCNTs and functionalised with diazonium salts yielding heavily functionalised CNTs, which greatly enhanced the interaction with the elastomer matrix. In addition to homogeneous dispersion, controllable alignments of CNTs in the matrices are also crucial to achieve improvement in composite properties and this will be discussed in the following sections. In addition to these methods, thermal and laser ablation are also other possible surface modification techniques [64].

There are certain reports showing the less effectiveness of non-covalent functionalization of CNTs over covalent binding. Jiang et al. [66] studied the effect of surface modification of MWCNTs by surfactant, hexadecyltrimethylammonium bromide (CTAB) and coupling agent, gamma-aminopropyltriethoxy silane (KH550), on the microstructure and electrical properties of rubber. The results showed that CTAB improves the dispersion of MWCNTs, but fails to improve the rubber-MWCNTs interfacial interaction. While the use of KH550 helped in the good dispersion of MWCNTs and induced strong interfacial interaction, on the other hand it often hindered the electron transport in the composites. These results were further confirmed by the temperature and pressure dependences of the electrical properties of the composites. The way of attachment of the functional groups on the described CNT composite is shown in Fig. 3 (physical adsorption in Fig. 3a and chemical interaction in Fig. 3b) [66]. Even though wide varieties of studies are going on about the dispersion of nanotubes, a complete disentanglement is not yet reported.

Even though the aggregation tendency of CNTs is the culprit, Kobashi et al. proved that these undesired CNT agglomerates can be utilized to fabricate advanced composites [67]. Stable highly concentrated CNT suspensions were made from long SWCNTs at above 3.0 wt% and the nanotube agglomerates formed were used for elastomer reinforcement. The agglomerates exhibit a dendritic network similar to venation and vein patterns and caused 10-fold increase in electrical conductivity for the rubber. The authors finally concluded that two dispersion strategies, i.e., isolated CNTs, and dendritic CNT agglomerates are complementary, and each demonstrated distinct advantages and disadvantages [67].

3. Fabrication of elastomer composites

Elastomers are widely used -from the small-scale biomaterials to the large-scale earth quake damping devices- because of their highly reversible deformation properties depending on curing. However, the initial modulus and durability of the elastomers are very poor. Also elastomeric applications generally require and make use of the large deformation extensibility and resilience of the elastomer [68]. Therefore various kinds of fillers such as metal oxides, carbon black (CB), silica particles and CNTs are usually employed for their effective reinforcement. Upon the incorporation of stiff fillers into elastomers, the stiffness enhances (i.e., enhance the initial stiffness and retain this stiffness enhancement for overall large strain deformation behavior) while retaining the important attributes of large strain resilient behavior and large strain-to break. The high and reversible deformability of elastomers is of great industrial importance. Their outstanding strength, long fatigue life, good creep, stress relaxation resistance and low cost make them the most popular material in technology. Fillers are added to rubber products as in vehicle tyres and shock mounts to enhance their stiffness and toughness properties. They also improve the processability, increase the toughness, fracture resistance and stress stransfer in elastomers. Filler reinforcement provides fabrication of

stronger, lighter or less expensive composites than their traditional neat counterparts. To improve the physical and mechanical properties of rubber, fillers like silica, $CaCO_3$, CB etc. have been used from early days. The most commonly available elastomeric composites are reinforced with CB particles which ranges in size from 100-1000Å [69-71].

The unique behaviour of CB filled elastomer composites is attributed to the presence of a rigid particulate phase and the interaction of the elastomer chains with this phase. But the main problem with these fillers is that a substantial improvement in properties is obtained only at higher filler loadings. As there is a demand for modern technological application for superior elastomeric composites, innovative reinforcements having better properties should be introduced [72]. Due to very small size and large surface area and hence surface properties, nanoparticles play an important role as fillers in this regard. By adding only a very small amount of nanoparticles into rubber, excellent enhancement in properties can be achieved. Being unique filler CNTs are expected to increase the property of all types of elastomers including rubbers. In the case of CNTs, a stronger filler/matrix interaction at the interface leads to a more immobilized rubber shell compared with filler particles of micro dimensions [66, 68]. Another important factor is the anisometry (shape factor) of the filler aggregates i.e. the ratio of the largest dimension of the particle to the shortest. In compounds containing fillers with identical surface area and chemical nature but with different shape, the storage modulus increases with increase in anisometry. This larger shape factor for CNTs explains higher reinforcements than CB. The alignment (in terms of both overall alignment as well as waviness of the nanotubes) and bonding detriments encountered while incorporating MWCNTs into thermoplastics may be used to make advantage in their incorporation into elastomers. Incorporation of nanotubes in elastomers like silicone rubber (SR) dramatically improves the properties of the resultant composites [69, 73]. CNTs act as effective crosslinks even in unvulcanized rubber at low filler loading [74].

Additive effects of the physical and chemical crosslinks of the chains play an important role at the beginning of the deformation and gives higher modulus than pure elastomer. Though rubbers are thermal and electrical insulators, incorporation of conductive fillers could produce conducting composite materials.

The development of CNT based elastomeric composites could demonstrate both the excellent energy absorption characteristics of the matrix components as well as the advanced structural properties of the CNTs. Recent experiments show that significant improvement in the mechanical properties of polymeric materials can be achieved by using even small volume fractions of CNTs as reinforcements [69]. Potential applications of CNT filled elastomer composites could vary from industrial materials such as rubber hoses, tyre components, sensing devices to electrical shielding and electrical heating equipments. The fabrication of high performance elastomer composites depend on the efficiency in load transfer from the matrix to the nanoparticles. If the percentage of reinforcement is very low or if it is well dispersed there are more strong interfaces that slow down the progress of the crack, thus making it applicable in light weight aerospace materials. However there are some critical issues concerned with such composites like the non uniform dispersion of nanotubes in the matrix (as discussed previously), increase in viscosity due to high aspect ratio and lack of control of the alignment or orientation of CNTs. Another problem to be addressed is the lack of a strong chemical bond between the nanotube and the elastomer matrix. This is due to the absence of an electrostatic force between the CNTs and the elastomer and the stress/deformation arising from the mismatch in the matrix-nanotube thermal expansion coefficients. Most of these issues can be solved by modifying CNTs and also during the preparation of the composites [54-55, 58-61]. All the aspects of these amazing composites are discussed in detail in this review.

3.1 Preparation techniques

The major composite manufacturing methods usually employed are explained here in detail.

3.1.1 Solvent casting

This method involves dispersion of both filler and matrix in separate suitable solvents and thereafter mixing the two. The solvent evaporates to get dry samples of the composite. Following this method, Bokobza et al. [75] formulated CNT/styrene butadiene rubber (SBR) composites and achieved a 45% increase in modulus and a 70% increase in the tensile strength with 1 phr (per hundred rubber) MWCNT. Solvent casting is found to be the most useful and effective method in the case of latex matrices as this does not require the dissolution of the elastomer in any additional solvent depending on the nature of the filler. But if the filler is not compatible with the aqueous elastomer matrix, both the elastomer and filler dispersions are made in other suitable solvents. Khalid et al. [71] also dispersed CNTs in NR by solvent casting using toluene. Even though this method is effective, the use of organic solvents like toluene cannot be welcomed.

3.1.2 Freeze drying

Freeze drying is a process whereby solutions are frozen in a cold bath and then the frozen solvents are removed through sublimation under vacuum, leading to the formation of porous structures. The nature, size, volume and morphology of pores depend on freeze temperature, solution concentration, nature of solvent and solute, and the control of the freeze direction. Aqueous, organic, colloidal and supercritical CO_2 solutions are used in this technique generally to produce porous structures [76]. A dispersion of filler in the polymer matrix is prepared by simple mixing and is allowed to condense in liquid N_2 and then it is compression molded. Up to now, this technique is not widely used to synthesize CNT/elastomer composites. Yu et al. [77] effectively synthesized CNT

polystyrene latex composites using freeze drying followed by compression molding method. The same technique can be proposed to prepare elastomer latex composites also.

3.1.3 Spray drying

A suspension of CNTs in elastomer can be converted to CNT/elastomer powder composites by spray drying process. For this, the suspension of CNTs (with or without functionalization)/elastomer/vulcanizing reagents is homogeneously mixed, atomized and dried by means of spray drying to obtain powders of composites. By means of spray drying process, uniform globules of polymers (diameter less than 10 μm) could be fabricated in which CNTs are well dispersed. Zhou et al. [72, 78] synthesized SBR powders containing CNTs with uniform diameters of about 5-10μm using spray drying process. Compared with those of pure SBR composites, the hardness and tear strength of the composites filled with 60phr CNTs are enhanced by 70 and 250% respectively, and the tensile strength of the composites with 50phr CNTs improved remarkably by 600%.

3.1.4 Latex stage compounding

Rubber latex can be compounded with CNTs along with curing agents. The main crosslinking method is using sulphur in the presence of ZnO, stearic acid, Tetramethyl Thiuram Disulfide (TMTD), 2,2'-Dithiobis(benzothiazole) (MBTS) etc. This process improves crosslinking between the polymer chains in the composites. In this process, at first the curing agents are mixed well with the latex by milling methods, which is called compounding and then the compounded latex is mixed with the CNTs [79]. This method is successfully utilised by Anand et al. [65] for preparing MWCNT/NR latex composites. They compounded the NR latex using ball milling and thereafter composites are formulated using mechanical mixing and noticed good improvement in mechanical, rheological and electrical properties.

3.1.5 Hetero coagulation approach

The typical heterocoagulation process is based on depositing small charged particles on the surface of larger particles of opposite charge. The method is based on ion exchange between cationic latex particles and anionic (oxidized) nanoparticles [80]. The electrostatic interaction between the filler and polymer is believed to enhance the filler–polymer adhesion [81]. Heterocoagulation method was also successfully used to prepare exfoliated clay filled polymer composites [82-83]. This technique is employed by Peng et al. [84] while preparing functionalized MWCNT/NR composites. The interaction between the charged particles binds them together to give well dispersed composite materials.

3.1.6 In-situ polymerization

In situ polymerization to fabricate CNT based composites involves the polymerization of corresponding monomers in situ within the CNT suspensions. This offers an easy and efficient method to disperse CNTs uniformly in the polymer matrix. The type of polymerization reaction, nature of sovents used, reaction conditions etc. may vary based on the type of composite required. Curing of elastomers can be done by directly adding curing agents also in situ. When the monomers polymerize in the presence of CNTs, covalent bonds can be formed between the monomer units as well as with the functionalized CNTs. These strong matrix-filler bonds enhance the interfacial interaction and lead to highly improved properties like mechanical strength of the composites [85-87]. This method is particularly used for polymers that cannot be prepared by solution processing (insoluble polymers) and melt mixing (thermally unstable polymers).

3.1.7 Melt blending/Extrusion

As the name indicates melt blending offers a high temperature shear mixing for composite fabrication. In this method, elastomers are melted in internal mixers or two roll mills by adding CNTs.

This is the most industrially preferred method of composite manufacturing since it avoids the usage of solvents. The machines used for this purpose are designed such a way that the screws inside it can move at high speeds which in turn results in efficient dispersion of CNT bundles inside the elastomer matrix. Even though this method is the best suited one for commercial scale, it has two disadvantages. One is the high possibility of efficient dispersion of CNTs only at higher concentration inside the elastomer matrix [88] and the second is the difficulty to add curing agents to elastomers at high processing temperatures. So this method is more concentrated on thermoplastics reinforced composites. However there are a few works reported on fabrication of elastomer composites also. For instance, Das et al.obtained good dispersion of CNTs in SBR and butadiene rubber (BR) blend following melt mixing [16]. They also fabricated [70] MWCNT/CR composites by adding the CNT dispersion using ethanol as dispersion agent in to mill mixed CR and obtained excellent mechanical properties.

3.1.8 Solid state shear pulverization

Polymer and CNTs were mixed and pulverized by pan mill or twin screw extruder and the polymers are grafted on CNTs. The major advantage of this technique includes its easy scale-up. This is a solvent less process [89]. Xia et al. [90] and Masuda et al. [91] prepared CNT/polymer composites via solid state shear pulverization and proved that this technique improves the dispersion rate of the nano fillers in the matrix and results in a major property enhancement. By this process powders of the composites are obtained.

Other methods of composite manufacture include growing a pre aligned array of CNTs in a substrate by CVD and then infiltration of a monomer in to these arrays and its polymerization. The resulting composite film showed good dispersion of nanotubes in the polymer and gave enhanced thermal stability. Electrophoretic deposition method is also possible by moving the charged particle

dispersed in a suitable solvent towards an electrode under an applied electric field. The functional groups on CNTs can solubilize them in water and can create a negative charge which helps them to move towards anode [88]. This offers advantages of low cost, uniformity of the coatings and possibility of depositing on complex shaped substrates. The techniques for CNT dispersion are not limited to those described above. Many of the recent studies are often based on the use of a combination of aforementioned techniques, such as ultrasonication plus ball milling [92], and ultrasonication plus extrusion [93-94] etc. By combining the latex stage compounding with self-assembly technique, Peng et al. synthesized MWCNT/NR latex composites and obtained good adhesion behaviour at <3 % CNTs content [95]. They suggested the enhanced state of dispersion based on morphology and thermal analyses as a result of the combined techniques.

3.2. Orientation of carbon nanotubes

The orientation and alignment of CNTs can influence the properties of CNT composites to a great extent. Orientation effects are mainly due to their high aspect ratio. The degree of alignment of nanotubes can be determined by X-ray diffraction and polarized Raman spectroscopy. The alignment of CNTs can be done during composite formation or aligned nanotubes can be incorporated into the polymer matrix [96]. If the composites are manufactured by extrusion or injection molding, there is a chance of tuning the alignment degree. This can be done by regulating the shear rate as well as the pressure applied [97]. This method helps to produce well aligned CNT composites in single step. In situ polymerization is also possible in which, viscosity of the nanotube monomer suspension affects the degree of alignment. The tubes can be aligned after composite formation also. This is done by mechanical stretching, electrospinning etc. Other methods of alignment also include filtration, plasma-enhanced chemical vapor deposition (PECVD), template, force field-induced alignment, magnetic field-induced alignment and liquid crystalline phase-induced alignment. Among all methods, the

spinning technique offers the greatest degree of alignment [20] due to the extrusion of the composite through a very small orifice during the process. The alignment depends on the fiber diameter and the amount and type of CNTs. SWCNTs can align more than MWCNTs. SWCNTs tend to orient parallel to each other in close proximity to maximize their interaction, thus forming bundles consisting of 100–500 tubes. As the amount of nanotubes increases, motions of the tubes are restricted because of agglomeration and thereby the alignment decreases [97]. Functionalisation also can affect nanotube alignment. For instance, when CNTs are oxidized, carboxyl or hydroxyl functional groups get attached on the terminals and forms COOH-terminated self-assembled monolayers. The tubes having lengths greater than the dimensions of such a monolayer, can align along the inter layer boundaries and these patterns are used for fabricating thin films and continuous ropes of CNTs with sophisticated structures. The CNTs can also be aligned by flowing gas through a suspension of it. The alignment in this case is due to the circulation of tubes in the suspension droplet under gas flow. The orientation depends on the nanotube chirality too [98]. The nanotube debundling prefers to occur in the middle region for armchair tubes whereas it occurs at the ends for zigzag tubes. In the case of armchair tubes, the preferred path for unzipping is parallel to the tube axis which results in straight zigzag-edged graphene ribbons. This is a little different from the zigzag tubes, where they have two energetically preferred helical unzipping directions. This is because of the fact that in these kind of tubes, two types of C–C bonds have to be opened. Thus the orientations of nanotubes in composites are functions of nanotube properties. In ex situ method CNTs are aligned in advance and then compounded with the polymer matrix by in situ polymerization of some monomers.

Filler orientation can influence the electrical conductivity of composites. The anisotropic conductivity of composites has been predicted by orientation of rods or fibres [98-99]. Wood et al. showed that the radial shear flow during manufacture removes the initial isotropy present in the system

[100], but the resulting film has SWCNTs distributed on the plane of the film. Since SWCNTs are randomly oriented in the resulting film, the direction in which sample strips are taken for characterization does not make any difference in the results. To utilize their novel properties, many researchers have focused on the dispersion and orientation of CNTs, and fabricated various CNT/elastomer composites [101-108]. Deng et al. [109] demonstrated that persistence length and reorientation of MWCNTs during stretch have a significant impact on mechanical properties, such as the modulus of the rubber composite. Hudziak et al. proposed a phenomenological model for magneto resistive effects in an above-percolation-threshold loaded Fe-filled MWCNT/elastomer composite by interpretation of resistance relaxation for a range of axial strain [110]. They observed a large instantaneous magnetoresistance at low axial strain as a result of conduction pathway breaking caused by preferential orientation of the conducting nanotubes perpendicular to the axial current flow as a result of the magnetic torque experienced by the ferromagnetic Fe-MWCNT [110]. The reorientation of nanotubes under strain in the samples may be responsible for the initial increase in modulus under strain and this is quantified in the Raman experiments by Frogley et al. [69]. The Raman measurements provide extra insight into the nature and efficiency of the interface in the composites as well as quantification of the strain induced reorientation of the nanotubes towards the axis of tensile strain. The reason is in composites the polymer chains are more oriented than that of the pure matrix, the orientation being induced by the high alignment of the CNTs upon application of the uniaxial deformation. Summing up, highly ordered CNTs are useful for many applications, such as field emission displays and sensors, data storage, and light-emitters. This also provides superior applications to the obtained well-aligned CNT/polymer composites.

4. Characterization of the elastomer composites

4.1. Structural analysis of the composites

4.1.1. Behaviour at the interface

While incorporation of CNTs in the elastomer matrix, good interfacial compatibility must be ensured in order to fabricate high performance composites. This interfacial interaction between elastomers and CNTs is investigated in the literature mainly by examining (i) the CNT/polymer interface, through Raman spectroscopy, bound rubber measurements and solid state nuclear magnetic resonance (NMR) spectroscopy (ii) the interaction at medium range, through dynamic-mechanical tests and (iii) the interaction at long range, through quasi-static measurements. The effect of medium range and long range CNT interactions on the properties of elastomers are explained in the following sections from dynamic-mechanical measurements and quasi-static measurements such as mechanical studies. Since the bound rubber measurements are included in section 4.2.2 of this same review, here the use of Raman and NMR spectroscopy is dealt with.

Raman spectroscopy is a powerful characterization tool for CNTs by providing the nature of two main absorption bands D (centred at $1300 \, \text{cm}^{-1}$ related to the presence of disordered structures or structural defects at the surface) and G (centred at $1600 \, \text{cm}^{-1}$ related to the graphite-like structures). The ratio between the intensity of the G and D bands (I_D/I_G) is a measure of the degree of CNT imperfection; and the shift in peak position along with it address the functionalization [62, 111]. Tip enhanced Raman spectroscopy (TERS) is a useful technique for CNT composites in many ways. This analysis gives information about the optical properties of CNTs [112], CNT dispersion and CNT-polymer interface. The intensity of G-band of CNTs in TERS strongly depends on the height of the bundle. Also the G-band frequency in TERS varies depending on the position of CNTs along the

bundles [113]. Very recently TERS studies revealed the interactions and local structural changes at MWCNT/SBR interface. The TERS is a combination of scanning probe microscopy and surface-enhanced Raman scattering and has high spatial resolution as high as 4 nm [114]. In their work Suzuki et al. collected same spots for both Raman spectra and TERS studies. Considerable deviations were observed in TERS peaks depending on the position of the composite samples analysed. The relative intensities of peaks change from position to position which indicates the distribution of MWCNTs in SBR. At lower CNT concentration, the peaks correspond to SBR are present larger in number and the position of specific vinyl and phenyl groups in SBR in the spectrum show the interaction between the filler and matrix [115]. Bokobza et al. also characterized the CNT/elastomer interactions from Raman spectroscopy under strain. They explained the CNT reinforcement in terms of the shift in position of the absorption wavenumber [116].

The significance of NMR spectroscopy in addressing the behavior of elastomer composites is well explained in a chapter in a book edited by our group [117]. Even though Park and Kim explained this technique based on silica reinforced composites, this chapter provides the basic understanding of NMR technique in addressing the filler-elastomer interactions. In the case of CNT composites, NMR spectroscopy also provides structural information by analyzing the H positions in the polymer [118]. An important parameter of interfacial interaction, crosslink density is calculated based on this method by Yu et al. They fabricated MWCNT/polyisoprene composite and had done the analysis by 1H solid-state NMR spectrometer. Here the crosslink density values obtained from swelling measurement shows higher reinforcement for the CNT reinforced samples, whereas the value from NMR method indicates lower number of chemical crosslinks for the composites compared to the neat polymer. This indicates that the MWCNTs disrupt chemical cross-linking process near the CNT-polymer interface. This also causes the accumulation of free radicals, or unpaired free electrons near the interface. But

since the swelling is a bulk phenomenon and deals with the total crosslink density of the entire sample, it shows higher crosslink density values than that obtained from NMR [119].

4.1.2. Microscopic morphology

The nature of dispersion of nanotubes in elastomer is mostly explored by microscopic techniques. The commonly used techniques include AFM, SEM and TEM. Confocal microscopy and optical microscopy are also used, but in order to visualize the nano strcucture the previous techniques are much better. Characteristic properties of the composites can also be explained based on their microscopic structure. Wang et al. explained the mechanical improvement obtained for the CNT/NR composites by proposing a cellular structure [120]. They made the composites by mill mixing with high shear stress and investigated the topography, modulus, and adhesive energy distribution maps of the resulting composites in terms of CNT loading with an AFM nanomechanical mapping technique. Those maps (Fig. 4a-c) were successfully used to identify and characterize heterogeneity of such composites. In the composite, the mechanical interfacial regions formed around CNTs together with CNTs divided elastomer matrix into small ''cells'' in which the matrix was occluded (Fig. 4d). And this entire structure was named as cellular. Bokobza et al. also [121] demonstrated the influence of MWCNTs on the mechanical properties of SBR through the AFM analysis.

The SEM and TEM techniques address the internal microstructure of the composites in addition to their surface morphology. Cross sectional SEM images of the cryo cut (in liquid nitrogen) and sputter coated (with gold) samples of MWCNT/styrene–butadiene–styrene composites were taken in order to explain their mechanical, electrical and electro-mechanical properties by Costa et al. and they could illustrate the good interfacial adhesion of CNTs with [122] the polymer. The well dispersion of MWCNTs as well as some large aggregates of nanotube clusters and voids in the composite is clearly seen in the cross-sectional SEM images of the MWCNT/polydimethyl siloxane

(PDMS) composite given in Fig. 5 [123]. The difference in the microstructure at lower and higher filler concentrations is clear from Fig. 5a and 5b which respectively represent the MWCNT/PDMS at 0.2 and 1.4 wt% of nanotubes. At 1.4 wt %, the continuous, percolative paths formed are also observed. Since the voids inside the composite can cause crack propagation under tension, the mechanical property between microtensile test and buckling method are influenced. Thus morphology is applied here as a tool to determine the mechanical as well as electrical properties in addition to observation of dispersion [123]. The TEM images of the PDMS composite containing exfoliated ionic liquid modified SWCNTs having 30 nm diameter are also shown in the same figure which illustrates the dispersion of CNTs in the presence of ionic liquids. Fig. 5d shows the high level of dispersion of modified SWCNTs in PDMS when compared with that containing entangled SWCNT bundles with a diameter of more than 100 nm (Fig. 5c). Moreover Oh et al. correlated this morphological observation with the dielectric and mechanical properties of the composites [124].

4.2. Determination of constrained elastomer in the composites

4.2.1. Gel fraction

The gel fractions (GF) of the vulcanizates are measured by the solvent extraction method. This parameter would characterize the crosslinking degrees of the vulcanizates. A certain amount of vulcanizates is put in an extractor with a suitable solvent and later dried into a constant weight. The GF is calculated using Eq. (1).

$$GF = \frac{w_2}{w_1} \times 100 \dots\dots\dots\dots\dots\dots\dots\dots\dots\dots\dots\dots\dots\dots\dots\dots (1)$$

where w_1 and w_2 are respectively the weights of the testing specimen before and after the extraction.

Khalid et al. [71] described the ability of radiation-induced cross linking in CNT/NR composites, by estimating the gel fractions. They found a rapid increase in GF of the composites with

an increase in radiation dose up to 150kGy which is attributed to the radiation-induced cross links formed through a free radical mechanism [125]. Therefore, as the radiation dose increases, more radicals are generated in the polymer matrix and consequently more cross linking occurs. However, at higher dose (above 150kGy), the gelation rate slows down because at this stage macromolecular chemical bonds are realized predominantly between already cross linked macromolecular networks. Therefore, it does not lead to a significant increase in the gel content despite an increase in cross linking density in spatial macromolecular lattices, with increase in radiation doses. However the GF increased with increase in the CNT loading and radiation dose. This is due to the different functional groups, such as carboxyl, phenolic, hydroxyl, aldehydic and ketonic, present on the CNT surfaces that would participate in physical as well as chemical bond formation at the interface between the CNT and rubber matrix up on irradiation [126] together with the free radical formation. This effect of radiation dose on the GF of CNT/rubber composite is given in Fig. 6.

The crosslinking degrees of vulcanizates with different CNT additives are shown in Fig. 7. It can be seen that the cross-linking degrees of the vulcanizates increase gradually with increasing CNT. With more CNTs added into the composites, the volume of CNTs in the vulcanizates increases [127] and this leads to enhanced GF values. After a particular concentration of CNTs, the GF values show a leveling effect as well.

4.2.2. Bound rubber content

Bound rubber has been attributed as being involved in polymer-filler interactions and the amount of bound rubber is considered as an important indicator of reinforcement. It is significant in non crosslinked samples. Soluble materials were extracted by immersing samples in toluene for days, followed by drying at room temperature [128]. The weights of the non-crosslinked samples before and after the extraction were measured, and thus the bound rubber contents were calculated. The bound

rubber test relies upon the determination of the quantity of elastomer adsorbed (Q_{ads}) on the filler surface, which is calculated using Eq. (2).

$$Q_{ads} = \frac{M_D - M_{CNT}}{M_{CNT}} \text{----------------------------------- (2)}$$

where Q_{ads} correspond to the amount of rubber adsorbed within the filler network, M_{CNT} the initial CNT mass and M_D is the mass of the dried centrifuged residue [128]. Nah et al. [129] suggested a weaker rubber-filler interaction for CNT/NR composites compared to the NR/CB composites based on the bound rubber content. Their comparison is shown in Fig. 8a. The reason for lower values of bound rubber for CNT samples may be a kind of slippage effect of the inner layers of nanotubes with respect to the outer layer; in other words, it could be explained on the basis of relatively weak adhesion between the layers. They also suggested that the outer layers of the CNTs have weak adhesion to rubber. However they obtained an increase in mechanical property for the CNT/NR composites, the reason for which is explained as the high aspect ratio of the CNTs.

Bound rubber depends on other characteristics of the filler (its structure, surface area, and the surface properties) and also on the chemical composition and functionality of the rubber [130]. It is inferred that the aggregate structure of CB is more efficient than the fibril structure of CNT for making bound rubbers, if the surface activity is similar. Fig. 8b shows a plot of volume expansion against bound rubber content. It is seen that the increase in volume expansion is approximately proportional to the amount of bound rubber. The volume expansion at large extensions also attributes to the formation of micro voids in well-reinforced CB-filled rubber compounds i.e a craze like phenomenon. Volume expansion may also occur in the bound rubber fraction by a meniscus instability mechanism [131]. Verge et al. [128] synthesized vulcanized CNT-based NBR composites by a two-step process involving a first melt blending and then sulfur-curing and they observed a substantially higher quantity of polymer chains remains bound/adsorbed on the CNT surface when the acrylonitrile (ACN) content

in NBR is increased. A larger quantity of CNTs appears thus bound to NBR containing higher ACN units, attesting for the expected interactions between the ACN units and CNTs. Moreover, these interactions stress the fact that ACN units are localized in the neighborhood of CNTs. Since ACN groups can generate free-radicals by hydrogen atom abstraction, it can be assumed that their proximity to CNTs favors the polymer-grafting on the CNT surface. In a recent work by Saatchi et al. the bound rubber is assumed to be critical for the mechanical and deformational properties, development of crosslinking density in matrix rubber and for polymer-filler interaction [132]. For comparison they made CB and MWCNTs reinforced SBR composites and analysed the experimental data using the Flory–Rehner model and the tube model theory. They proposed a three-phase composite model including rigid particles, semi-rigid bound rubber and matrix rubber for the CB filled SBR and further confirmed the less tendency of bound rubber formation by CNTs compared to CB. They proposed that the final properties of MWCNT/SBR system originate from the polymer-filler interaction and high aspect ratio of the MWCNT reinforcement than bound rubber content. This polymer-filler interaction was found to be good for all the composite systems studied, according to the Kraus interaction parameter and Heinrich coupling density factor.

4.3. Mechanical properties

The fiber like structure of CNTs, their low density and high aspect ratio make them very useful for the reinforcement of elastomers. When such fillers are added to an elastomer its tensile modulus, tensile strength and hardness increase depending upon the nanotube loading, dispersion and alignment in the matrix. The tensile strength increases with CNT content due to high surface area of CNTs in contact with the elastomer molecules. The elongation at break is also expected to increase with nanotube addition; however this trend varies in different systems. The interfacial interaction between the polymer and the filler and also the homogeneous dispersion of filler in the matrix increase

the stiffness and ductility of the composites and cause elongation at break also to improve. The mechanical properties of CNT reinforced elastomer composites are summarized in Table 4. Adedigba et al. [141] demonstrated a linear relationship between the Young's modulus of the CNT/NR composites and percentage of CNT addition. They reinforced NR latex with MWCNTs and noticed an increment of about 124% in Young's modulus at 10 phr CNT loading. The improvement in modulus as well as stress strain behavior is attributed to the effectiveness of CNTs to uniformly transfer the applied stress through the matrix, which is related to the large surface area of CNTs.

Long back, Guth et al. [142-143] successfully evaluated Young's modulus from the stress–strain experiments and derived an equation to evaluate the value of apparent aspect ratio of rod like particles. This Guth–Gold–Smallwood equation is represented by Eq. (3).

$$E = E_0 \left(1 + 0.67\, \phi f + 1.62\, \phi^2 f^2\right) \text{-------------------------------------- (3)}$$

where E and E_0 are the Young's modulus of the filled and neat elastomer respectively, Φ is the volume fraction of the filler and f is the shape factor or the aspect ratio of a non-spherical particle. When the filler concentration and aspect ratio are very less, the third quadratic term of the above equation can be neglected. Initially for deriving Eq. (3) rigid, anisotropic fillers with relatively low aspect ratio were considerd, but high aspect ratio CNTs are also flexible to this equation.

Perez et al. [68] used another form of Guth equation as shown by Eq. (4) to correlate the elastic moduli of polymeric composites containing MWCNTs with the experimental values.

$$E = E_0 \left(1 + 2.5\, \phi f + 14.1\, \phi^2 f^2\right) \text{----------------------------------- (4)}$$

where E_0 and E represent elastic moduli (Young's modulus can also) of the unfilled and filled polymer. The quadratic term in this equation corresponds to the effect of aspect ratio and volume

fraction of fillers on the elastic modulus of composites and on the interaction between the dispersed particles.

The stress–strain curves for CNT/NR composites are represented in Fig. 9a. Bhattacharyya et al. [144] observed the typical non-linear ''S curve'' described in the kinetic theory of rubber elasticity. It is useful in that case to plot the so called reduced (or Mooney) stress as a function of the extension ratio as shown in Fig. 9b. The plot (Fig. 9b) of reduced stress vs $1/\alpha$ illustrates the elastic behavior of rubber-like materials. It shows that the modulus is increasing with the increase of filler volume fraction, which is in qualitative agreement with the Mooney–Rivlin equation (Eq. (5)), at least in the moderately large deformation regime.

$$\sigma = 2C_1(\alpha - 1/\alpha^2) + 2C_2(1 - 1/\alpha^3) \quad \ldots\ldots\ldots\ldots\ldots\ldots\ldots\ldots\ldots\ldots \quad (5)$$

where C_1 and C_2 are constants, σ is the retractive stress and α is the extension ratio.

The upturn observed in Fig. 9b at low inverse extension ratio is related to the stress-induced crystallization of NR [145-146]. And the authors have explained this on the basis of modified Mooney Rivlin equation [147].

$$\sigma = 2\left(\frac{C_1 + C_2}{\alpha}\right)F_\alpha \quad \text{---} \quad (6)$$

where C_1 and C_2 are dependents of α and the function $F(\alpha)$ is $F(\alpha) = \alpha - \frac{1}{\alpha^2} + \frac{\alpha_m}{3}\left(\frac{\alpha}{\alpha_m}\right)^3 + \ldots..$

α_m is the maximum extension ratio. When $\alpha < \alpha_m$ this equation becomes Mooney Rivlin equation (Eq. (5)).

A similar behavior although in low magnitude has been reported by Bokobza et al. [148] with silica nanoparticles filled rubber in the unvulcanized state due to a rigid network formation. This ensures a similar type of networking behavior in CNTs also. This as well as the hydrodynamic effect

contributes towards the more significant reinforcement and network formation in CNT/elastomer composites. Cantournet et al. [149] thoroughly investigated the mechanical behaviour of CNT elastomer composites and proposed a constitutive model for explaining their behaviour. They observed an increase in the initial stiffness and the subsequent strain-induced stiffening at large strains with MWCNT content. The weight percentage of CNTs is also found to be influencing the tensile strength, tensile stretch at break and the strain to failure. They noticed a 2.5 times increase in the modulus for a 12.2wt% MWCNT/elastomer composite when compared to the neat elastomer. Comparatively, a similar weight fraction of CB filler provides a modulus 1.3 times that of the neat elastomer [150]. Fig. 10a and 10b represents [149] the uniaxial tension load-unload true stress vs true strain plots. These data show an ability to substantially increase the tensile stiffness and retain the stiffness enhancement during large strain deformation as well as the ability to increase the tensile strength and the tensile strain-at-break. The developed hyper elastic constitutive model for composite materials is based on the volume fraction of matrix and MWCNT content. The model is capable of predicting the effects of MWCNT content on the large deformation stress strain behavior of the composite materials in tension and compression modes and it is in agreement with experimental observation.

Chemical modifications of CNTs, enable the interaction of the functional groups on the CNTs with the polymer matrix and helps in the homogenous dispersion of the nanotube fillers and consequently, the interfacial bonding and load transfer could be enhanced which increases the elastic modulus and ultimate tensile strength when compared to the unfunctionalised CNTs. This was shown by Park et al. [151]. They used functionalized and unfunctionalized SWCNTs in the polymer matrix. It was also observed that a larger aspect ratio was imperative in enhancing the strength through comparison with functionalized MWCNT reinforced composite. A maximum in the work of fracture was indicated at low nanotube volume fractions, which could be facilitated through bridging effect by

the CNTs. This implies that the toughness of the composite could be diminished at increased CNT loading due to network formation of the nanotubes. Phenol functionalized MWCNTs enhanced the tensile strength and Young's Modulus of SBR composites respectively from 0.17 MPa (SBR) to 0.48 MPa and from 0.25 MPa to 0.83 MPa at 10wt% concentration [152]. The homogenous dispersion of CNT-Phenol in SBR is thought to be responsible for the considerable enhancement in the reported properties [152]. The mechanical improvement is better explained by Wang et al. [120] by a cellular structure for the obtained CNT/NR composites. They made the composites by mill mixing with high shear stress and investigated the topography, modulus, and adhesive energy distribution maps of the resulting composites in terms of CNT loading. Due to the three-dimensional structure of CNTs and the mechanical interfacial regions formed within the composite (as explained in Fig. 4), the mechanical properties were greatly enhanced.

Sato et al. [153] prepared r-SWCNT soot filled SBR compound suitable as tread material for high performance tyres, vibration-proof material and/or shock dampeners. The r-SWCNT soot at higher concentration offered higher reinforcement and lower resilience in comparison with CB at the same concentration in contrast to the general rubber behavior of decrease in resilience with increasing filler content. In a similar way, Frogley et al. [69] observed a dramatic enhancement in the initial modulus for SWCNT/SR composites, as a function of filler loading and applied strain and thereafter a reduction in the ultimate properties at around 10-20% strain. This special trend is observed in most of the elastomer (or rubber) composites and is considered to be arising from the trapping and releasing of rubber chains within the filler clusters. In situ Raman spectroscopy experiments explained and quantified this initial increase in modulus as due to the break-down of the effective interface between the phases and reorientation of nanotubes under strain [112]. For nanotubes the high aspect ratio and low density of bundles and their well dispersion in the matrix contribute towards this high

reinforcement. Other than the *in situ* measurements of the strain dependent Raman spectrum macroscopic tensile tests also explains the increase in modulus at low strain rate [111, 113]. However the other composite properties variation was not correlated with this observance [69].

To obtain high performance rubber composites that combine improved mechanical and tribological properties, the method of melt compounding has been effectively utilized by Likobzar et al. [154]. They attained large extent of exfoliation and intercalation of MWCNTs in hydrogenated NBR (HNBR) matrix along with CNT/rubber cross-link formation. It has been established that the hardness, the tensile and tear strengths, and the apparent cross-link density varied with increasing ACN content of HNBR. The elongation at break exhibited a maximum at certain ACN content for both unhydrogenated and hydrogenated rubbers and is attributed to the optimal cross-linking at this ethylene or butadiene/ACN segment ratio. The value of the tensile strength also depends on the hydrogenation of NBR. By contrast, the tear strength was lower for hydrogenated in comparison to unhydrogenated rubbers. From the viewpoint of wear resistance the unhydrogenated rubbers were much better than the hydrogenated ones due to their lower coefficient of friction [154]. It is also emphasized that the observed improvement in the wear rate for HNBR/MWCNTs strongly depends on the configuration of the tribological tests as well as the increase in ACN content.

Nanotube size also influences mechanical properties of the composite [155]. If L and ℓ are the nanotube length and the characteristic network mesh size respectively, at $L\,\ell^{-1} \sim 1$, the effect of the filler particles is relatively small and when $L\,\ell^{-1} \gg 1$ there is a sharp increase in the mechanical modulus. Even though CNTs improve mechanical properties, the chance of CNT bundling and breakage and thereby reduction in aspect ratios while fabricating the composite cannot be ruled out. This in turn causes the expected reinforcement strength of the tubes with the matrices to decrease and must be solved.

4.4. *Viscoelastic Behavior*

Viscoelasticity is not specific to elastomers only, but all macromolecules exhibit viscoelasticity above their softening temperatures [156]. Because of the coiled structure, both the movement of chain segments within one coil and the movement of entire coils with respect to each other are possible for macromolecules. Near the softening point, the chain segments become mobile and the material slowly changes its shape under the influence of a deformation force [157]. Further temperature increase removes the segmental contacts within and between the coils more and more, and the segments become more and more mobile. Thus, a considerable deformation, such as stretching of the polymeric material, is possible even with a relatively small deformation force. Because of the presence of both the inter as well as intra molecular links in the polymer chains, even if the elastomer chains undergo deformation at higher temperature, they cannot move apart from each other. So the stretched elastomer returns to its original shape as soon as the deforming force is removed (Fig. 11). As the thermally induced macromolecular motion described above is responsible for viscoelasticity, the viscoelastic properties of elastomers are inherently temperature-dependent [158-159, 70]. Here in this section we are explaining the flow behavior of rubber CNT composites in two ways- depending on the crosslinking chemistry. At first the viscoelasticity of uncured composite is discussed followed by the cure kinetics.

4.4.1. *Rheology and dynamic mechanical properties*

The terms rheology and viscoelasticity are related closely to each other and often explained together. Rheology is the study of the flow behavior of a material under conditions in which they can flow rather than deform [157]. Rheological behavior of elastomer composites is very significant as it is related to the composite processing, its structure and other properties [157]. Rheological response

varies based on the nature, type, aspect ratio, concentration and mode of dispersion of fillers, nature of the elastomers and the matrix-filler interfacial interactions [160-163]. All viscoelastic materials have two components for the modulus, arising from the viscous and the elastic parts. The variations of these two -loss modulus and storage modulus- along with the material's viscosity as a function of various factors such as frequency, strain, temperature etc. are the important rheological observations which can characterize the rheological properties of composites.

Percolation is an important aspect of rheology and behavior of the composites varies above and below the percolation level [164-165]. Similar to the electrical percolation behavior (which will be decribed in the following section), the rheological percolation of composites is characterized by a transition from a rheological state (where the viscosity or elastic modulus changes significantly with increasing filler content) to a solid-like behavior (where the viscosity or elastic modulus doesn't or slightly change with filler content) [157, 161]. The particular concentration at which this transition occurs is known as the rheological percolation threshold. Different from the electrical percolation threshold, this rheological threshold value is highly dependent on temperature. This is due to the fact that rheological response of composites is dominated by the elastomer chain mobility, which always enhance with increase in temperature [162]. Whereas in the case of electrical percolation threshold, since it depends on the CNT network formation through which conduction occurs, the temperature effect is low. The amount of CNTs needed to achieve rheological percolation threshold is much lower than that required for electrical percolation. This is due to the contribution of polymer part towards the former whereas only the filler part is active in the case of the latter. The dispersion of CNTs can lower the rheological threshold further [166-167]. At low concentrations, the non-interacting nanotubes homogeneously dispersed in the polymer matrix take a very long time to re-aggregate, provided the matrix viscosity is high enough to suppress fast Brownian motion. The rheology of such dispersions

remains that of a viscous liquid, with the response as a linear function of tube concentration. At concentrations above the threshold there is a clear emergence of an elastic gel of entangled nanotubes in their homogeneously dispersed state [167]. Composites containing entangled CNTs have distinct rubber modulus at low frequencies and also there is a characteristic superposition between the mixing time and the frequency of rheological testing, similar to the time/temperature superposition in classical glass-forming polymers. Usually uniform dispersion of CNTs provides effective polymer-filler interaction or reinforcement and causes the viscosity of the matrices to increase as a function of filler loading over the entire range of shear rates. A higher viscosity reduces the colloidal movement of the particles especially latex and hence improves colloidal stability [65]. The viscosity of the composites usually decreases with increase in shear rate. This pseudo plastic nature or shear thinning behavior is more predominant in the case of samples with high filler loadings. Shear thinning decrease contributes to better dispersion state of CNTs as well. Shanmugharaj et al. [63] reported that the value of ΔS increases on loading pure as well as silane functionalized CNTs and the composite of pure CNT exhibited higher ΔS value compared to NR vulcanizates, which may be due to the presence of filler aggregation leading to resistance to polymer chain mobility. However, ΔS decreases for the functionalized CNT composites and it may be due to the decrease in the effective volume percentage of loaded CNT by silane functionalization. Kuan et al. [168] showed that CNT can increase the melt viscosity and can reduce the variation of processing viscosity of PU. They prepared CNT/waterborne polyurethane (WPU) composites by using two approaches of covalent bonding (system1) and ionic bonding (system 2) to improve the filler polymer compatibility. This indicates that CNTs can stabilize the viscosity of polymer melting, especially in system 1 (Fig. 12a). After it was molten, a few CNTs aggregate again and the phase separation phenomenon of composite appears in system 2 (Fig. 12b). High processing temperature destroys the ionic bonding, which causes the interface between CNTs

and WPU to diminish. It leads to the phase separation of composite. Xia et al. [169] prepared well-dispersed and long-term stable CNTs/polyol dispersions by a mechanochemical approach with the aid of a dispersing agent followed by preparing CNT/PU composites by polymerization in situ.

The variation of viscosity of CNTs-polyol dispersions with shear rate was determined at different temperatures and the data obtained fitted well with the Herschel–Bulkley model. The viscosities (η) of Herschel–Bulkley suspensions were calculated according to Eq. (7)

$$\eta = \tau_o \gamma + a \gamma^{n-1}$$ -- (7)

Where γ is the shear rate, a and τo are constants and n is the shear thinning exponent. When n> 1, the fluid exhibits a shear-thickening behavior; when n= 1, the fluid exhibits a Bingham plastic behavior; and when n< 1, the fluid exhibits a shear thinning behavior. When τ_o=0, Eq. (7) is equal to a power law model. It is considered that η, k, τ_o values are related to the dispersion state of nanotubes.

For both MWCNTs and SWCNTs, the shear thinning exponent decreases with concentration indicating significant thinning behaviour. Also, with increase in temperature, shear thinning decreases ensuring better CNT dispersion at high temperature. Xia et al. [169] analyzed the variation of viscosity of MWCNT-polyol and SWCNT-polyol dispersions at a particular shear rate and at 60 °C with CNTs concentration and the experimental viscosity values fitted very well with Eq. (8)

$$\eta = \eta_0 \left(1 + 0.67 fC + 1.62 f^2 C^2\right)$$-- (8)

where f is the aspect ratio (ratio of the longest to shortest diameter of particles), η_0 is the viscosity at zero CNT concentration and C is the concentration of CNTs. From TEM analysis, they got higher f values for MWCNTs than SWCNTs. In contrast to SWCNT/PU composite, the more reinforcing effect, i.e., higher modulus obtained for MWCNT/PU composite should relate to their higher viscosity, more shear thinning behaviour of MWCNT-polyol dispersion and higher shape factor of MWCNT in

polyol dispersion. These composites also exhibit the unique ability of solid like behaviour at low shear region.

Bhattacharyya et al. [144] demonstrated variation in storage modulus with temperature and strain amplitude very clearly. Fig. 13a [144] shows the variation of storage modulus (log E) as a function of temperature for the various nanotube compositions. It is observed from the figure that the storage modulus of neat rubber depends on the frequency and temperature, but is independent of the strain amplitude. However in the case of rubber composites it strongly depends on the dynamic deformation especially at higher concentration of fillers (Fig. 13b). In this case, the value of storage modulus decreases with increase in strain amplitude. This non linear behavior of filled rubbers is known as Payne effect and can be explained by the existence of a filler network in the rubber matrix above the percolation threshold [16, 144]. When the shear amplitude is increased, these filler networks break down leading to the lowering of storage modulus. At low temperature the polymer, NR is in the glassy state with a modulus around 0.6 GPa. With increasing temperature the elastic tensile modulus suddenly drops down by 3 orders of magnitude corresponding to the glass-rubber transition. This modulus drop can be ascribed to an energy dissipation phenomenon involving cooperative motions of long chain sequences. Above glass transition temperature (T_g), the composite films exhibit a huge increase in the storage modulus with increase in the filler wt%, for example in case of composite with 8.3 wt% of CNT the relaxed modulus at T_g + 70 K is 75 times higher than that of the pure matrix. Also the initial tensile modulus determined from tensile tests is lower than the storage modulus for CNT/NR composites where as they are equal for pure NR films. This could be related to the observed Payne effect when the dynamic strain amplitude is increased. It is clear from the figure that the initial storage modulus is increasing with the filler content and decreasing with the strain amplitude (Fig. 13b). This strong Payne effect is consistent with the strong Mullins effect observed when the sample underwent

cyclic tensile tests, and the reasons for both effects are explained to be the same. The dynamic mechanical analyses are quite useful in finding out the interactions occurring in the molecular level, for instance, the filler-filler and filler-polymer chains interactions. More detailed explanations of Mullins and Payne effects can be seen from the works of Klueppel, Lang and Soffu et al. [170-172]

Fig. 14 shows the correlation of Eq. (4) with the relative increase in the modulus determined from dynamic mechanical analysis [68]. In fact the storage modulus reflects the elastic modulus of the rubber materials, which measures the recoverable strain energy in a deformed specimen. It has been reported that the Guth model (Eq. (4)) and the Halpin–Tsai (Eq. (9) [10]) model fit very well (both models depends on filler aspect ratios) with the experimental data after considering the aspect ratio of 40-45 for MWCNTs in SBR.

$$E = E_0 \frac{(1 + 2f\phi\sigma)}{(1 - \phi\sigma)} \quad \dots\dots\dots\dots\dots\dots\dots\dots\dots\dots\dots\dots\dots\dots\dots \quad (9)$$

where σ is given by

$$\sigma = \frac{\left[E_f / (E_o - 1) \right]}{\left[E_f / (E_o + 2f) \right]}$$

E_f is the modulus of the filler. In elastomeric composites, $E_f \gg E_0$, so Eq. (9) reduces to Eq. (10).

$$E = E_0 \frac{(1 + 2f\phi)}{(1 - \phi)} \quad \dots\dots\dots\dots\dots\dots\dots\dots\dots\dots\dots\dots\dots\dots \quad (10)$$

In the case of CNT/rubber composites, the high specific surface areas and essential modulus of CNTs enhance the stiffness of rubber which results in an increment in the storage modulus values. In the case of CNT/NR composite, the modulus is increased after the addition of CNTs [68]. With the increase of temperature, the stiffness of NR is also enhanced due to the influence of CNTs. The storage modulus of CNT/NR composites is also high due to the improved dispersion of CNTs in the NR matrix and good interfacial bonding between them. The addition of CNTs reduces the volume percentage of NR in composites, which lowers hysteresis loss of the composites under a dynamic

condition. This can be beneficial for some of the applications of rubber products, such as tyres. The presence of CNTs also affects the cure kinetics of rubber due to the increase in activation energy of NR and thus more energy is needed for the curing of the composites.

4.4.2. Curing behavior of composites

The curing kinetics of rubber materials is one of the key factors in determining their composite properties [173]. Cure chemistry and kinetics of rubber reinforced CNTs especially the effect of modified CNTs on elastomer vulcanization processes are little addressed [174-175]. The chemical nature of the filler significantly affects the crosslinking process of elastomers. Scorch time is a measure of premature vulcanization of rubber which indicates the time during which a rubber compound can be processed at a given temperature before curing begins. Sui et al. [173] observed that the vulcanization time, scorch time and optimum cure time decreased and the maximum torque increased after adding acid treated and ball milled CNTs into NR. In addition, the over-curing reversion of CNT/NR was alleviated. The time for reaching the maximum torque of the composites containing treated CNTs is found to be a little longer than that of neat NR and CB filled NR, which reflects the lower vulcanizing rate of CNT/NR composites. The reason for the highest maximum torque of the CNT/NR composites is that the CNTs with ultra-high modulus effectively restrict the changes in polymer molecular configuration, and thus enhancing the modulus of the rubber composites.

In the vulcanizing curves of neat NR and NR composites (Fig. 15a), the last region of the vulcanization process shows the reduction in the over-curing reversion of NR due to the addition of CNTs, when compared to the neat NR and NR/CB composites [173]. It helps to eliminate the difference in crosslinking degree between the surface and bulk of the thick rubber sample arising from the low thermal conductivity of the rubber materials. It is clear that the presence of CNTs affects the

curing process of NR. The reason for this is the increase in activation energy during curing reaction of

NR with the addition of CNTs so that more energy is needed for the curing of CNT/NR composites.

Though Sui et al. reported decreased curing properties for acid treated CNTs this fact is to be critically

addressed and it must be the part of another review.

The major techniques used to study rubber vulcanization include differential scanning

calorimetry (DSC), oscillating disk rheometry (vulcanizing curve), and chemical extraction. However

the vulcanizing kinetic parameters of rubber materials can be gained conveniently using data in the

vulcanizing curve which reflect the change of curing degree with time at a constant temperature. Yue

et al. [137] used two kinds of vulcanizing agents, dicumyl peroxide (DCP) and 2,5-dimethyl-2,5-

ditbutylperoxy hexane (Varox), for the curing of composites based on HNBR and SR. Fig. 15b shows

that the vulcanization time of the composites filled with Varox, increased with the content of CNTs.

When maximum curing is achieved, the modulus of the composites dramatically decreases with CNTs

(after 15 phr CNTs), which is in contrast to that of the traditional filler composites. The different

curves 1, 2, 3, 4, 5 and 6 in the figure denote the samples containing 0, 2, 10, 15, 30 and 40 % of

CNTs respectively. Combining the results of the two kinds of composites, the effect of CNTs on the

vulcanization of rubber is attributed to the strong absorption effect of CNTs to the liquid vulcanizing

agent, i.e. Varox, which originates from its special hollow structure and extremely high specific area.

At higher than 30 phr, the composites with Varox cannot even be cross-linked and present in viscous

state. Hence they concluded that Varox is not a good vulcanizing agent for composites filled with

CNTs. On the contrary, the cross-linking effect of DCP for rubber is not seriously influenced by the

presence of CNTs probably because of the solid state and chemical structure of DCP. Sui et al. [133]

also studied the vulcanization kinetics indicating the influence of CNTs on the curing process of NR.

This time the activation energy in curing reaction of NR is increased by the addition of CNTs, and

more energy is needed for the curing of CNT/NR composites. The dispersion of CNTs in the matrix and the interfacial bonding were also observed to be improved. Presence of metal oxides also alters rubber curing rate in their CNT composites as widely reported [176-182].

Lu et al. [138] reported on the vulcanization properties of neat SBR and its composites filled with CNTs and CB. There exist three phases along the vulcanization curves of the composites. The first phase is the scorch delay or induction period during which most of the accelerator reactions occur. The second region is the curing reaction period during which the network structure forms. The cure time of the composites filled with CNTs is longer than that filled with CB, that is, CNTs must have decelerated the vulcanization of SBR composites. In the last period, the network matures by overcuring reversion, equilibrium, or additional but slower cross-linking depending on the nature of the composites. Here the rubber composites filled with CNTs are vulcanizing additionally, and those filled with CB and pure SBR are in equilibrium or even in overcuring reversion, which is harmful (loss or gain of mechanical properties) to the vulcanization of rubber. Wang et al. [120] observed that acid treated CNT/NR latex composites prepared by the spray drying process require more vulcanization than pristine CNT/NR compounds. Moreover, they reported that vulcanizing reversions did not occur in the filled samples. Similar effects were observed by Zhou et al. [78] while analyzing acid treated CNT/SBR composites. However they didn't mention about the effect of functionalization on vulcanization process. This is addressed by Shanmugharaj et al. [63], who found that 3-aminopropyltriethoxysilane functionalized CNTs increased the scorch time and optimum cure time in the sulfur vulcanization of NR.

In an intensive survey, Bujans et al. [183] showed the influence of pristine and functionalized CNTs on ethylene propylene diene terpolymer (EPDM) composites by analyzing the vulcanization time, scorch and optimum cure time. It is found that functionalized CNTs noticeably affected the

curing process, reducing the vulcanization time and delta torque, due to the presence of acid sites on the CNTs surface which reduced the peroxide efficiency. For this reason, triallyl cyanurate (TAC), highly reactive towards free radicals, was used as coagent to increase the crosslinking efficiency without affecting the cure rate or scorch. The activation energy in curing reaction of EPDM was decreased by CNT addition and in particular with functionalized CNTs, and hence, a lower energy is needed to cure the EPDM composites. The involvement of sulfonic acid groups in the peroxide vulcanization process affected notably the crosslink density of the polymer. The vulcanization curve (Fig. 16) showed a reduction of maximum torque, which confirms the involvement of benzenesulfonic groups in the mechanism of peroxide vulcanization. However, CNTs accompanied by ionic liquid can speed up, the curing reaction again [70]. Generally, the reinforcing CB shows acceleration activity with lowering the cure time as compared with the corresponding gum compounds [184], but here, the inert graphite-like surface of CNTs is not able to promote the sulfur curing activity like CB. Similar effects and an increase in the activation energy for the curing reaction of NR have been found in MWCNT/NR [133] composites also. Both pure and functionalized CNT in NR vulcanizates increase the scorch time and optimum cure time significantly due to absorption of basic accelerator by the particular functional groups [63].

4.5. *Thermal properties*

Thermal conductivity of polymer composites depends on the filler aspect ratio, conductivity and interfacial thermal resistance between the filler and polymer matrix [88,185-189]. Dispersion and orientation states of CNTs leading to the formation of networks also enhance the thermal conductivity [188]. Typically, thermal conductivity of composites increases with increase in filler loading and do not exhibit a percolation threshold behavior as a function of loading. The incorporation of

nanoparticles especially the highly electron dense nanotubes affect the thermal stabilities of

elastomers. The DSC technique based on the assumption that the heat of reaction is only due to the

cross linking reaction and is proportional to the extent of the reaction is a typical method to analyze

the thermal properties of the composites. Hydrogen bond action and physical adsorption between

functional groups of CNTs and the polymer molecules affect the thermal transition of polymer

molecules and its other thermal behavior. Adedigba et al. [141] noted an increase in T_g for NR

composites and found that this is due to the restriction of the macromolecular chain of the rubber by

the filler CNT. Since CNTs can uniformly distribute the heat, melting temperature is also found to

increase. However the improvement in thermal stability obtained for them was not very high.

The thermal conductivity of polymers is determined theoretically by following Debye

equation (Eq. (11)).

$$\lambda = \frac{C_p vl}{3} \dots\dots\dots\dots\dots\dots\dots (11)$$

where C_p is the specific heat capacity per unit volume; v is the average phonon velocity; and l is the

phonon mean freepath. The specific heat capacity is related to the thermal conductivity, λ by Eq. (12)

provided the non-steady state methods like hot wire and hot plate method, temperature wave method

and laser flash technique [190-191] are employed for measurement.

$$\lambda = \alpha C_p \rho \dots\dots\dots\dots\dots\dots\dots (12)$$

where α, C_p and ρ are the thermal diffusivity, heat capacity and density, respectively.

Two models are used to find out the thermal conductivity of the composites, which are the

parallel model and series model. In the parallel or rule of mixture model, it is assumed that each phase

contributes independently to the overall conductivity, proportional to its volume fraction (Eq. (13)).

This model assumes the presence of a conducting filler network within the composite and is more applicable in the case of long and continuous fiber composites.

$$k_c = k_p \phi_p + k_m \phi_m \quad \text{.........................} (13)$$

where k_c, k_p and k_m are the thermal conductivities of the composite, particle and matrix respectively, and Φ_p and Φ_m volume fractions of particles and matrix.

Series model assumes no contact between the particles and thus the particle contribution is confined to the region of matrix-chains alone [171]. The conductivity of composites according to the series model is predicted by Eq. (14).

$$k_c = \frac{1}{\left(\dfrac{\phi_m}{k_m}\right) + \left(\dfrac{\phi_p}{k_p}\right)} \quad \text{..} (14)$$

The electrically conducting mechanism of polymer composites is associated with the formation of certain filler conducting paths [172]. If the fillers are conductive they can form conductive percolating network even at very low concentration. In the case of thermal conductivity the formation of thermal conductive paths has great importance. Even though no rapid increase was observed in the thermal conductivity at the percolation threshold (different from the electrical conductivity mechanism), the percolation model was applied to thermal conductivity of composites and suspensions. In order to estimate the thermal conductivity percolation Foygel et al. [187] applied Monte Carlo simulations to classical percolation based on Eq. (15)

$$k(\phi; f) = k_o [\phi - \phi_c f]^{tf} \quad \text{...............................} (15)$$

where k is the thermal conductivity, k_0 is a pre-exponential factor related to the conductivity of fillers and their contacts, ϕ_c is the critical volume fraction for percolation and t is the critical exponent showing the percolating network characteristics [171].

CNTs with functional groups on their surfaces could have greatly enhanced affinity towards polymers. The T_g of the composites of such modified CNTs are found to be high. The T_g value increases with CNT addition as well. Also, the CNTs can absorb some vulcanizing reagents in the case of rubber composites and decelerate the vulcanization of the composites and can reduce the heat release area in the storage modulus versus temperature curve [188-189]. With increasing CNT addition, the vulcanization duration and maximum torsion of the composites increase gradually at the same time due to the same fact. This can also be influenced by the presence of functional groups on the tubes especially acidic groups, which can prevent the formation of vulcanization initiating groups [190]. The increment of maximum torsion might be due to high Young's modulus of the added CNTs. It is well known that the hydrodynamic reinforcement occurs in the conventional fillers giving rise to an increase in the modulus in polymer matrix or an increase in the viscosity of liquids. Compared with conventional fillers such as CB, carbon fiber etc., the high aspect ratio, smaller particle size, larger interfacial area and stronger polymer- filler interaction of CNTs create thick shells of CNTs with elastomers. It is found that in the CNT/SBR composites, CNTs resulted in more immobilized rubber shells which might exhibit higher storage modulus for the rubber composites [16, 127].

Even though metals exhibit similar kind of mechanisms for thermal and electrical conduction, both of these differ as heat conduction is not only due to valence electrons but also due to phonons. Since CNTs have many times thermal conductivity compared to commonly used metals, their incorporation to elastomers can contribute much towards the composite thermal conductivity. Whereas the electrical conductivity depends on the formation of conductive filler networks, the thermal conductivity based on phonon transport depends on several pathways different from CNTs to CNTs [16]. Ma et al. [157] compared the thermal conductivities of composites containing modified and unmodified CNTs (Fig. 17), and found higher conductivity for the pristine CNT composite than those

containing amino-functionalized CNTs. They succeeded in enhancing the conductivity by incorporating silver nanoparticles onto the CNT surface (Fig. 17). Because of the superior thermal conductivity of silver (429 W/(m K)) and the reduced Ag-CNT interfacial resistance and enhanced phonon conduction, heat flows through the composite sample.

Huang et al. [191] obtained high thermally conductive silicone CNT/elastomer composites by using in situ addition of polymers into CNT arrays and established the effect of composite alignment. As shown in Fig. 18, the thermal conductivity of the aligned composites with only 0.4 vol % filler loading is respectively 116% and 105% higher than that of pure elastomer and dispersed composites. Kim et al. [104] also proved the influence of alignment of CNTs on thermal conductivity of composites. They got substantial improvement in thermal conductivity (0.70 W/mK) by aligning 5 wt% CNTs in EPDM (0.28 W/mK). The comparison of thermal stability behaviour of CNTs, clay and liquid crystalline polymer on the styrene-(ethylene butylene)-styrene-based elastomer by Saengsuwan et al. revealed interesting facts [192]. An enhancement in thermal stability is observed for CNTs and clay filled systems. The reason for this improvement can be attributed to the decrease in polymer degradation rate since the network layer structure acts as a shield and re-emits the incident radiation back into the gas phase. The presence of CNT also increases the thermal conductivity of the polymer and thus increasing the time taken to protect the heat of the polymer. The enthalpy of the composite system was lower than the neat and found decreasing with increase in filler content. They also studied the kinetic information on thermal degradation using Flynn-Wall-Ozawa (F-W-O) method. This is a simple method for determining the activation energy from the mass loss and temperature data, obtained at several heating rates. The equation for this model is represented by Eq. (16).

$$\ln \beta = \left[\frac{AE_a}{Rg(\alpha)} \right] - 5.3305 - 1.0516 \frac{E_a}{RT} \quad \text{------------------------------} \quad (16)$$

where β is the heating rate in °C min^{-1}, E_a is the activation energy (KJ mol^{-1}), A is a pre-exponential factor, R is the universal gas constant (J K^{-1}mol^{-1}), T is absolute temperature (K), and $g(\alpha)$ is an integral reaction type of kinetic function. From the analysis, it is found that the activation energy of CNTs is very high which is evidenced by the enhanced thermal stability of CNT incorporated samples in air. The kinetic parameters are also calculated by Kissinger model (Eq. (17)).

$$\ln\left(\frac{\beta}{T_{max}^2}\right) = \ln\left[n\left(1-\alpha_{max}\right)^{n-1}\left(\frac{AR}{E_a}\right)\right] - \frac{E_a}{RT_{max}} \quad\text{-----------------}\ (17)$$

This model is related to the temperature (T_{max}) at the maximum mass-loss rate $(d\alpha/dt)_{max}$ and the activation energy determined from this method is apparent and independent of the reaction mechanism. The kinetic parameters calculated for all samples were observed to be different, but the results for activation energy calculated using Kissinger method followed the same trend as that of F-W-O method. The decomposition order (n) for CNT system showed the highest value, indicating the complex nature of the composite, whereas the value of n for the other two systems were found to be lower than the neat elastomer even if the systems were complex [192].

4.6. *Electrical properties*

CNTs have clearly demonstrated their capability as fillers to make insulating polymers conductive. To transfer the composite from the insulating state into the conductive state, a critical filler loading must be required [193]. This critical concentration, known as the percolation threshold is marked by a sudden increase in composite electrical conductivity by several orders of magnitude. This observation of an enhancement in electrical conductivity by several orders of magnitude at very low percolation thresholds (<0.1 wt%) of CNTs in polymer matrices without compromising other

performance aspects of the polymers such as their low weight, optical clarity, low melt viscosities etc., has triggered an enormous interest in this specific area. Among various composites, nanotube-filled polymers could be used potentially for transparent conductive coatings, electrostatic dissipation, electrostatic painting and EMI shielding applications [193-194]. Often, at the percolation threshold, the filler forms a continuous network inside the polymer matrix, and increase in the filler loading further usually has little effect on the composite electrical resistivity i.e. this interconnecting filler network formed results in a sharp drop of the electrical resistance of the composites. When the concentration of these particles increases above percolation threshold, the formed network like structure will be responsible for the conduction [75].

Anand et al. [65] found very good improvement in the conductivity values of NR even at small loadings of SWCNTs. When CNTs are added to an elastomer, it will be dispersed in the elastomer and this will increase the electrical conductivity due to the presence of free electrons. CNTs show very good enhancement in the conductivity value at smaller filler loading also [116]. The very high aspect ratio of the nanotubes is mainly responsible for this percolation behavior at very low concentrations. Above the percolation threshold, the material behaves as an ohmic conductor with conductivity almost independent of frequency. Even if they succeeded in describing the phenomenon, they didn't get a much higher improvement in the conductivity value [65]. Verge et al. [128] produced vulcanized CNT/NBR composites by melt blending in the Brabender internal mixer. It was shown that during the blending process, the polymer chains are grafted onto the CNT surface via a free-radical mechanism. Indeed, NBR generates free-radicals from its ACN units upon heating and/or shearing. As a result of the high inherent affinity between the CNTs and ACN units, and due to the formation of ACN-based free-radicals leading to NBR-grafting on CNTs, increasing the ACN relative content along NBR chains triggers higher polymer-grafting on the nanotube surface. The higher rate of

disentanglement of CNT bundles and their dispersion in NBR matrices with higher ACN relative content should favor the formation of a percolation network and likely reduce the electrical percolation threshold. They noticed an increase in the percolation threshold even with lower acrylonitrile NBR. Das et al. [70] illustrated the variation in electrical conductivity of SBR and BR blends by preparing the composites from two methods-wet chemical method and dry mix method. The CNTs formed very good network even at very small concentrations when they were dispersed by wet chemical method. This is clearly indicated in Fig. 19a and 19b. The authors could explain well the conduction mechanism occurring in CNTs along with the morphology of the CNT network.

Bokobza et al. [10] studied the effect of filler loading on the volume resistivity of CB and MWCNT filled composites based on insulating SBR. A continuous network is formed at lower filler loading with MWCNT bundles compared with CB. The higher aspect ratio of the nanotube bundles which increases the probability of particle-particle contacts explains this low percolation threshold. Their results are in agreement with those of Flandin et al. [195] and of Thongruang et al. [196] who showed that the percolation threshold concentration in composites is around 10-15 wt% for carbon fiber and high structure CB and around 40-50 wt% for graphite and low structure CB. Since the resistivity of the unfilled elastomer is several orders of magnitude larger than that of the filled vulcanizate, any rearrangement of the filler particle distribution induced, for example a deformation, leads to a change in the vulcanizate conductivity. Significant changes in electrical resistivity against deformation in CB filled composites have already been reported in the literature [10,197-201].

The important uses of electrically conducting composites (volume conductivity$>10^{-10}$ S/cm) are shown in Fig. 20a. As already discussed the electrical conduction mechanism depends on percolation theory which explains an insulator-to-conductor transition, on increasing the conducting filler concentration. Below the percolation region, conductive network does not exist and the electrical

properties are only contributed by the polymer matrix. In contrast, above the percolation range, conductive filler networks and multiple electron paths exist and so the electrical conductivity of the composite shows a saturation plateau, as shown in Fig. 20b [157]. The electrical percolation threshold is found to decrease by using ethanol as dispersion agent, compared to dry mixing, correlating with improved optical dispersion. However, different studies of CNT-filled elastomers have shown that this is not the case always. In previous investigations, the reason for the missing direct correlation between thermal and electrical conductivity has been related to the contact resistance between adjacent CNTs in the composite [16]. The mechanism of charge carrier transport in composites with conductive carbon particles has been analyzed extensively by Sheng et al., showing the conductivity is limited by the tunneling of charge carriers over nanoscopic gaps between neighboring particles with potential-barrier modulation by thermal fluctuations [202]. The morphological properties of these gaps can be characterized by dielectric spectroscopy, where typical gap distances between 3 and 8 nm have been found for CB-filled elastomers. The dielectric data show that similar gaps are also present in CNT-elastomer composites [16]. The impact of the gaps on the thermal conductivity is even more pronounced because the thermal transport through the CNT is dominated by phonons [203], which cannot tunnel but instead are scattered and reflected at the boundaries, i.e. at the gaps. This reduces the thermal conductivity of the CNT network drastically, implying that the thermal transport of the composite is governed by the elastomer. On the other hand, the electronic contribution is about 15 times higher than the thermal conductivity of rubber. But, this is too small, in comparison with many magnitudes of order between the electrical conductivities of CNT and rubber, to allow for a percolation behavior of the electron thermal conductivity. The electrical conductivity values for various nanotube elastomer composites are given in Table 5.

Dependence of conductivity of the MWCNTs/rubber composites on the surfactants, CTAB and KH550 is demonstrated by Jiang et al. [66] as in Fig. 21c. They proposed two main factors that can affect the conductivity of the composites with different modifiers- good dispersion, which is helpful to improve the conduction due to the formation of conductive network and the interfacial interaction that produces energy barrier and blocks the transport of electrons. In the case of KH550, most of the MWCNTs are tightly combined with the rubber and relatively thick rubber layers exist among the CNTs, which cause a high transport barrier of electrons by tunneling mechanism. This factor results in a low conductivity of the MWCNTs/rubber composites. The composites with MWCNTs modified with CTAB display a relatively high conductivity because of physical interfacial action. In this case, it produces a considerable lower transport barrier for electron among the CNTs. In addition, the NH_3^+ in CTAB is also helpful to the transport of electrons because the amine salt can decrease the energy barrier for the charge transport. In case of the combination of both surfactants, KH550 and CTAB, the composites not only exhibited stronger interfacial interaction but also offered better dispersion. It is reasonable that the conductivity of this kind of composites is intermediate.

A series of polymer-based composites with various modified CNT (m-MWCNT) volume fractions were prepared in order to address the percolation threshold as closely as possible. Fig. 21a clearly shows a metal-insulator transition at the volume fraction, $\Phi_{m\text{-}MWCNT} \approx 0.01$. Percolation theory helps to describe the conductivity of the composite near the metal-insulator transition with power laws as indicated in Eq. (18) [203, 205].

$$\sigma\left(\phi_{m-MWCNT}\right) \propto \sigma\left(\phi_{m-MWCNT} - \phi_c\right)^t, \text{ for } \Phi_{m\text{-}MWCNT} > \Phi c \ \dots\dots\dots\dots\dots\dots\dots\dots\dots\dots \text{ (18)}$$

where Φ_c is the percolation threshold and t is the critical exponent in the conducting region. The best fits of the conductivity data to the log-log plots of the power laws give $\Phi_c = 0.01$ and t = 3.45 (inset in

Fig. 21a). This small Φ_c indicates the good dispersion of m-MWCNT in the rubber host, its high aspect ratio (about 100) and the unique physical properties, so that little content of m-MWCNT in the composites could form a percolation cluster. A plot of the AC conductivity as a function of the frequency in Fig. 21b tells about the conductivity dependence on frequency. Chemically modified nanotube, m-MWCNT/methyl vinyl silicone rubber (VMQ) composites were prepared [206] by treating the surface of MWCNT using c-aminopropyl triethoxy silane. Based on the percolation threshold, two kinds of electrical behavior are possible, namely the insulators with conductivity dependent on the frequency (for composites at $\Phi_{m\text{-}MWCNT} < 0.01$) and the conductors with conductivity independent of frequency (for composites at $\Phi_{m\text{-}MWCNT} > 0.01$). Compared to the MWCNT/VMQ composite, m-MWCNT/VMQ composite has better interface compatibility due to a strong interaction between m-MWCNT and VMQ. The conductivity is as high as 10^{-2} (S m^{-1}) in the m-MWCNT/VMQ composite at 0.03 $\Phi_{m\text{-}MWCNT}$ value, which is a 7-order of magnitude larger than that of rubber matrix. However, Skakalova and coworkers [207] have obtained a better improvement in electrical conductivity (14-order of magnitude) for the modified nanotubes/polymer composites. The effect of CNTs on the stability of the mechanical and electrical properties of recycled waste rubber was better investigated by Mahmoud et al. [208]. Their results indicate that the addition of CNTs to the recycled rubber improves its electrical conductivity by more than two orders of magnitude. The stiffness of the recycled rubber also increased by 6, 15, and 28 times as a result of the addition of different concentrations of the CNTs to it. This piece of work is found to be useful as it involves recycling mechanism of polymer too. The recent work on CNT/rubber by Bokobza et al. also showed a correlation between the mechanical and electrical behaviour of the composite [116]. The electrical conductivity is reported to be depending on the processing condition and is found to be very sensitive. They obtained the percolation at very lower content of CNTs, 0.5 phr for all the three composite

systems studied NR, SBR and EPDM. Raman spectroscopy revealed the penetration of elastomer chains in to the filler agglomerates and the decreased filler-filler interactions. The CNT orientation influences the electrical conductivity even above the percolation threshold. When the filled composite is stretched uniaxially, both polymeric chains and anisotropic filler particles align and this is evidenced from the increased electrical resistivity of the composites with strain. This also points towards the decrease in the number of nanotube contacts and thus better dispersion. An interesting property of drastic increase in electric resistance of MWCN/PU conducting composite was observed by Shang et al., in the presence of organic vapors. They explained the reason as the matrix swelling induced by the solvent absorption that expands the gap between the fillers and found that the electrical response behavior of the composite depends on solvent-polymer interaction, temperature and vapor pressure [209].

The ionic liquid assisted better dispersion of CNTs is combined with the electrical conductivity requirement by Kim et al. and prepared SWCNT/SR composite as a useful material to electrodes [210]. The sheet resistance of the obtained stretchable composite is significantly decreased by the imidazolium-based ionic liquid assisted dispersion. The obtained material is useful as stretchable conductor that requires a constant conductivity when a high tensile strain up to 200% is applied. Thus the dispersion of nanotubes in the matrix has a key role in enhancing the elastomer conductivities.

4.7. Dielectric properties

CNT composites with high dielectric constant are increasing attention in many technological fields. But, though there is an increase in dielectric constant, these composites show an increase in dielectric loss and a significant decrease in dielectric strength, which are undesirable for many practical applications. To increase the dielectric constant by minimizing the increase in dielectric loss

in CNT-polymer composites is a matter of great importance. It should also be noted that covalent functionalization on CNT surface can damage their intrinsic properties like electrical conductivity [211]. The study of dielectric constant becomes important in this context. Ryan et al. [212] compared the electric and dielectric properties of MWCNT/PDMS composites based on pristine and functionalised nanotubes (MWCNTs-OH). They succeeded in demonstrating the feasibility of using core-shell MWCNTs to increase the dielectric constant by reducing the dielectric loss of the composites for the first time. Hydroxylated MWCNTs (MWCNTs-OH) represent one of the simplest types of core-shell MWCNTs. In core-shell MWCNTs, the outer graphene layer is covalently functionalized to become non-conducting, whereas the unmodified inner layers remain conducting. This leads to increase the dielectric constant while lessening the increase in electrical conductivity and dielectric loss of the CNT-polymer composites. The room temperature dielectric loss of composites as a function of MWCNT mass fraction (wt %) at 10 kHz is shown in Fig. 22a. It is clear that the dielectric loss (~0.63) of the 9 wt % MWCNT-OH/PDMS composite is much lower than that (~1.25) of the 6 wt % pristine MWCNT/PDMS composite. It is also found that the dielectric constant and dielectric loss of the 9 wt % MWCNT pristine-PDMS composite are ~1631 and 10 (obtained from Fig. 22a which indicates that the dielectric loss either reaches or exceeds the instrument's maximum measurement limit, that is 10) respectively. Whereas the dielectric constant of the 9 wt% MWCNT-OH/PDMS composite (~1249) is close to that of the 9 wt % MWCNT pristine-PDMS composite (~1382), but its dielectric loss (~0.80) is much lower than that (~2.31) of the same pristine CNT composite. Yet the impact of covalent functionalization of CNT surfaces on the values of dielectric constant and the dielectric loss of the composites compared with pristine CNTs remains essentially unclear. Seok et al. [213] determined the dielectric constant of the MWCNT/silicone elastomer composite within room temperature to 180°C range at 50 Hz and 100 kHz of frequency. They

observed a similar range in permittivity (ε') values (3-5), in both frequencies, and it is found to be

increasing with increase in the CNT content. Fritzsche et al. [214] synthesised CNT/NR hybrid

composites and noticed a significant increase in dielectric properties up to ε'=103 with increase in

CNT. They interpreted this large permittivity value as a combined effect of nanoscopic gaps between

adjacent nanotubes and a percolation network with bottle-necks and dead ends of the CNTs on various

length-scales. Since the permittivity is a measure of the polarization in the sample, the amount of

interfaces between CNTs and polymer is more pronounced. They observed a relaxation process at low

frequencies for the sample containing less amount of CNT (about 3 phr). Also this relaxation process

is increasing in strength and is more shifted to higher frequencies with increase in CNT. This behavior

is similar to CB filled composites [215-216]. In such cases the bound rubber between CB particles,

obstructs the electrical contact between them. When the gaps between the filler particles are of

nanometer size, free electrons tunnel between the particles. This movement of electrons by tunnelling

over the gaps is referred as the relaxation process. The characteristic frequency of the relaxation

transition observed at high frequencies can be related to the distance between adjacent filler particles

[217-218]. The dependence of frequency on dielectric properties of the CNT/ blend composites in the

presence of different ionic liquids has been explored by Das and co workers (Fig. 22b). For the

CNT/(S-SBR/BR) composite, the permittivity value is a constant throughout the frequency range

whereas for the compounds containing ionic liquids a different behavior is observed [70]. The

composite comprised with AMIC ionic liquid shows the highest ε' value ($\sim 2\times 10^4$) compared to the

other composites. For the samples containing other ionic liquids the relaxation process is seen at low

frequencies indicating a large gap between the nanotubes whereas for AMIC containing sample, the

relaxation process is shifted to very high frequencies (1–10 MHz). So the smallest gap size is achieved

with AMIC resulting in the best contact between the tubes and therefore in a high conductivity. All

these factors point out to the formation of an effective percolation network in the presence of the reactive ionic liquid AMIC.

The frequency independence on the dielectric permittivity of CNT/PU composites was explained by Barick et al. [219]. The magnitude of ε_r does not vary significantly with the concentration of MWCNT as well. This is because the relaxation time for realignment of interfacial dipoles along the direction of external electric field is reduced with increase in frequency. It is also observed that the loss tangent values of both neat TPU and its composites exponentially decay with increase in frequency at lower region (up to 10^5Hz), and it rapidly increases thereafter. With increase in CNT loading the tan δ of the composites enhances up to 10^5 Hz but above which it reduces than that of the neat TPU. The significant increment of loss tangent with MWCNT concentration is due to the high electrical conductivity of CNTs. The authors pointed out that the composite system is suitable for developing capacitors [219]. In short, the low dielectric loss and high permittivity which are often necessary for making good dielectric materials for capacitors are satisfied with CNT based systems provided a good dispersion is achieved.

5. Carbon nanotube hybrid composites

The generally accepted definition of hybrid composites is that it is a material created by dispersing two or more inorganic nanoparticulates in to a macroscopic organic matrix. Because of the extra ordinarily large interfacial third phase, hybrid composites constitute fast growing area of the field of nanotechnology. They should be considered as an attractive, versatile, technological platform for future electronic, optical, magnetic, and biomedical applications. Multi nano component materials are attaining wider attention as they can provide combined properties such as electro-opto-mechanical, chemo-electro-mechanical, thermoelectrical etc. The synergistic effect of various nanoparticles causes in the improvement of properties of the composites. Famá et al. [220] illustrated the influence of multi

components in determining the properties of the composites by wrapping MWCNTs with an aqueous

solution ofstarch-iodine complex. Even though starch packaging are used in cushions and protections

against shock and vibration during transportation [221], the use of starch based materials has been

strongly limited because of their poor mechanical properties and high permeation compared to other

non-natural polymers [222]. By successfully incorporating CNTs all these limitations are negotiated.

Litina et al. [223] used the modified clay and CNT in the polystyrene polyisoprene block co polymer

by solution intercalation and found that the composite prepared from the ester modified CNT/clay

system is exfoliated and the composite formed by incorporating clay/unmodified CNT is intercalated.

Here they used CNTs, developed on clay-supported nickel nanoparticles following the CVD. The tube

surfaces are modified by ester groups in subsequent step. The hybrid composite is identified as the last

one in the general schematic representations for the formation of CNT composites (CNT with

spherical fillers in Fig. 23).

Fritzsche et al. [89] demonstrated that the incorporation of CNT in silica filled NR resulted in

good dispersion of CNTs. The composite showed enhanced mechanical stiffness, tensile strength,

modulus, and electrical conductivity with quite low amounts of CNT, though the tear resistance under

dynamical loading is slightly reduced. The technique used here was dry mixing. The tensile strength

increased from 14 to 17 MPa when part of the silica was exchanged by 10 phr CNT and the elongation

at break was successively reduced. Nevertheless the energy at break increases by about 30% if 6 phr

silica is exchanged by 6 phr CNT, which appears to be an optimum CNT concentration corresponding

to a volume fraction of 1.5%. The modulus at 100%, representing a measure for the reinforcement at

low strains, also increased from 2 to 8 MPa. They also prepared CNT-based filler hybrid systems

involving various rubbers like SBR, BR, EPDM and NR using wet mixing method (ethanol and other

solvents as dispersing agents). Lorenz et al. [134] used different techniques to disperse MWCNT in

various elastomers using an internal mixer. Two classical reinforcing fillers, silica together with the bi-functional organo-silane were used for the hybrid systems. Both solvent assisted and dry mixing techniques were employed. It is found that on the addition of CNTs to NR-silica composites, the fatigue crack propagation rate could slightly be reduced at moderate levels.

The electrical conductivity of the hybrid filler systems is also found to be generally larger as compared to the pure CNT or CB composites due to higher shear forces in the hybrid systems. The reinforcement of SBR with CB and MWCNTs is investigated by Bokobza et al. [148] and the obtained composites showed good improvement in mechanical and electrical conductivity with a lower percolation threshold than those samples containing only CNTs. Synergistic effect of CB in presence of nanofillers (nanoclay and nano fiber) on mechanical and dynamic mechanical properties of NR matrix is discussed by Bhattacharya et al. In the presence of regular loadings of CB, both nanofillers lowered the wear characteristics of NR composites by virtue of black-nanofiller synergy [224]. Improved abrasion resistance was observed not only at low experimental conditions, but at high levels also. Due to the enhanced efficiency of the heat dissipation path way through the networks of ''nanoblocks'' and ''nanochannels'' the hybrid composite is expected to have better conductivities. Abrasion followed stick-slip process and bimodal distribution of wear was observed, resulting in the formation of intrinsic and aggregated particles. While the intrinsic particles remain almost invariant, the aggregated particle size decreased significantly with CB loading in the composites resulting in the reduced material dissociation. The designed compounds lied within the high performance window of strong wet grip and low rolling resistance, while abrasion resistance improved amazingly. In a recent work by our group good solvent sensors were fabricated by making use of the synergy between MWCNTs and reduced graphene oxides in NR matrix [225].

In the case of MWCNT/EPDM composites, the CNTs were dispersed fairly well in the polymer matrix at lower concentration, but they were aggregated at higher concentrations [135]. With increasing the proportion of CNTs, the mechanical properties such as tensile strength and elastic moduli were improved, whereas the elongation at break was decreased (Fig. 24a). On the other hand, in the case of MWCNT/organo clay/EPDM composites, the clay platelets used along with MWCNTs, improve the dispersion of CNTs in the polymer matrix irrespective of the filler content, which is observed clearly from the TEM images (Fig. 24b). The better dispersion of the filler and co-filler led to further improved mechanical and electrical properties of the composites [226-227]. The strain response of the MWCNT/EPDM composites showed characteristic piezoresistivity under deformation, which proves the potential of the composites for being suitable as sensor materials [135]. All these observations lead to the growing importance of hybrid composites.

6. Applications of elastomer carbon nanotube composites

6.1. Overview

Elastomer composites containing conducting fillers such as CB, carbon fiber, and metal fiber have been extensively investigated for multi-functional applications such as structural reinforcement [228], EMI shielding, electronic packaging, radar absorbing materials and high charge storage capacitors. Addition of CNTs is promising in improving the flame retardancy of elastomers as well [54, 229]. These nanofillers have the unique ability to delay ignition, reduce smoke emissions and eliminate slumping and dripping of the molten polymer by formation of a strong, stable char. Some applications such as flame retardant material include wire and cable covers, battery jars and electrical enclosures, small appliances and home interior decoration materials. The CNT composites have potential applications in automotive industry that could lead to better quality, lower cost, less fuel consumption and lower environmental emissions. Those applications include electrostatic painting of

exterior panels, shielding of automotive electronics and addition of nanofibers to tyres to improve stiffness. Recent researches developed a high performance rubber sealing material resisting 260°C / 240 MPa using a special composite of surface controlled MWCNT, which can act as a sealing material. This composite material can be used at low temperatures in a real oil field, which can avoid the energy crisis [135]. High performance CNT composites out of NR and aligned MWCNTs with large elastic modulus and thermal and electrical conductivities were reported by Sui et al. [228] and Kim et al. [104].

Recently, Hata and co-workers [231] developed a new viscoelastic material from CNTs that is similar to SR, but maintains temperature independent viscoelasticity at a range of temperatures from -196 to 1000°C in an oxygen-free environment, unlike the traditional composites. Among many other applications, temperature-invariant rubbery material made from CNTs could be used as dampeners (antivibration mounts) for high-vacuum furnaces and even aerospace vehicles that travel to the cold interstellar space. These composites remain flexible over the entire temperature range. This CNT rubber can be stretched in the direction of applied stress up to 5% strain and the porous network structure, coupled with excellent thermal transport properties intrinsically associated with CNTs, allows the CNT rubber for rapid and efficient heat dissipation to prevent significant heat accumulation. CNT rubber composite materials with exotic viscoelastic properties can outperform the existing elastomers. Even though it is difficult to picturise all the applications of elastomer composites, a few of them are illustrated in Fig. 25.

In addition, conducting rubber composite out of EPDM, MWCNT and clay is used as strain sensors [141]. In the same way, MWCNT/SR composite gives a positive piezoresistance both parallel and perpendicular to the direction of applied pressure [170]. Conductive thermoplastic elastomer composites of PP/EPDM with three kinds of carbon fillers including CB, MWCNT and hybrid CNT-

CB show piezoresistive properties depending on the nature of filler, concentration and percolation threshold [232]. At low filler concentration high pressure-resistance sensitivity and at high concentration low pressure-resistance sensitivity is observed. These composites are well suited for fabricating pressure sensors, the detailed study of which is given in the next section. There are certain other kinds of sensors useful for health monitoring [233] and for detecting dangerous deformations and vibrations of vehicle parts as well.

CNTs having high dielectric constant are very effective for synthesising composite dielectrics. Such composites are very beneficial as actuators for artificial muscles, capacitors for energy storage, sensors for mechanical strain, humidity, and gases and in flexible electronics [234-239]. CNTs can act as the electric or light induced heating sources for liquid crystalline elastomers. They are efficient heat absorbers and can convert heat energy to light energy [240]. This is really important in the field of electronics specifically in solar cells or light emitting diodes. The three dimensional network structure formed by boron doping of CNTs by CVD behaves like elastomer solids and these materials have unique properties. These oil absorbing sponge-like solids possess multi functionalities such as ultra-light weight, super-hydrophobicity, high porosity, thermal stability and mechanical flexibility [241]. Moreover photo-actuating materials based on the commercial elastomer EVA filled with well-dispersed MWCNTs were also developed as potential materials for the fabrication of smart actuators [242].

6.2. Sensing

Recently electrically conducting flexible rubber composites (CRC) containing CNTs have received much attention as potential materials for vapour, strain and pressure sensors [185-186, 228, 243-246]. Upon external forces, CRC deformation takes place with the micro scale change of inter-electrical conduction in rubber matrices due to the change of contact resistance, and CRC exhibits

macro scale piezoresistivity. This effect can be more explained as follows. The electrical conductivity of CNT composites depends on the resistance of CNTs and contacts between them at junction points based on the stress applied to the material. The stress is transferred to the junction points via the stiff nanotubes causing the resistance change sensitive to small material deformations [247]. Extensive studies on this resistance-strain sensitivity reveal interesting results and corresponding models were reported [248]. The effect of strain on the electrical resistance of CNT/SR composites by in situ polymerization [249] has been reported by Zeng et al. Knite et al. also described simultaneously existing giant effects -strain sensing and gas sensing- based on CNT/polyisoprene composites [250]. Conducting EPDM/MWCNTs/organo-clay rubber composite was reported as flexible strain sensors [135]. Here the organo-clay exfoliates the MWCNT bundles inside the rubber matrix and this led towards sensing. Fig. 26 describes the strain sensing properties of MWCNT/EPDM composite at 20 wt% of MWCNTs during extension and compression. When the MWCNT/EPDM composite sheet was extended upon micro strain, the resistance increased significantly (Fig. 26a). However, there are still some problems that must be resolved to get composites exhibiting significantly improved properties like mechanical strength and conductivity.

For predicting the piezoresistance of the MWCNT/polymer composite films Park et al. [247] proposed the Eq. (19).

$$\frac{\Delta R}{R_0} \approx \begin{cases} k\varepsilon \rightarrow (0 \le \varepsilon \le \varepsilon^c) \\ k\varepsilon + u(\varepsilon - \varepsilon^c)N \rightarrow (\varepsilon > \varepsilon^c) \end{cases} \quad \ldots\ldots\ldots\ldots\ldots (19)$$

where ΔR is the change in resistance, R_0 is the initial resistance, k is the slope of the linear region, e is the strain of film, ε^c is the critical strain at which the number of contacting MWCNTs begins to decrease significantly, and N is the tunneling resistance between adjacent MWCNTs.

The piezoresistance of MWCNT/SR composite under uniaxial pressure was studied by Wang et al. [170] and they found that the carboxyl radical (-COOH) on MWCNT avoids the second aggregation and improve the degree of homogeneous dispersion of MWCNT in rubber, thus enhancing the piezoresistive properties. They studied the variation of electrical resistance with pressure for unmodified CNTs (Sample A), carboxylated CNTs (Sample B) and neat SR (Sample C) as observable in Fig. 26b and the former two samples exhibit positive piezoresistance. Also a sharper and more linear increase of sample B than sample A is found because of homogeneous dispersion of MWCNTs under 0-2.86 MPa uniaxial pressure.

In composites containing homogeneous CNTs, as pressure is applied they are forced to align with the direction of stretching, as shown in Fig. 27a. As a result, the number of contacting CNTs reduces and the tunneling resistance increases. This is why such composites display positive piezoresistance quantified by Park's equation (Eq. (19)). But, for the composite with aggregating CNTs, the aggregations are treated as particles, and their piezoresistivity is different from that of homogeneous CNTs filled composites. For this case, the simplified Eq. (20) by Hussain [251] explains the change of electrical resistivity with pressure.

$$\rho = \rho_1 \left(\frac{1 - \phi_c}{\phi - \phi_c} \right)^w \quad \text{..............................} (20)$$

where ρ is the resistivity of composite, ρ_1 the resistivity of particle, ϕ_c the critical percolation fraction, ϕ the current particle fraction, and w is an exponent. When the composite is subjected to stress, the volume is compressed and the particle's fraction increases, with a resulting decrease in resistivity. However, as shown in Fig. 27b, the thickness of the sample also decreases, that result in an increase in the resistance between two electrodes. So, for sample A, the trend of the resistivity change is opposite to that of the resistance change, which may have a negative effect on sensitivity and sensing linearity.

Sensing characteristics under twisting and bending deformations allow the material to be useful in wearable electronics. The change in zero strain resistance of CNT/PU sheets by 1-2% in the subsequent cycles (100 cycles) fabricated by Shin et al. [252] (Fig. 28) shows the composite's capability in retaining its original shape whereas the resistance of the neat matrix was observed to be constant during all bending and twisting cycles. In short the conducting CNTs in elastomers open up the door towards smart sensor devices useful in flexible electronics and textiles provided good filler rubber compatibility is achieved.

6.3. Electromagnetic interference (EMI) shielding

EMI shielding and electrostatic discharge (ESD) protections are the major applications of conductive polymer composites [17]. The radiation leakage is a serious issue to be prevented and the shielding materials do it by the mechanism of reflection. Currently used, metal coated polymers (MCP) and CB filled polymers for EMI shielding and ESD protection has many limitations. For CB-filled polymers, the high concentration of the CB required to achieve good electrical properties reduces certain composite mechanical properties and ease of processing, while increasing the cost. It also results in damage to the packaged electronics. The importance of CNTs in shielding the EM radiation is well addressed in a review of Hu et al. [253]. In order to effectively shield the radiation, the conducting surface should be unbroken and the holes if present in the shield must be smaller than the wavelength of the particular EM radiation. In CNT case, multiple-reflection within the internal surfaces and between external surfaces decreases the overall shielding effectiveness. Thermoplastic elastomer tri-block copolymers styrene–butadiene–styrene (SBS) reinforced with CNT has good shielding properties [254]. CNTs are used as strategic materials such as EMI/radio frequency shielding in computer, cellular phone housing etc.

A very detailed study about the electromagnetic interference theory and the polymer composites as EMI shielding materials can be seen in a very recent review of Thomassin et al. in Materials Science and Engineering: R: Reports [255]. They discussed various carbon fillers (CB, carbon fiber, CNT and graphene) based polymer composites, their synthesis, electrical properties and the dependence of all these factors on EMI shielding property. They found that the shielding efficiency greatly enhances with high level of CNT dispersion within the matrix, synergizing nanotubes with metal particles and mode of fabrication methods. In addition to reflection, the phenomenon of absorption also plays role in regulating shielding. Very recently Kwon et al. satisfied the need of flexible EMI shielding materials by developing conducting adhesives out of MWCNTs decorated with nanoscale silver particles and microscale silver flakes embedded NBR [256]. A maximum shielding effectiveness of about ~75 dB at 1 GHz was achieved and this as well as the conductivity varies according to the Ag flake concentration. Here reflection was observed to be the major shielding mechanism [51] Functionalized MWCNTs filled PU composite foams exhibiting lower EMI shelding values than their pristine counterparts are also reported [257].

6.4. Electroactivity

Electroactive CNT composites are used in fabricating low-cost, integrated micro devices capable of working in extreme environments. Such devices are used in bio-inspired sensors to detect flow field, pressure and temperature gradient. The fabricated conducting and mechanically robust MWCNT (0.1-10 wt%) /PDMS composites exhibited piezo- and pyro-resistivity as well as self-recovery properties [258]. In this case the nanotubes are aligned and so a performance/conductivity-morphology relationship [258] exists. This is due to the carrier hopping mechanism between the aligned anisotropic MWCNTs at specific volume fraction percolation. A large and effective dielectric

anisotropy is reported in a nematic liquid-crystalline elastomer containing very low (~ 0.01%) concentration of CNTs. Here the nanotubes were aligned along the nematic director and the resulting composite showed good electromechanical property. When a constant field (~ 1 MV/m) is applied, the composite shows a uniaxial stress (~ 1 kPa) as the torque induced by the electric field is transmitted to the rubber network. The authors succeeded in deriving the influence of field strength, nanotube concentration and reproducibility at various cycles on the composite behavior and in tailoring the material for making electrically driven actuators [259].

Bendable and twistable electrothermal actuators are prepared from a layer of PDMS sandwiched between two layers of CNT/PDMS composite by Seo et al. Upon heating one of the outer layers (CNT/PDMS), a thermal gradient forms in the direction of the middle layer (PDMS) thickness and as a result the structure bends towards the opposite unheated side. Also when two such sandwich structures were parallelly arranged on the same body and heated as in the above case, the two bend in opposite directions finally resulting in a twisting motion [260]. Silicone dielectric elastomer actuators were fabricated using covalently functionalized MWCNT filled silicone copolymer. Poly(azidopropylmethyl)-co-(dimethylsiloxane) (silicone-N3) is used for modifying CNTs through nitrene addition reaction. The silicone grafted MWCNTs uniformly disperse in the matrix because of the enhanced compatibility of the filler with the medium and the passivation layers of the modified nanotubes. The resulting composites possess superior mechanical and dielectric properties in addition to the electromechanical characteristics [261].

6.5. MEMS and MAMS

MEMS or microelectromechanical systems form the basics of several industrially significant devices such as sensors, actuators, displays, optical switches, energy harvesting devices, transducers etc. Since nanotechnology joins hand with this field it can also be called nanoelectromechanical

systems or NEMS. Using the low-cost MEMS technology, CNT/PDMS composite is applied in fabricating piezoresistors by Kim et al. They have observed good mechanical, electrical and pressure sensing properties for the composites at various filler loadings. The gauge factor of the CNT/PDMS composites showed values 1.38 - 12.4 according to the CNT concentration. In addition to nanosensors such materials are useful in microfluidic systems as well [262]. By aligning CNTs on the polymer surface CNT/PDMS composites were formulated [263]. Such composite showed excellent electrical properties, rheological properties, room temperature micropatternability and elasticity. Surface potential measurements reveal the increased charge storage capacity and stability of the CNT/PDMS composite when compared to neat PDMS and CNTs over a measurement period of 280 h. The authors have illustrated the power generation in this corona-charged composite by ball drop experiment and the composite is proposed to be suitable as elastic electrets.

The polymer PDMS is widely used in MEMS because of its structural applications. In another work, conducting MWCNT/PDMS composites were fabricated by monolithic integration. Fabrication processes including PDMS patterning, micromolding, and bonding techniques were employed. Such composites are applicable in elastomeric strain gauges, capacitive pressure sensors, microfluidic channels with heaters, electrodes and sensors [264]. Buckling is another phenomenon to be addressed before manufacturing the micromechanical devices. In the case of SWCNTs filled elastomer composites, the buckle wavelength is proportional to $\frac{3}{4}^{th}$ power of the CNT radius whereas for MWCNTs, it linearly increases with the number of walls. When two parallel nanotubes on the elastomer surface are considered, they interact and buckle together at the same wavelength below a critical spacing. For the coupled buckling, the larger tube dominates as the cobuckling wavelength is close to the wavelength of larger CNTs [265].

Microwave-absorbing materials (MAMS) made from CNT/elastomer composites are widely applied in wireless communication. CNTs are capable of absorbing microwave radiation and this capability is found to increase with their functionalization and rate of dispersion. Multiscale hybrid CNT/microwire composite was reported for improved microwave absorption and used in shielding applications [266]. The property of microwave absorption of the composite varies with the thickness of the material, working frequency, complex permittivity and permeability. Zhang et al. investigated the effect of fabrication method on the microwave absorption property of MWCNT/PVC/NBR composites. The composite made by premixing with PVC had a higher dielectric loss and thus better microwave absorbing performance than that made by premixing with NBR at the same MWCNT concentration. The former had a minimum reflection loss of 49.5 dB at the optimum composite thickness of 1.96 mm due to a high dielectric loss and moderate permittivity. Upon the addition of SiC to the composite the reflection loss decreased to 34.9 dB at 3 mm thickness due to an impedance mismatch at the air–material interface since the permittivity increased [257]. The radiation absorption property of the CNT elastomer composites were a matter of discussion in many literature [267-269]. A very recent work of Rath et al. reported the multi functional properties including radar absorption of the acid functionalized MWCNTs filled poly(vinylidene fluoride) (PVDF) composites. The electromagnetic wave absorption of the composite was studied in the X-band (6-12 GHz) and a reflective loss of 37dB was obtained at 0.25 wt % filler concentration [270]. In another case mechanically strong microwave absorbers are made from MWCNTs/HNBR/rare earth acrylate. But when compared to the previous cases, here lower values for reflection losses (9 dB for lanthanum reinforced and 13.5 dB for samarium reinforced composites) and broader absorption bands were reported [271]

Based on the various properties discussed here, it could be concluded that the amazing properties of CNTs are yet to be explored. These cylindrical carbon tubes can make wonders and this will contribute tremendous application in various fields of science and technology.

7. Conclusions and future outlook

This review provides an overview about the research works in CNT reinforced elastomers and the properties and applications of such type of composites. Huge progress in CNT applications based on elastomer composites can only be realized when a proper dispersion of the entangled agglomerates of as-prepared CNT products is achieved, without damaging their unique properties. The various preparation methods of CNT composites are described. Efforts have also been made to discuss the influence of surfactants on the dispersion of nanotubes in suitable solvents. Due to high aspect ratio, large surface area and low mass density CNTs possess improved mechanical properties. Moreover CNTs are thermally and electrically conductive due to the presence of pi electrons. As a result when such particles are incorporated in to an elastomer matrix the properties are found to increase. Different nanofillers can together add towards further enhancement in properties of the polymers. Through a combination of benefits of each type of filler, these hybrid composites could potentially exhibit improved characteristics with regard to single-filler materials. However the critical challenge is the development of means and ways to promote and increase the dispersion and alignment of CNTs in the matrix. The alignment of CNTs in a polymer matrix could be increased by ex situ alignment due to force, electrical and magnetic field-induced methods, and liquid crystalline phase could also induce the orientation of CNTs along the direction of the applied field. Recent developments in the field of CNT/elastomer systems were included in this survey. Basic items about CNT based elastomeric composites, such as: dispersion of CNT in the matrix, interface, medium and long range interaction,

reinforcement etc. are clearly identified and highlighted. In conclusion, this literature work in CNT-based elastomeric composites has demonstrated the potential of this new form of carbon as reinforcing filler for rubber materials in many applications especially in the field of electronics. However certain problems are still there which are to be explored in future in order to completely exploit the unusual properties of CNTs. Some of the issues are the following:

1. The techniques for obtaining a good dispersion of CNTs in elastomers matrix is still under study. Effective methods for segregating the nanotube bundles and also the suitable surfactant for improving the interaction between the matrix and the tubes and the techniques for analyzing the effectiveness of distribution of the particles etc. should be developed.

2. The initial high cost of CNT made it an expensive filler material which caused a bad impression when the application side is concerned. Even if the cost is reduced to very high extent nowadays, more efforts should be taken to prepare the nanotubes by simpler and economical means. In addition simpler methods should be optimized for functionalization and alignment techniques.

3. Though some specific fields of electronics are introduced here, more developments should be achieved in the area of elastomer nanotube composites to make it widely applicable in fields of wearable electronics, robotics etc.

4. Graphene, graphitic fillers and other eco friendly fillers like cellulose, starch etc. overtake CNTs in its journey for the formation of composites. The toxicity of nanotubes, its biodegradability etc are some of the important aspects that should be addressed in future.

Acknowledgement

APPENDIX

ACN, Acrylonitrile

AFM, Atomic force microscopy

BMI, 1-butyl 3-methyl imidazolium bis(trifluoromethyl-sulphonyl)imide

BR, Butadiene rubber

CB, Carbon Black

CNTs, Carbon nanotubes

CR, Chloroprene rubber

CRC, Conducting flexible rubber composites

CTAB, Hexadecyltrimethylammonium bromide

CVD, Chemical vapor deposition

DCP, Dicumyl peroxide

DSC, Differential scanning calorimetry

EMI, Electromagnetic interference

EMIT, 1-Ethyl-3-methyl imidazolium thiocyanate

EPDM, Ethylene propylene diene rubber

ESD, Electrostatic discharge

FTIR, Fourier transformation infra red

F-W-O, Flynn-Wall-Ozawa

GF, Gel fraction

HNBR, Hydrogenated nitrile rubber

HXNBR, Hydrogenated carboxylated acrylonitrile–butadiene rubber

KH550, Gamma-aminopropyltriethoxy silane

MAMS, Microwave-absorbing materials

MBTS, 2,2'-Dithiobis(benzothiazole)

MCP, Metal coated polymers

MEMS, Microelectromechanical systems

MWCNT, Multi walled carbon nanotube

NaDDBS, Sodium dodecyl benzene sulphonate

NBR, Acrylonitrile butadiene rubber or Nitrile rubber

NMR, Nuclear magnetic resonance

NR, Natural rubber

PDMS, Polydimethyl siloxane

PECVD, Plasma-enhanced chemical vapor deposition

PmPV, poly (m-phenylene vinylene-co-2, 5-dioctyloxy p-phenylene vinylene)

PS-NH$_2$, Amine terminated polystyrene

PVA, Polyvinyl alcohol

PVDF, Poly(vinylidene fluoride)

PU, Polyurethane

RTVSR, Room temperature cured silicone rubber

SBR, Styrene butadiene rubber

SBS, Styrene-butadiene-styrene or poly(styrene-b-butadiene-b-styrene)

SDS, Sodium dodecyl sulphate

SEM, Scanning electron microscope

SR, Silicone rubber

SWCNT, Single walled carbon nanotube

TAC, Triallyl cyanurate

TEM, Transmission electron microscopy

TERS, Tip enhanced Raman spectroscopy

TGA, Thermo gravimetric analysis

T$_g$, Glass transition temperature

TMTD, Tetramethyl thiuram disulfide

TPNR, Thermoplastic natural rubber

Triton X-100, Isooctyl phenoxy polyethoxy ethanol

TTDPD, Trihexyl tetradecyl phosphonium decanoate

VMQ, Methyl vinyl silicone rubber

WPU, Waterborne polyurethane

XNBR, Carboxylated nitrile butadiene rubber

XPS, X ray photo electron spectroscopy

References

[1]   S. Iijima, *Nature,* 1991, **354,** 56-58.

[2]   T. Uchida and S. Kumar, *J. Appl. Polym. Sci.,* 2005, **98**, 985-989.

[3]   S.J. Tans, A.R.M. Verschueren and C. Dekker, *Nature,* 1998, **393**, 49-52.

[4]   R.J. Young, C.A. Cooper and M. Halsall, *Composites Part A,* 2001, **32**, 401-411.

[5]   G. Gao, T. Çagin and W.A. Goddard, *Nanotechnology,* 1998, **9**, 184-191

[6]   S. Berber, Y.K. Kwon and D.Tomanek, *Phys. Rev. Lett.,* 2000, **84**, 4613-4616.

[7]   J.G. Smith, J.W. Connell, D.M. Delozier, P.T. Lillehei, K.A. Watson, Y. Lin, B. Zhou and Y.P. Sun, *Polymer,* 2004, **45**, 825-836.

[8]   P. Costa, C. Silvia, J.C. Viana and S.L. Mendez, *Comp. Part B Eng.,* 2014, **57**, 242-249.

[9]   S. Giordani, S.D. Bergin, V. Nicolosi, S. Lebedkin, M.M. Kappes, W.J. Blau and J.N. Coleman, *J. Phys Chem B,* 2006, **110**, 15708-15718.

[10] L. Bokobza, *Polymer,* 2007, **48**, 4907-4920.

[11] H.H. Le, M.N. Sriharish, S. Henning, J. Klehm, M. Menzel, W. Frank and H.J. Radusch, *Comp. Sci. Technol.,* 2014, **90**, 180-186.

[12] P.J.F.Harris, Carbon nanotubes and related structures, new materials for the twenty- first century. Cambridge University Press, Cambridge, UK 1999

[13] W. Marx and A. Barth, http.//cdn.intechopen.com/pdfs-wm/10022.pdf.

[14] K. Subramaniam, A. Das, D. Steinhauser, M. Klüppel and G. Heinrich, *Eur. Polym. J.,* 2011, **47**, 2234-2243.

[15] J.M. Tour, J.L. Hudson, R. Kirshnamoorti, K. Yurekli and C.A. Mitchell, US 2007/0259994, 2007.

[16] A. Das, K.W. Stöckelhuber, R. Jurk, M. Saphiannikova, J. Fritzsche, H. Lorenz, M. Klüppel and G. Heinrich, *Polymer,* 2008, **49**, 5276-5283.

[17] A. Fletcher, M.C. Gupta, K.L. Dudley and E. Vedeler, *Compos. Sci. Technol.,* 2010, **70**, 953-958.

[18] A.L. Kalamkarov, A.V. Georgiades, S.K. Rokkam, V.P. Veedu and M.N. Ghasemi-Nejhad, *Int. J. Solids Structur.,* 2006, **43**, 6832–6854. .

[19] M. Monthioux, L. Noe, L. Dussault, J.C. Dupin, N. Latorre, T. Ubieto, E. Romeo, C. Royo, A. Monzo´n and C. Guimon, *J. Mater. Chem.,* 2007, **17**, 4611–4618.

[20] X.L. Xie, Y.W. Mai and X.P. Zhou, *Mater. Sci. Eng. R,* 2005, **49**, 89-112.

[21] J.L. Delgado, M.A. Herranz and N. Martı´n, *J. Mater. Chem.,* 2008, **18**, 1417–1426.

[22] L. Liu, G. Guo, C. Jayanthi and S. Wu, *Phys. Rev. Lett.,* 2002, **88**, 217206-217210.

[23] N. Behabtu, C. Y. Colin, E. T. Dmitri, K. Olga, W. Xuan, W.K. M. Anson and E. A. Bengio, *Science* 2013, **339**, 182-186.

[24]   J. Qiu, J. Terrones , J. J. Vilatela , M. E. Vickers , J. A. Elliott and A. H. Windle, *ACS Nano*, 2013, **7,** 8412–8422

[25]   A. S. Wu and T. W. Chou, *Mater. Today*, 2012, **15**, 302–310

[26]   T.W. Ebbesen and P.M. Ajayan, *Nature,* 1992, **358**, 220–222.

[27]   G. Ting, P. Nikolaev, A. Thess, D. Colbert and R. Smalley, *Chem. Phys. Lett.,* 1995, **243**, 49-54.

[28]   I. Nobuhito, A.M. Mohd, S. Eiji and F. Akihiko, *Sci. Technol. Adv. Mater.,* 2007, **8**, 292-295.

[29]   J.L. Pinilla, R. Moliner, I. Suelves, M. Lazaro, Y. Echegoyen and J. Palacios, *Int. J. Hydrog. Energ.,* 2007, **32**, 4821-4829.

[30]   A. Eftekhari, P. Jafarkhani and F. Moztarzadeh, *Carbon,* 2006, **44**, 1343-1346.

[31]   J. Zhang, H. Zou, Q. Qing, Y. Yang, Q. Li, Z. Liu, X. Guo and Z. Du, *J. Phys. Chem. B,* 2003, **107**, 3712 -3718.

[32]   W. Li, Y. Bai, Y. Zhang, M. Sun, R. Cheng, X. Xu, Y. Chen and Y. Mo, *Synth. Met.,* 2005, **155**, 509-515.

[33]   P.X. Hou, S. Bai, Q.H. Yang, C. Liu and H.M. Cheng, *Carbon,* 2002, **40**, 81-85.

[34]   V. Djordjević, J. Djustebek, J. Cvetićanin, S. Velićknović, M. Veljković, M. Bokorov, B. Babić Stojić and O. Nešković, *J. Optoelectron. Adv. Mater.,* 2006, **8**, 1631-1634.

[35]   J.M. Bonard, T. Stora, J.P. Salvetat, F. Maier, T. Stöckli, C. Duschl, L. Forró c, A.H. Walt and A. Châtelain, *Adv. Mater.* 1997, **9**, 827-831.

[36]   B. Zheng, Y. Li and J. Liu, *Appl. Phys. A Mater. Sci., Process* 2002, **74**, 345-348.

[37]   L. Thiên-Nga, K. Hernadi, E. Ljubovic, S. Garaj and L. Forr´o, *Nano Lett.,* 2002, **2**, 1349-1352.

[38]   S. Curran, A.P. Davey, J. Coleman, A. Dalton, B. McCarthy, S. Maier, A. Drury, D. Gray, M. Brennan, K. Ryder, M. Lamy de la Chapelle, C. Journet, P. Bernier, H.J. Byrne, D.L. Carroll, P.M. Ajayan, S. Lefrant and W. Blau, *Synth. Met.,* 1999, **103**, 2559-2562.

[39]   D.L. Shi, X.Q. Feng, Y.G.Y. Huang, K.C. Hwang and H.J. Gao, *J. Eng. Mater. Technol.,* 2004, **126**, 250-257.

[40]   L.A. Girifalco, M. Hodak and R.S. Lee, *Phys. Rev. B, Condens. Matter Mater. Phys.,* 2000, **62**, 13104-13110.

[41]   M.S. Strano, V.C. Moore, M.K. Miller, M.J. Allen, E.H. Haroz, C. Kittrell, R.H. Hauge and R.E. Smalley, *J. Nanosci. Nanotechnol.,* 2003, **3**, 81-86.

[42]   R. Haggenmüller, H.H. Gommans, A.G. Rinzler, J.E. Fischer and K.I.Winey, *Chem. Phys. Lett.,* 2000, **330,** 219-225.

[43]   J. Zhaoxia, K.P. Pramoda, X. Guoqin and H.G. Suat, *Chem. Phys. Lett.,* 2001, **337**, 43-47.

[44]   G. Broza and K. Schulte, *Polym. Eng. Sci.,* 2008, **48**, 2033-2038.

[45]   P. Pötschke, A.R. Battachyya and A. Janke, *Eur. Polym. J.,* 2004, **40**, 137-148.

[46]   M. Kwiatkowska, G. Broza, K. Schulte and Z. Roslaniec, *Rev. Adv. Mater. Sci.,* 2006, **12**, 154-159.

[47]   Z. Roslaniec, G. Broza and K. Schulte, *Compos. Interf.,* 2003, **10**, 95-102.

[48]   D. Bonduel, M. Mainil, M. Alexandre, F. Monteverde and P. Dubois, *Chem. Commun.,* 2005, **14**, 781-783.

[49]   J. Sandler, G. Broza, M. Nolte, K. Schulte, Y.M. Lam and M.S.P. Shaffer, *J. Macromol. Sci., Part B, Phys.,* 2003, **42**, 479-488.

[50]   M.S.P. Shaffer and A.H.Windle, *Adv. Mater.,* 1999, **11**, 937-941.

[51]   V.K. Varadan and J. Xie, *Smart Mater. Struct.,* 2002, **11**, 610-616.

[52]   B. Likozar, *Scientia Iranica Transaction F, Nanotechnol., 2*010, **17**, 35-42.

[53]   K. Subramaniam, A. Das and G. Heinrich, *Compos. Sci. Technol.,* 2011, **71**, 1441-1449.

[54]   K. Subramaniam, A. Das, L. Häußler, C. Harnisch, K.W. Stöckelhuber and G. Heinrich, *Polym. Degrad. Stab.,* 2012, **97**, 776-785.

[55]   L. Liu, Z. Zheng, C. Gu and X. Wang, *Compos. Sci. Technol.,* 2010, **70**, 1697-1703.

[56]   H.H. Le, X.T. Hoang, A. Das, U. Gohs, K.W. Stoeckelhuber, R. Boldt, G. Heinrich, R. Adhikari and H.J. Radusch, *Carbon,* 2012, **50**, 4543–4556.

[57]   F. Semeriyanov, A. Chervanyov, R. Jurk, K. Subramaniam, S. König, M. Roscher, A. Das, K.W. Stöckelhuber and G. Heinrich, *J. Appl. Phys.,* 2013, **113**, 103706-13.

[58]   J. Liu, A.G. Rinzler, H.J. Dai, H.J. Hafner, R.K. Bradley, P.J. Boul, A. Lu, T. Iversion, K. Shelimov, C.B. Huffman, F. Rodriguez Macias, Y.S. Shon, T.R. Lee, D.T. Colbert and R.E. Smalley, *Science,* 1998, **280**, 1253-1256.

[59]   M.J. O'Connel, S.M. Bachilo, C.B. Huffman, V.C. Moore, M.S. Strano, E.H. Haroz, K.L. Rialon, P.J. Boul, W.H. Noon, C. Kittrell, J. Ma, R.H. Hauge, R.B. Weisman and R.E. Smalley, *Science,* 2002, **297**, 593-596.

[60]   H. Hyung, J.D. Fortner, J.B. Hughes and J.H. Kim, *Environ. Sci. Technol.,* 2007, **41**, 179-184.

[61]   C.A. Dyke and J.M. Tour, *J. Phys. Chem. A,* 2004, **108**, 11151-11159.

[62]   L.A.S.A. Prado, A. Kopyniecka, S. Chandrasekaran, G. Broza, Z. Roslaniec and K. Schulte *Macromol. Mater. Eng.,* 2013, **298**, 359–370.

[63]   A.M. Shanmugharaj, J.H. Bae, K.Y. Lee, W.H. Noh, S.H. Lee and S.H. Ryu, *Compos. Sci. Technol.,* 2007, **67**, 1813-1822.

[64]   D.H. Marsh, G.A. Rance, M.H. Zaka, R.J. Whitby and A.N. Khlobistov, *Phys. Chem. Chem. Phys.,* 2007, **9**, 5490-5496.

[65]   K.A. Anand, T.S. Jose, R. Alex, R. Joseph, A.K. Anoop, J.T. Sunil, A. Rosamma and J. Rani, *Int. J. Polymer Mater.,* 2010, **59**, 33-44.

[66]   M.J. Jiang, Z.M. Dang, S.H. Yao and J. Bai, *Chem. Phys. Lett.,* 2008, **457**, 352-356.

[67]   K. Kobashi, S. Ata, T. Yamada, D.N. Futaba, M. Yumura and K. Hata, *Chem. Sci.,* 2013, **4**, 727-733

[68]   L.D. Perez, M.A. Zuluaga, T. Kyu, J.E. Mark and B.L. Lopez, *Polym. Eng. Sci.,* 2009, **49**, 866-874.

[69]   M.D. Frogley, D. Ravich and H.D. Wagner, *Compos. Sci. Technol.,* 2003, **63**, 1647-1654.

[70]   A. Das, K.W. Stockelhuber, R. Jurk, J. Fritzsche, M. Kluppel and G. Heinrich, *Carbon,* 2009, **47**, 3313-3321.

[71]   M. Khalid, A.F. Ismail, C.T. Ratnam, Y. Faridah, W. Rashmi and M.F. Al Khatib, *Radiat. Phys. Chem.,* 2010, **79**, 1279-1285.

[72]   X.W. Zhou, Y.F. Zhu and J. Liang, *Mater. Res. Bull.,* 2007, **42**, 456-464.

[73] K.Q. Xiao and L.C. Zhang, *J. Mater. Sci.,* 2004, **39**, 4481-4486.

[74] D. Baskaran, J.W. Mays and M.S. Bratcher, *Angew Chem. Int. Ed.,* 2004, **43**, 2138-2142.

[75] L. Bokobza and C. Belin, *J. Appl. Polym. Sci.,* 2007, **105**, 2054-2061.

[76] L. Qian and H. Zhang, *J. Chem. Technol. Biotechnol.,* 2011, **86**, 172-184.

[77] J. Yu, K. Lu, E. Sourty, N. Grossiord, C.E. Koning and J. Loos, *Carbon,* 2007, **45**, 2897-2903.

[78] X. Zhou, Y. Zhu, Q. Gong and J. Liang, *Mater. Lett.,* 2006, **60**, 3769-3775.

[79] D. Ponnamma, H.J. Maria, A.K. Chandra and S. Thomas, Rubber Nanocomposites, Latest Trends and Concepts. In Advances in Elastomers II. Springer Berlin Heidelberg. 2013, pp. 69-107.

[80] Y.J. Xu, B. Higgins and W.J. Brittain, *Polymer,* 2005, **46**, 799-810.

[81] E.J. Park, S.H. Hong, D.W. Park and S.E. Shim, *Colloid Polym. Sci.,* 2010, **288**, 47-53.

[82] X.Y. Huang and W.J. Brittain, *Macromolecules,* 2001, **34**, 3255-3260.

[83] Y.J. Xu, W.J. Brittain, C.C. Xue and R.K. Eby, *Polymer,* 2004, **45**, 3735-3746.

[84] Z. Peng, C. Feng, Y. Luo, Y. Li and L.X. Kong, *Carbon,* 2010, **48**, 4497-4503.

[85] B.Z. Tang and H.Y. Xu, *Macromolecules,* 1999, **32**, 2569-2576.

[86] J.H. Fan, M.X. Wan, D.B. Zhu, B.H. Chang, Z.W. Pan and S.S. Xie, *J. Appl. Polym. Sci.,* 1999, **74**, 2605-2610.

[87] A. Star, J.F. Stoddart, D. Steuerman, M. Diehl, A. Boukai, E.W. Wong, X. Yang, S.W. Chung, H. Choi and J.R. Heath, *Angew Chem. Int. Ed.,* 2001, **40**, 1721-1725.

[88] M. Moniruzzaman and K.I. Winey, *Macromolecules,* 2006, **39**, 5194-5205.

[89] J. Fritzsche, H. Lorenz and M. Klüppel, Elastomer carbon nanotubes composites. In, Polymer-carbon nanotube composites, Preparation, properties and applications. Ed. T. McNally, P. Pötschke, Woodhead Publishing Limited, 2011 pp. 193-229.

[90] H. Xia, Q. Wang, K. Li and G.H. Hu, *J. Appl. Polym. Sci*., 2004, **93**, 378-386.

[91] J. Masuda and J.M. Torkelson, *Macromolecules,* 2008, **41**, 5974-5977.

[92] T. Villmow, P. Potschke, S. Pegel, L. Haussler and B. Kretzschmar, *Polymer,* 2008, **49**, 3500-3509.

[93] P.C. Ma, S.Q. Wang, B.Z. Tang and J.K. Kim, *J. Nanosci. Nanotechnol.,* 2009, **9**, 749-753.

[94] M. Moniruzzaman, F.M. Du, N. Romero and K.I.Winey, *Polymer,* 2006, **47**, 293-298.

[95] Z. Peng, C. Feng, Y. Luo, Y. Li, Z. Yi and L.X. Kong, *J. Appl. Polym. Sci.,* 2012, **125**, 3920-3928.

[96] P.S. Goh, A.F. Ismail and B.C. Ng, *Comp. Part A Appl. Sci. Manufactur.,* 2014, **56**, 103-126.

[97] A.A. Aziz, A.I.H. Dayang, A.B. Suriani and M.R. Mahmood, *Adv. Mater. Res.,* 2014, **832**, 338-343.

[98] X. Zheng, M.G. Forest, R. Lipton, R. Zhou and Q. Wang, *Adv. Funct. Mater.,* 2005, **15**, 627-638.

[99] M.G. Forest, X.Y. Zheng, R.H. Zhou, Q. Wang and R. Lipton, *Adv. Funct. Mater.,* 2005, **15**, 2029-2035.

[100] J.R. Wood, Q. Zhao and H.D. Wagner, *Comp. Part A,* 2001, **32**, 391-399.

[101] Q. Zhao, R. Tannenbaum and K.I. Jacob, *Carbon,* 2006, **44**, 1740-1745.

[102] D. Zhu, C. Xu, N. Nakura and M. Matsuo, *Carbon,* 2002, **40**, 363-373.

[103] K. Kueseng and K.I. Jacob, *Eur. Polym. J.,* 2006, **42**, 220-227.

[104] Y.A. Kim, T. Hayashi, M. Endo, Y. Gotoh, N. Wada and J. Seiyama, *Scr. Mater.,* 2006, **54**, 31-35.

[105] L. Zhang, Q.Q. Ni, A. Shiga, T. Natsuki and Y. Fu, *Polym. Eng. Sci.,* 2011, **51**, 1525-1532.

[106] T.T. Pham, V. Sridhar and J.K. Kim, *Polym. Compos.,* 2009, **30,** 121-130.

[107]   T.P. Chua, M. Mariatti, A. Azizan and A.A. Rashid, *Compos. Sci. Technol.,* 2010, **70**, 671-677.

[108] N. Yan, K. Wu, Y.H. Zhan and H.S. Xia, *Plast. Rubber Compos.,* 2009, **38**, 290-296.

[109] F. Deng, M. Ito, T. Noguchi, L. Wang, H. Ueki, K. Niihara, Y.A. Kim, M. Endo and Q. Zheng, *ACS Nano,* 2011, **5**, 3858-3866.

[110] S. Hudziak, A. Darfeuille, R. Zhang, T. Peijs, G. Mountjoy, G. Bertoni and M. Baxendale, *Nanotechnol.,* 2010, **21**, 125505/1-9.

[111] L. Bokobza and J. Zhang, *eXPRESS Polym. Lett.,* 2012, **6**, 601–608

[112] N. Peica, C. Thomsen and J. Maultzsch, *Phys. Status Solidi. B,* 2010, **247**, 2818-2822.

[113] N. Peica, C. Thomsen and J. Maultzsch, *Nanoscale Res. Lett.,* 2011, **6**, 1-7.

[114] P. Verma, T. Ichimura, T. Yano, Y. Saito and S. Kawata, *Laser Photon Rev.,* 2010, **4**, 548–561.

[115] T. Suzuki, X. Yan, Y. Kitahama, H. Sato, T. Itoh, T. Miura and Y. Ozaki, *J. Phys. Chem. C,* 2013, **117**, 1436-1440

[116] L.Bokobza, *Polym. Adv. Technol.,* 2012, **23**, 1543-1549.

[117] S.J. Park and B.J. Kim, Studies on solid-state NMR and surface energetics of silicas for improving filler-elastomer interactions in nanocomposites. In: Rubber Nanocomposites preparation, properties, and applications. Ed. R. Stephen and S. Thomas, John Wiley & Sons (Asia) Pvt Ltd, 2010

[118] S.S. Mahapatra, S.K. Yadav, H.J. Yoo and J.W. Cho, *J. Mater. Chem.,* 2011, **21**, 7686-7691

[119] J. Yu, B. Tonpheng, G. Gröbner and O. Andersson, *Macromolecules,* 2012, **45**, 2841−2849

[120] D. Wang, S. Fujinami, K. Nakajima, K. Niihara, S. Inukai, H. Ueki, A. Magario, T. Noguchi, M. Endo and T. Nishi, *Carbon,* 2010, **48**, 3708-3714.

[121] L. Bokobza, B. Bresson, G. Garnaud and J. Zhang, *Compos. Interf.,* 2012, **19**, 285-295

[122] P. Costa, J. Silva, V. Sencadas, R. Simoes, J.C. Viana and S. Lanceros-Me´ndez, *J. Mater. Sci.,* 2013, **48**,1172-1179.

[123] J.B. Lee and D.Y. Khang, *Compos. Sci. Technol.,* 2012, **72**, 1257-1263

[124] K. Oh, J.Y. Lee, S.S. Lee, M. Park, D. Kim and H. Kim, *Compos. Sci. Technol.,* 2013, **83**, 40-46

[125] A. Charlesby, *J. Polym. Sci. Part A, Polym. Chem.,* 1953, **11**, 513-520.

[126] E. Menzibal, L. Cruz, C.F. Jasso, G. Burillo and V.I. Dakin, *Radiat. Phys. Chem.,* 1996, **47**, 305-309.

[127] X.W. Zhou, Y.F. Zhu, J. Liang and S.Y. Yu, J. *Mater. Sci. Technol.,* 2010, **26**, 1127-1132.

[128] P. Verge, S. Peeterbroeck, L. Bonnaud and P. Dubois, *Compos. Sci. Technol.,* 2010, **70**, 1453-1459.

[129] C. Nah, J.Y. Lim, B.H. Cho, C.K. Hong and A.N. Gent, *J. Appl. Polym. Sci.,* 2010, **118**, 1574-1581.

[130] E.M. Dannenberg, *Rubber Chem. Technol.,* 1986, **59**, 512-524.

[131] E.J. Kramer and H.H. Kausch, Crazing in Polymers. Ed Springer-Verlag, New York 1983. pp. 1-56.

[132] M.M. Saatchi and A. Shojaei, *Polym. Int.,* 2012, **61**, 664-672.

[133] G. Sui, W.H. Zhong, X.P. Yang and Y.H. Yu, *Mater. Sci. Eng. A,* 2008, **485**, 524-531.

[134] H. Lorenz, J. Fritzsche, A. Das, K.W. Stöckelhuber, R. Jurk, G. Heinrich and M. Klüppel, *Compos. Sci. Technol.,* 2009, **69**, 2135-2143.

[135] I. Kang, M.A. Khaleque, Y. Yoo, P.J. Yoon, S.Y. Kim and K.T. Lim, *Compos. Part A,* 2011, **42**, 623-630.

[136] A. De Falco, S. Goyanes, G.H. Rubiolo, I. Mondragon and A. Marzocca, *Appl. Surf. Sci.,* 2007, **254**, 262-265.

[137] D. Yue, Y. Liu and Z. Shen, *J. Mater. Sci.,* 2006, **41**, 2541-2544.

[138] L. Lu, Y. Zhai, Y. Zhang, C. Ong and S. Guo, *Appl. Surf. Sci.,* 2008, **255**, 2162-2166.

[139] B.K. Lim, S.H. Lee, J.S. Park and S.O. Kim, *Macromol. Res.,* 2009, **17**, 666-671.

[140] S. Inukai, K. Niihara, T. Noguchi, H. Ueki, A. Magario, E. Yamada, S. Inagaki and M. Endo, *Ind. Eng. Chem. Res.,* 2011, **50**, 8016-8022.

[141] A. Adedigba, Abdul-Lateef, M.A. Harthi and M.A. Atieh, *Arab. J. Sci. Eng.,* 2010, **35**, 49-56.

[142] E. Guth, *J. Appl. Phys.,* 1945, **16**, 20-25.

[143] H.M. Smallwood, *J. Appl. Phys.,* 1944, **15**, 758-767.

[144] S. Bhattacharyya, C. Sinturel, O. Bahloul, M.L. Saboungi, S. Thomas and J.P. Salvetat, *Carbon,* 2008, **46**, 1037-1045.

[145] M. Tosaka, D. Kawakami, K. Senoo, S. Kohjiya, Y. Ikeda and S. Toki, *Macromolecules,* 2006, **39**, 5100-5105.

[146] J.M. Chenal, L. Chazeau, L. Guy, Y. Bomal and C. Gauthier, *Polymer,* 2007, **48**, 1042-1046.

[147] F.R. Costa, S. Pradhan, U. Wagenknecht, A.K. Bhowmick and G. Heinrich, *J. Polym. Sci., Part B, Polym. Phys.,* 2010, **48**, 2302-2311.

[148] L. Bokobza and J.P. Chauvin, *Polymer,* 2005, **46**, 4144-4151.

[149] S. Cantournet, M.C. Boyce and A.H. Tsou, *J. Mech. Phys. Solids,* 2007, **55**, 1321-1339.

[150] J. Bergstrom and M. Boyce, *Rubber Chem. Technol.,* 1999, **72**, 633-656.

[151] S.H. Park and P.R. Bandaru, *Polymer,* 2010, **51**, 5071-5077.

[152] T. Laoui, *Fullerenes Nanotubes Carbon Nanostruct.,* 2013, **21**, 89-101.

[153] Y. Sato, K. Hasegawa, Y. Nodasaka, K. Motomiya, M. Namura, N. Ito, B. Jeyadevan and K. Tohji, *Carbon,* 2008, **46**, 1506-1517.

[154] B. Likozar and Z. Major, *Appl. Surf. Sci.,* 2010, **257**, 565-573.

[155] A.A. Gavrilov, A.V. Chertovich, P.G. Khalatur and A.R. Khokhlov, *Soft Matt.,* 2013, **9**, 4067-4072.

[156] S.T. Huxtable, D.G. Cahill, S. Shenogin, L. Xue, R. Ozisik, P. Barone, M. Usrey, M.S. Strano, G. Siddons, M. Shim and P. Keblinski, *Nat. Mater.,* 2003, **2**, 731-734.

[157] P.C. Ma, N.A. Siddiqui, G. Marom and J.K. Kim, *Compos. Part A,* 2010, **41**, 1345-1367.

[158]   L. Dai, *Angew Chem. Int. Ed.,* 2011, **50**, 4744-4746.

[159] Y. Agari, A. Ueda and S. Nagai, *J. Appl. Polym. Sci.,* 1993, **49**, 1625-1634.

[160] C. Liu, J. Zhang, J. He and G. Hu, *Polymer,* 2003, **44**, 7529-7532.

[161] F. Du, R.C. Scogna, W. Zhou, S. Brand, J.E. Fischer and K.I. Winey, *Macromolecules,* 2004, **37**, 9048-9055.

[162] Y.Y. Huang, S.V. Ahir and E.M. Terentjev, *Phys. Rev. B Condens. Matter Mater. Phys.,* 2006, **73**, 125422/1-125422/9.

[163] Z. Fan and S.G. Advani, *J. Rheol.,* 2007, **51**, 585-604.

[164] S.V. Ahir, Y.Y. Huang and E.M. Terentjev, *Polymer,* 2008, **49**, 3841-3854.

[165] B. Vigolo, C. Coulon, M. Maugey, C. Zakri and P. Poulin, *Science,* 2005, **309**, 920-923.

[166] S.K. Peddini, C.P. Bosnyak, N.M. Henderson, C.J. Ellison and D.R. Paul, *Polymer,* 2014, **55**, 258-270.

[167] M. Alimardani, F. Abbassi-Sourki and G.R. Bakhshandeh, *Compos. Part B Eng.,* 2014, **56**, 149-156.

[168] H.C. Kuan, C.M. Ma, W.P. Chang, S.M. Yuen, H.H. Wu and T.M. Lee, *Compos. Sci. Technol.,* 2005, **65**, 1703-1710.

[169] H. Xia and M. Song, *Soft Matt.,* 2005, **1**, 386-394.

[170] P. Wang, S. Geng and T. Ding, *Compos. Sci. Technol.,* 2010, **70**, 1571-1573.

[171] Z. Han and A. Fina, *Progr. Polym. Sci.,* 2011, **36**, 914-944.

[172] J.W. Shen, X.M. Chen and W.Y. Huang, *J. Appl. Polym. Sci.,* 2003, **88**, 1864-1869.

[173] G. Sui, W.H. Zhong, X.P. Yang, Y.H. Yu and S.H. Zhao, *Polym. Adv. Technol.,* 2008, **19**, 1543-1549.

[174] A.R. Payne, Reinforcement of elastomers. Ed. G. Kraus, Interscience Publishers, New York, 1965, pp. 69.

[175] A. Mongruel and M. Cartault, *J. Rheol.,* 2006, **50,** 115-136.

[176] H.M. da Costa, L.L.Y. Visconte, R.C.R. Nunes and C.R.G. Furtado, *J. Appl. Polym. Sci.,* 2003, **87**, 1194-1203.

[177] B. Likozar, *Polym. Eng. Sci.,* 2011, **51**, 542-549.

[178] G. Sui, W. Zhong, X. Yang and S. Zhao, *Macromol. Mater. Eng.,* 2007, **292**, 1020-1026.

[179] M.M. Saatchi and A. Shojaei, *Polym. Int.,* 2012, **61**, 664-672.

[180] L.D. Perez, M.A. Zuluaga, T. Kyu, J.E. Mark and B.L. Lopez, *Polym. Eng. Sci.,* 2009, **49**, 866-874.

[181] A. De Falco, A.J. Marzocca, M.A. Corcuera, A. Eceiza, I. Mondragon, G.H. Rubiolo and S. Goyanes, *J. Appl. Polym. Sci.,* 2009, **113**, 2851-2857.

[182] C. Kummerlöwe, N. Vennemann, E. Yankova, M. Wanitschek, C. Größ, T. Heider, F. Haberkorn and A. Siebert, *Polym. Eng. Sci.,* 2012, **53**, 849-856

[183] F.B. Bujans, R. Verdejo, M. Pérez-Cabero, S. Agouram, I. Rodríguez-Ramos, A. Guerrero-Ruiz and M.A. López-Manchado, *Eur. Polym. J.,* 2009, **45**, 1017-1023.

[184] A. Das, A.K. Ghosh, S. Pal and D.K. Basu, *Polym. Adv. Technol.,* 2004, **15**, 197-208.

[185] C. Guthy, F. Du, S. Brand, K.I. Winey and J.E. Fischer, *J. Heat Transfer.,* 2007, **129**, 1096-1099.

[186] D. Bigg, Thermal conductivity of hetero phase polymer compositions. Thermal and Electrical Conductivity of Polymer Materials. Berlin/Heidelberg, Springer, 1995, p. 1-30.

[187] M. Foygel, R.D. Morris, D. Anez, S. French and V.L. Sobolev, *Phys. Rev. B, Condens. Matter Mater. Phys.,* 2005, **71**, 104201/1-8.

[188] J. Zhao, F. Du, W. Cui, P. Zhu, X. Zhou and X. Xie, *Compos. Part A, Appl. Sci. Manufactur.,* 2014, **58**, 1-6.

[189] M. Alimardani, F. Abbassi-Sourki and G.R. Bakhshandeh, *Iran Polym. J.,* 2012, **21**, 809-820.

[190] R. Gulotty, M. Castellino, P. Jagdale, A. Tagliaferro and A.A. Balandin, *ACS nano,* 2013, **7**, 5114–5121.

[191] H. Huang, C. Liu, Y. Wu and S. Fan, *Adv. Mater.,* 2005, **17**, 1652-1656.

[192] S. Saengsuwan and S. Saikrasun, *J. Therm. Anal. Calorim.,* 2011, **110**, 1395-1406.

[193] K. Czaniková, M. Omastová, I. Krupa, P. Kasák, E. Pavlová and D. Chorvát Jr, Elastomeric actuators based on ethylene-vinyl acetate and carbon nanotubes. In chemistry, the key to our sustainable future. Springer Netherlands 2014, pp. 1-14

[194] M. Ji, H. Deng, D. Yan, X. Li, L. Duan and Q. Fu, *Compos. Sci. Technol.,* 2014, **92**, 16-26.

[195] L. Flandin, A. Chang, S. Nazarenko, A. Hiltner and E. Baer, *J. Appl. Polym. Sci.,* 2000, **76**, 894-905.

[196] W. Thongruang, C.M. Balik and R.J. Spontac, *J. Polym. Sci. Part B, Polym. Phys.,* 2002, **40**, 1013-1025.

[197] A.R. Payne, *J. Appl. Polym. Sci.,* 1965, **9**, 1073-1082.

[198] AR Payne and R.E. Whittaker, *Rubber Chem. Technol.,* 1971, **44**, 440-478.

[199] J.B. Donnet, A. Voet, Chemistry & Physics of Carbon volume 2. New York and Basel, Marcel Dekker Inc, 1976 .

[200] K.P. Sau, T.K. Chaki and D. Khastgir, *J. Appl. Polym. Sci.,* 1999, **71**, 887-895.

[201] N.C. Das, T.K. Chaki and D. Khastgir, *Polym. Int.,* 2002, **51**, 156-163.

[202] P. Sheng, E.K. Sichel and J.I. Gittleman, *Phys. Rev. Lett.,* 1978, **40**, 1197-1200.

[203] C.W. Nan, *Prog. Mater. Sci.,* 1993, **37**, 1-116.

[204] N.K. Preetha, P. Thomas and R. Joseph, *Mater. Des.,* 2012, **41**, 23-30.

[205] Z.M. Dang, Y. Shen and C.W. Nan, *Appl. Phys. Lett.,* 2002, **81**, 4814-4816.

[206] M.J. Jiang, Z.M. Dang and H.P. Xu, *Eur. Polym. J.,* 2007, **43**, 4924-4930.

[207] V. Skakalova, U. Dettlaff-Weglikowska and S. Roth, *Synth. Met.,* 2005, **152**, 349-352.

[208] W.E. Mahmoud, E.H. El-Mossalamy and H.M. Arafa, *J. Appl. Polym. Sci.,* 2011, **121**, 502-507.

[209] S. Shang, W. Zeng and X. Tao, *Sens. Actuators B,* 2012, **166-167**, 330-337.

[210] T.A. Kim, H.S. Kim, S.S. Lee and M. Park, *Carbon,* 2012, **50**, 444-449.

[211] V. Georgakilas, K. Kordatos, M. Prato, D.M. Guldi, M. Holzinger and A. Hirsch, *J. Am. Chem. Soc.,* 2002, **124**, 760-761.

[212] R.K. Ryan, J. Alireza, P Basudev, P. Srikanth, S. Kristina, C. Jian and G. Shaoqin, *J. Phys. Chem. C,* 2009, **113**, 17626-17629.

88

[213] P. Il-Seok, J.K. Kwang, N. Jae-Do, L. Joonsoo and Y. Woosoon, *Polym. Eng. Sci.,* 2007, **47**, 1396-1405.

[214] J. Fritzsche, H. Lorenz and M. Klüppel, *Macromol. Mater. Eng.,* 2009, **294**, 551-560.

[215] J.G. Meier, J.W. Mani and M. Klüppel, *Phys. Rev. B, Condens. Matter Mater. Phys.,* 2007, **75**, 054202/1-10.

[216] M. Klüppel, *Adv. Polym. Sci.,* 2003, **164**, 1-86.

[217] A. Allaoui and S. Ba, *Compos. Sci. Technol.,* 2002, **62**, 1993-1998.

[218] B. Kozinsky and N. Marzari, *Phys. Rev. Lett.,* 2006, **96**, 166801/1-4.

[219] A.K. Barick and D.K. Tripathy, *Mater. Sci. Eng. B,* 2011, **176**, 1435-1447.

[220] L. Fama, L. Gerschenson and S. Goyanes, *Carbohydr. Polym.,* 2009, **75**, 230-235.

[221] H.S. Villada, H.A. Acosta and R.J. Velasco, *Temas Agrarios,* 2007, **12**, 5-13.

[222] N.M.L. Hansen and D. Plackett, *Biomacromolecules,* 2008, **9**, 1494-1505.

[223] K. Litina, A. Miriouni, D. Gournis, M.A. Karakassides, N. Georgiou, E. Klontzas, E. Ntoukas and A. Avgeropoulos, *Eur. Polym. J.,* 2006, **42**, 2098-2107.

[224] M. Bhattacharya and A.K. Bhowmick, *J. Mater. Sci.,* 2010, **45**, 6126-6138.

[225] D. Ponnamma, K.K. Sadasivuni, M. Strankowski, Q. Guo and S. Thomas, *Soft Matt.,* 2013, **9**, 10343-10353.

[226] K. K. Sadasivuni, A. Saiter, N. Gautier, S. Thomas and Y. Grohens, *Colloid Polym.* Sci., 2013, **291**, 1729-1740.

[227] K. K. Sadasivuni, D. Ponnamma, S. Thomas and Y. Grohens, *Prog. Polym. Sci.*, 2014, **39**, 749–780.

[228] G. Heinrich and T.A. Vilgis, *Macromolecules,* 1993, **26**, 1109-1119.

[229] P. Kim, L. Shi, A. Majumdar and P.L. McEuen, *Phys. Rev. Lett.,* 2001, **87**, 215502/1-215502/4.

[230] G. Sui, W. Zhong, X. Yang and S. Zhao, *Macromol. Mater. Eng.,* 2007, **292**, 1020-1026.

[231] M. Xu, D.N. Futaba, T. Yamada, M. Yumura and K. Hata, *Science,* 2010, **330**, 1364-1368.

[232] K. Shehzad, J.W. Zha, Z.F. Zhang, J.K. Yuan and Z.M. Dang, *J. Adv. Phy.,* 2013, **2**, 70-74.

[233] J.H. Kim, J.M. Kim, I. Kang and J.Y. Cha, Int Confer Nanotechnol Biosensors. Singapore, IACSIT Press 2011, **2**, 38-41.

[234] R. Krupke, F. Hennrich, H.V. Lohneysen and M.M. Kappes, *Science,* 2003, **301**, 344-347.

[235] L. Wang and Z.M. Dang, *Appl. Phys. Lett.,* 2005, **87**, 042903/1-3.

[236] K. Ahmad, W. Pan and S.L. Shi, *Appl. Phys. Lett.,* 2006, **89**, 133122/1-3.

[237] Z.M. Dang, L. Wang, Y. Yin, Q. Zhang and Q.Q. Lei, *Adv. Mater.,* 2007, **19**, 852-857.

[238] M.J. Jiang, Z.M. Dang and H.P. Xu, *Appl. Phys. Lett.,* 2007, **90**, 042914/1-3.

[239] Q. Li, Q. Xue, L. Hao, X. Gao and Q. Zheng, *Compos. Sci. Technol.,* 2008, **68**, 2290-2296.

[240] Y. Ji, J.E. Marshall and E.M. Terentjev, *Polymer,* 2012, **4**, 316-340.

[241] D.P. Hashim, N.T. Narayanan, J.M. Romo-Herrera, D.A. Cullen, M.G. Hahm, P. Lezzi, J.R. Suttle, D. Kelkhoff, E. Munõz-Sandoval, S. Ganguli, A.K. Roy, D.J. Smith, R. Vajtai, B.G. Sumpter, V. Meunier, H. Terrones, M. Terrones and P.M. Ajayan, *Nat. Sci. Rep.,* 2012, **2**, 363/1-8.

[242] K. Czaniková, N. Torras, J. Esteve, I. Krupa, P. Kasák, E. Pavlova, D. Račko, I. Chodák and M. Omastová, *Sens. Actuat. B Chem.,* 2013, **186**, 701-710

[243] T. Sekitani, Y. Noguchi, K. Hata, T. Fukushima, T. Aida and T. Someya, *Science,* 2008, **321**, 1468-1472.

[244] K. K. Sadasivuni, D. Ponnamm, P. Kasak, I. Krupa and M. A. S A Al-Maadeed, *Mater. Chem. Phys.*, 2014, DOI: 10.1016/j.matchemphys.2014.06.055.

[245] S. K. Kumar, M. Castro, I. Pillin, J. F. Feller, S. Thomas and Y. Grohens, *Polym. Adv. Technol.*, 2013, **24**, 487–494.

[246] S. K. Kumar, M. Castro, A. Saiter, L. Delbreilhc, J. F. Feller, S. Thomas and Y. Grohens, *Mater. Lett.*, 2013, **96**, 109–112.

[247] M. Park, H. Kim and J.P. Youngblood, *Nanotechnol.,* 2008, **19**, 055705/1-7.

[248] X. Song, S. Liu, Z. Gan, Q. Lv, H. Cao and H. Yan, *Microelectron. Eng.,* 2009, **86**, 2330-2333.

[249] Y. Zeng, H. Liu, J. Chen and H. Ge, *J. Wuhan Univ. Technol. Mater. Sci. Ed.,* 2011, **26**, 812-816.

[250] M. Knite, I. Klemenok, G. Shakale, V. Teteris and J. Zicans, *J. Alloys Compd.,* 2007, **434-435**, 850-853.

[251] M. Hussain, Y. Choa and K. Niihara, *Compos. Part A,* 2001, **32**, 1689-1696.

[252] M.K. Shin, J. Oh, M. Lima, M.E. Kozlov, S.J. Kim and R.H. Baughman, *Adv. Mater.,* 2010, **22**, 2663-2667.

[253] L. Hu, D.S. Hecht and G. Gru¨ner, *Chem. Rev.,* 2010, **110**, 5790–5844

[254] H. Koerner, W. Liu, M. Alexander, P. Mirau, H. Dowty and R.A. Vaia, *Polymer,* 2005, **46**,4405-4420.

[255] J.M. Thomassin, C. Jérôme, T. Pardoen, C. Bailly, I. Huynen and C. Detrembleur, *Mater. Sci. Eng., R, Reports,* 2013, **74**, 211-232

[256] S. Kwon, R. Ma, U. Kim, H.R. Choi and S. Baik, *Carbon,* 2014, **68**, 118-124.

[257] S. Zhang, Y. Zhai and Y. Zhang, *J. Appl. Polym. Sci.,* 2013, **130**, 345-351.

[258] K. Hilmar, P. Nathan, D. Heather, J. Shane, A. Max and V. Richard, Piezo- and pyro-resistivity of carbon nanotube-elastomer nanocomposites. American Physical Society, 2004, Palais des Congres de Montreal, Montreal, Quebec, Canada

[259] S. Courty, J. Mine, A.R. Tajbakhsh and E.M. Terentjev, *Europhys. Lett.,* 2003, **64**, 654-658.

[260] D.K. Seo, T.J. Kang, D.W. Kim, Y.H. Kim and D. Kyun, *Nanotechnol.,* 2012, **23**, 075501.

[261] S.K. Yadav, I.J. Kim, H.J. Kim, J. Kim, S.M. Hong and C.M. Koo*, J. Mater. Chem. C,* 2013, **1**, 5463-5470

[262] D. Kim, J.E. Han, H. Park and K.S.Yun, Simple and low-cost patterning of carbon nanotube on PDMS for flexible MEMS. 978-1-4577-0156-6/11/, Transducers'11, Beijing, China, 2011

[263] W.J. Xu, M. Kranz, S.H. Kim and M.G. Allen, *J. Micromech. Microeng.,* 2010, **20**, 104003-104010.

[264] J.M. Engel, N. Chen, K. Ryu, S. Pandya, C. Tucker, Y. Yang and C. Liu, Multi-layer embedment of conductive and non-conductive pdms for all-elastomer MEMS, The 12th Solid

State Sensors, Actuator, and Microsystems Workshop (Hilton Head 2006), Hilton Head Island, SC, 2006.

[265] J. Xiao, H. Jiang, D.Y. Khang, J. Wu, Y. Huang and J.A. Rogers, *J. Appl. Phys.,* 2008, **104**, 033543.

[266] F.X. Qina, C. Brosseau and H.X. Peng, *Chem. Phys. Lett.,* 2013, **579**, 40-44.

[267] Z. Liu, G. Bai, Y. Huang, F. Li, Y. Ma, T. Guo and Y. Chen, *J. Phys. Chem. C,* 2007, **111**, 13696-13700.

[268] Z. Liu, G. Bai, Y. Huang, Y. Ma, F. Du, F. Li and Y. Chen, *Carbon,* 2007, **45**, 821-827.

[269] Q. Ling, J. Sun, Q. Zhao and Q. Zhou, *Polym. Plast. Technol. Eng.,* 2010, **49**, 481-486.

[270] S.K. Rath, S. Dubey, G.S. Kumar, S. Kumar, A.K. Patra, J. Bahadur and T.U. Patro, *J. Mater. Sci.,* 2014, **49**, 103-113.

[271] W. Wu, Y. Zhai, Y. Zhang and W. Ren, *Compos. Part B Eng.,* 2014, **56**, 497-503.

Figure Captions

Fig. 1. Contribution of different continents to CNT production [Reprinted from ref 13 with permission].

Fig. 2. Various structural forms of nanotubes (a) SWCNT (b) MWCNT (c) Torus (d) Nanobud (e) Cup stacked CNTs (i) and Different types of SWCNTs (ii) [Reprinted from ref 18,19 and 21 with permission].

Fig. 3. Schematic representation of (a) physical adsorption between MWCNTs and CTAB and (b) chemical interaction of KH550 with MWCNTs and rubber [Reprinted from ref 66 with permission].

Fig. 4. Typical (a) AFM tapping mode height image (b) Nanomechanical mapping adhesive energy (J/m^2) (c) Young's modulus (MPa) distribution images and (d) three-dimensional cellular structure of CNT(60phr)/NR [Reprinted from ref 120 with permission]

Fig. 5. Cross-sectional SEM images of the cured (a) 0.2 wt% and (c) 1.4 wt% MWCNT/PDMS composites. TEM images of (c) SWCNT/PDMS and (d) IL-SWCNT/PDMS (8 wt% IL) composites containing 1.6 wt% SWCNT [Reprinted from ref 123 and 124 with permission].

Fig. 6. Effect of radiation dose on the gel fraction of rubber/CNT composites. SMR indicates Standard Malaysian Rubber. [Reprinted from ref 71 with permission]

Fig. 7. Cross linking degrees of the vulcanizates filled with different CNTs addition [Reprinted from ref 127 with permission]

Fig. 8. Variation in bound rubber content of CNT/NR and CB/NR (a) with filler loadings and (b) with volume expansion [Reprinted from ref 129 with permission].

Fig. 9. (a) Stress–strain curves for pure NR latex and its composites (b) variation in the value of modulus with filler volume fraction [Reprinted from ref 144 with permission]

Fig. 10. (a) Uniaxial tension load–unload true stress vs. true strain at a strain rate of 0.01/s to a strain of 0.4 for the elastomer and the MWCNT/elastomer composites and (b) uniaxial tension true stress vs true strain at a strain rate of 0.01/s taken to failure; the inset plot reports the initial axial modulus as a function of weight fraction MWCNT [Reprinted from ref 149 with permission]

Fig. 11. A model of the viscoelastic deformation of polymers in the rubber elastic state [Reprinted from ref 188 with permission]

Fig. 12. Viscosity of CNT/WPU composites vs time at various compositions when the processing temperature is 200°C (system 1-covalent bonding system) (a) System 2-ionic bonding system (b) [Reprinted from ref 168 with permission].

Fig. 13. Variation of storage modulus **(**a) with temperature (b) with strain amplitude [Reprinted from ref 144 with permission].

Fig. 14. Elastic modulus of the NBR and SBR elastomers reinforced with the nanotubes from DMA measurements, and fitted to the Guth model [Reprinted from ref 64 with permission]

Fig. 15. Vulcanizing curves of (a) neat NR and NR composites and (b) CNT/SR composite [Reprinted from ref 173 and 137 with permission].

Fig. 16. Depressive effect of CNTs with 2% PTSA (p-toluenesulfonic acid) on EPDM vulcanization at 160°C. Comparison of the vulcanization kinetic of EPDM, 5CNT–EPDM and 5S/CNT–EPDM [Reprinted from ref 183 with permission].

Fig.17. Comparison of thermal conductivities of composites containing CNTs with different functionalities (data in bracket indicate% increase in thermal conductivity against the polymer matrix) [Reprinted from ref 93 with permission].

Fig.18. The enhanced values of thermal conductivity vs weight fractions of the CNTs. The inset is a comparison of measured thermal conductivity values of different samples [Reprinted from ref 191 with permission].

Fig. 19. Variation of electrical conductivity (a) with CNT content (b) with frequency [Reprinted from ref 16 with permission].

Fig. 20. Typical applications of conducting composites (a) and a schematic of percolation phenomenon and conducting network in conducting composites (b) [Reprinted from ref 93 with permission]

Fig.21. Dependence of the conductivity of the m-MWCNT/VMQ composites on the (a) m-MWCNT volume fraction, fm-MWCNT, at room temperature and 100 Hz and the inset shows the best fits of the conductivity to Eq. (17) (b) on frequency at room temperature [206](c) Dependence of conductivities of the MWCNT/VMQ composites with the modified MWCNTs at two concentrations (0.9 vol% and 1.6 vol%) on the modifiers at 10^2 Hz [Reprinted from ref 206 and 66 with permission].

Fig. 22. a) Room temperature dielectric loss of both MWCNT/PDMS composites as a function of MWCNT mass fraction (wt %) at 10 kHz [212] b) Dependence of permittivity of 3 phr CNTs loaded SSBR/BR matrix in presence of different ionic liquid measured at 20 °C [Reprinted from ref 212 and 70 with permission].

Fig. 23. A schematic representation for CNT/elastomer composites.

Fig. 24. TEM images of the MWCNT/organo-clay/EPDM composites a)10 wt% MWCNT, b) 10 wt% MWCNT/6 wt% Cloisite 15A [Reprinted from ref 135 with permission].

Fig. 25. Major application of CNT/elastomer composites a) Home appliances b) switches c) pressure sensing skin in robotics d) strain sensor attached to tyre engineering e) energy storage application as capacitors and f) cables

Fig. 26. Strain response of the MWCNT/EPDM composite containing 20 wt % of MWCNT during compression and extension [135] (b) Changes of electrical resistance under various pressures for the samples A-C (Sample A = Uunmodified-MWCNTs, Sample B= Carboxylated-MWCNTs, Sample C=Silicon Rubber) [Reprinted from ref 135 and 170 with permission]

Fig. 27. A schematic representation of the deformation in homogeneous-MWCNTs and aggregated-MWCNTs filled composites [Reprinted from ref 170 with permission].

Fig. 28. Dependence of zero strain resistance (R/R_0) on the number of bending and twisting cycles. The sample shape induced by bending and twisting is shown in the insets [Reprinted from ref 252 with permission]

Table 1

Description of single walled carbon nanotubes.

SWCNT	Chiral Angle θ	C_h	Geometry
Armchair	30°	(n, n) where n=m	Cis
Zig Zag	0°	(n,0) where m=0	Trans
Chiral	0°<θ<30°	(n,m)	Mixture

Table 2

Theoretical and experimental properties of CNTs [20].

Property	CNTs	Graphite
Specific gravity	0.8 g/cm^3 for SWCNT; 1.8 g/cm^3 for MWCNT (theoretical)	2.26 g/cm^3
Elastic modulus	1 TPa for SWCNT; 0.3–1 TPa for MWCNT	1 TPa (in-plane)
Strength	50–500 GPa for SWCNT; 10– 60GPa for MWCNT	9.6 GPa
Electrical resistivity	5–50 μΩ.cm	50 μΩ cm (in-plane)
Thermal conductivity	3000 W m^{-1} K^{-1} (theoretical) 3000 W m^{-1} K^{-1} (in-plane)	6 W m^{-1} K^{-1} (c-axis)
Magnetic susceptibility	22 x10^6 emu/g (perpendicular with plane) 0.5 x10^6 EMU/g (parallel with plane)	6x10^{-6} emu/cm^3
Thermal expansion	Negligible (theoretical)	1 x 10^6 K^{-1} (in-plane), 29 x10^6 K^{-1} (c-axis)
Thermal stability	>700 °C (in air); 2800 °C (in vacuum)	450–650 °C (in air)
Specific surface area	10–20 m^2/g	0.6 m^2/g

Table 3

Methods of covalent sidewall functionalization [61].

Methodology	Mode of reaction	Addend	Degree of functionalization	Mode of attachment
Benzene diazonium salt	The diazonium salt reacts with Carbon atoms of CNT	aryl	1 addend in every 10 carbons	Aryl groups attaches to sidewall of CNTs
Diazonium in oleum	The diazonium salt reacts with Carbon atoms of CNT	aryl	1 addend in every 20 carbons	Aryl groups attaches to sidewall of CNTs
Fluorination	Fluorine gas is passed in to CNTs and then nucleophilic substitution with alkyl amino functionalities	amino group or alkyl or aryl group	1 addend in every 2 carbons	Creates side wall amino functional groups and also subsequent reaction with RMgBr/RLi creates alkyl or aryl group.
Plasma treatment	By passing CF_4 gas via plasma treatment, which enhances the reactivity with aliphatic amines	alkyl or aryl group	1 addend in every 2 carbons	Gives fluorinated CNTs which on subsequent reaction creates alkyl/aryl groups.
Radical Chemistry	Reaction with free radicals created in situ.	alkyl	1 addend in every 6 carbons	Alkyl or aryl radicals get attach to sidewalls.
Billups reaction	Reductive alkylation reactions involving reaction with Li/NH_3 and RI	alkyl,aryl	1 addend in every 17 carbons	Give alkylated CNTs and results in complete exfoliation.
Prato reaction	1,3 dipolar cycloaddition of azomethine ylides to CNTs	pyrrolidine	1 addend in every 100 carbons	<u>N-methylpyrrolidine</u> derivative or pyrrolidinofullerene or pyrrolidino fullerene in 82% yield.
Bingel reaction	Haloderivative of malonate ion is reacted with a base and thereafter with CNTs	cyclopropane	1 addend in every 50 carbons	Cyclopropyl group formed as a result of the reaction get attached to the sidewalls.
Nitrene	Nitrene is reacted with CNTs	cyclopropane	1 addend in every 25 carbons	Cycloaddition of nitrene to CNTs
Dichlorocarbene	$:CCl_2$ is reacted with CNTs	cyclopropane	1 addend in every 25 carbons	Cycloaddition of carbene to CNTs

Table 4.

Mechanical properties of CNT reinforced rubber composites.

Elastomer	Processing	Reinforcement	CNT concentration	Cure time (min)	Modulus (MPa)	Tensile strength (MPa)	Elongation at break (%)
NR [133]	Solution	-	25phr/0phr Purified CNTs	7.1 /4.71 (150°C)	9.8 ± 0.4 /1.8 ± 0.2 (M300)	19.8 ± 2.5/7.2 ± 0.6	510 ± 20/680 ± 20
		-	25phr/0phrBall-milled CNTs	9.2 /4.71 (150°C)	12.5 ± 0.3 /1.8 ± 0.2 (M300)	24.8 ± 2.0/ 7.2 ± 0.6	495 ± 15/ 680 ± 20
TPNR	Dry		3 wt%/0 wt% MWCNT (CCVD)		440/340 (Y'modulus)	17.5/12.8	~15/310
NR [134]	Dry	-	3 : 40phr MWCNT:Silica)/0phr	-	4.8/1 Stress at M100	29/12	470/480
SBR / BR (70/30) [134]	solution	-	3 : 60phr (MWCNT:Silica)/0phr	-	6.1/1 Stress at M100	16.2/1.15	203/129
EPDM [134]	solution	-	3 : 40phr (MWCNT:CB) /0phr	-	5.5/1.1 M100	17.2/2.5	299/299
EPDM [135]	Dry	-	10 wt% MWCNT	17 min (170°C)	0.03 Elastic modulus	6.70	-
		-	10 wt%/6 wt% MWCNT/Cloisiite15A	17 min (170°C)	0.06 Elastic modulus	15.79	-
NR [63]	Dry at 30 °C	-	1phr/0phr MWCNT	6.1 /5.1 (150°C)	2.22/1.65 (M100)	20.0/21.7	481/593
		Silane functionalized	1phr/0phr MWCNT	6.3/5.1 (150°C)	2.11/1.65 (M100)	26.2/21.7	559/593
SBR/ BR (50/50)	Solution	EMIT	5phr /0phr MWCNT	3.5 /6.7 (160°C)	2.28/0.95 (M100)	5.07/1.22	348/151

[70]		TTDPD	5phr /0phr MWCNT	4.3 /6.7 (160°C)	2.94 /0.95(M100)	4.58/1.22	227/151
SBR [136]	Solution	-	0.66 wt%/0 wt% MWCNT	-	-	1.045/0.818	~170/220
HNBR [137]	-	-	25phr CNTs	8.38 (170°C)	7.0 (M300)	18.6	647
HXNBR [138]	Dry at 30 °C	-	2phr/0phr MWCNT	8.3/13.6 (170°C)	1.10±0.02 /0.90 ± 0.01 (M100)	15.7 ±0.5/ 13.3 ±0.2	622 ± 6/ 600 ± 3
HNBR [52]	Solution	BMPy BF4	- MWCNT-OH	4.5 min 180°C	14.2 (elastic modulus)	19.2	193
SBS [139]	Solution	PS-NH$_2$	0.4wt%/0wt% MWCNTs	-	~78/72.5 (Y'modulus)	~0.225/ 0.145	~890/790
SBS [140]	Dry at 60°-65°C	-	9wt%/ 0wt% MWCNTs	1 hr 120°C	4.0/2.1 (M100)	40/30	830/840
RTVSR [69]	Solution	-	1wt%/ 0wt% SWCNTs	-	~3/1(initial modulus)	~3.5/3.25	~240/400
NBR [41]	Dry	-	15phr/0phr MWCNTs	-	~2.7/1.7 (M100)	~5.3/2.7	-

Table 5

Electrical properties of elastomer/CNT composites.

Elastomer	Concentration of filler	Electrical conductivity
NR [134]	3 : 40phr MWCNT:Silica)	3.2×10^{-3} (S/m)
SBR / BR (70/30) [134]	3 : 60phr (MWCNT:Silica)	1.1×10^{-2} (S/m)
EPDM [134]	3 : 40phr (MWCNT:CB)	2.1×10^{-1} (S/m)
EPDM [135]	10 wt% MWCNT	9298 (Ω/m)
	10 :6 wt% MWCNT:Cloisite15A	224 (Ω/m)
XNBR [204]	3.9 phr MWCNT	0.07 (S/cm)
SBR/ BR (50/50) [70]	5phr MWCNT	2.4×10^{-3} (S /cm)
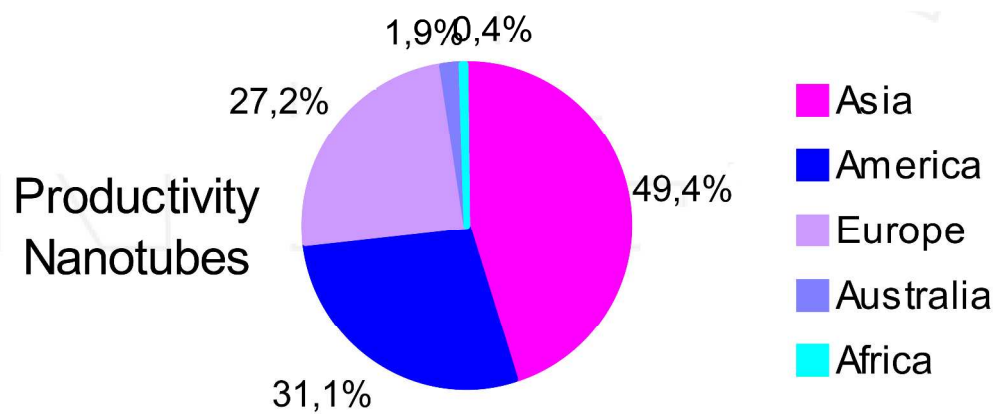
Figure 1- Contribution of different continents to CNT production [Reprinted from ref 13 with permission].
1111x535mm (96 x 96 DPI)

SWCNT   MWCNT   Torus   CNT Nanobud   Cup stacked

(m,n) = (5,5)
θ =30 , Arm-chair

(m,n) = (9,0)
θ = 0 , Zig-zag

(m,n) = (10,5)
0 < θ < 30, Chiral
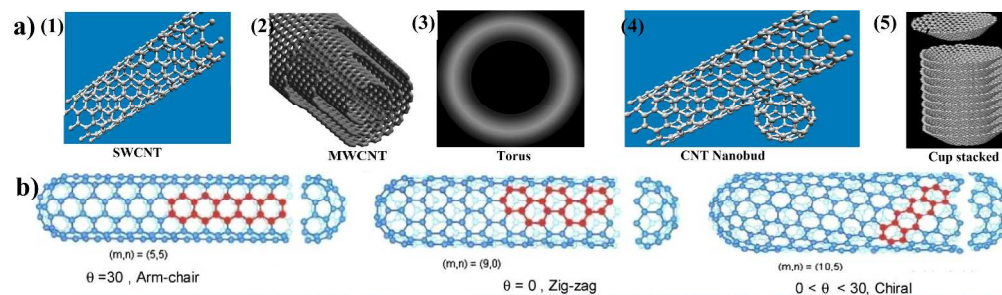
Figure 2- Various structural forms of nanotubes (a) SWCNT (b) MWCNT (c) Torus (d) Nanobud (e) Cup stacked CNTs (i) and Different types of SWCNTs (ii) [Reprinted from ref 18,19 and 21 with permission].
1354x387mm (96 x 96 DPI)

Figure 3- Schematic representation of (a) physical adsorption between MWCNTs and CTAB and (b) chemical interaction of KH550 with MWCNTs and rubber [Reprinted from ref 66 with permission].
1688x1088mm (96 x 96 DPI)
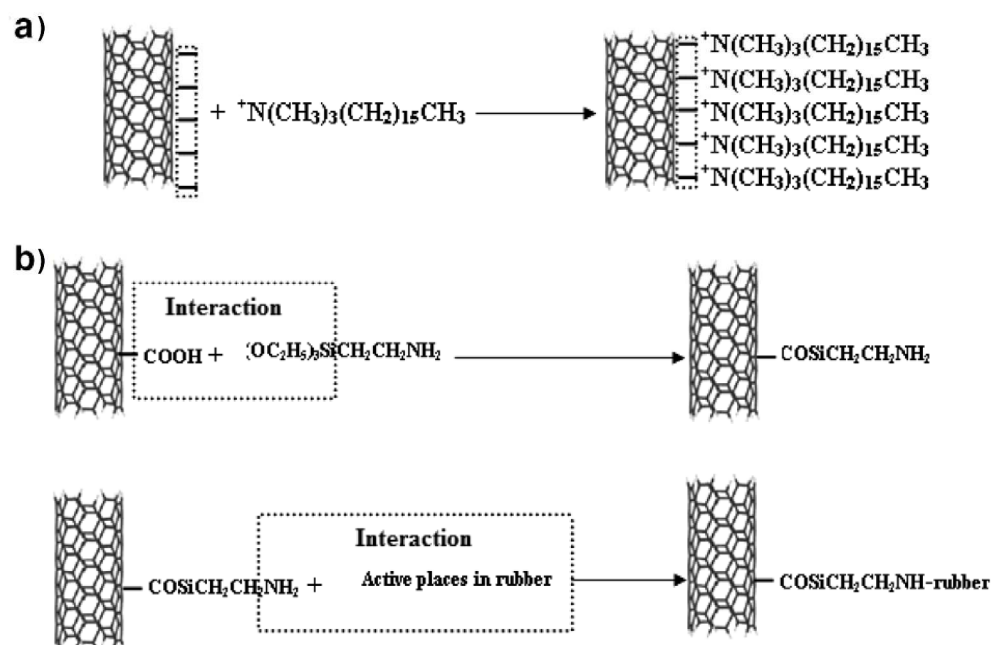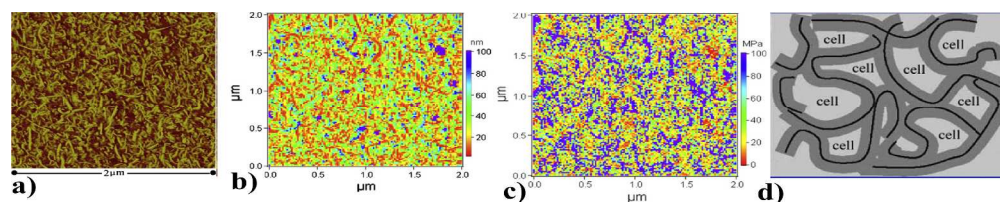
Figure 4- Typical (a) AFM tapping mode height image (b) Nanomechanical mapping adhesive energy (J/m2) (c) Young's modulus (MPa) distribution images and (d) three-dimensional cellular structure of CNT(60phr)/NR [Reprinted from ref 120 with permission]
812x153mm (96 x 96 DPI)
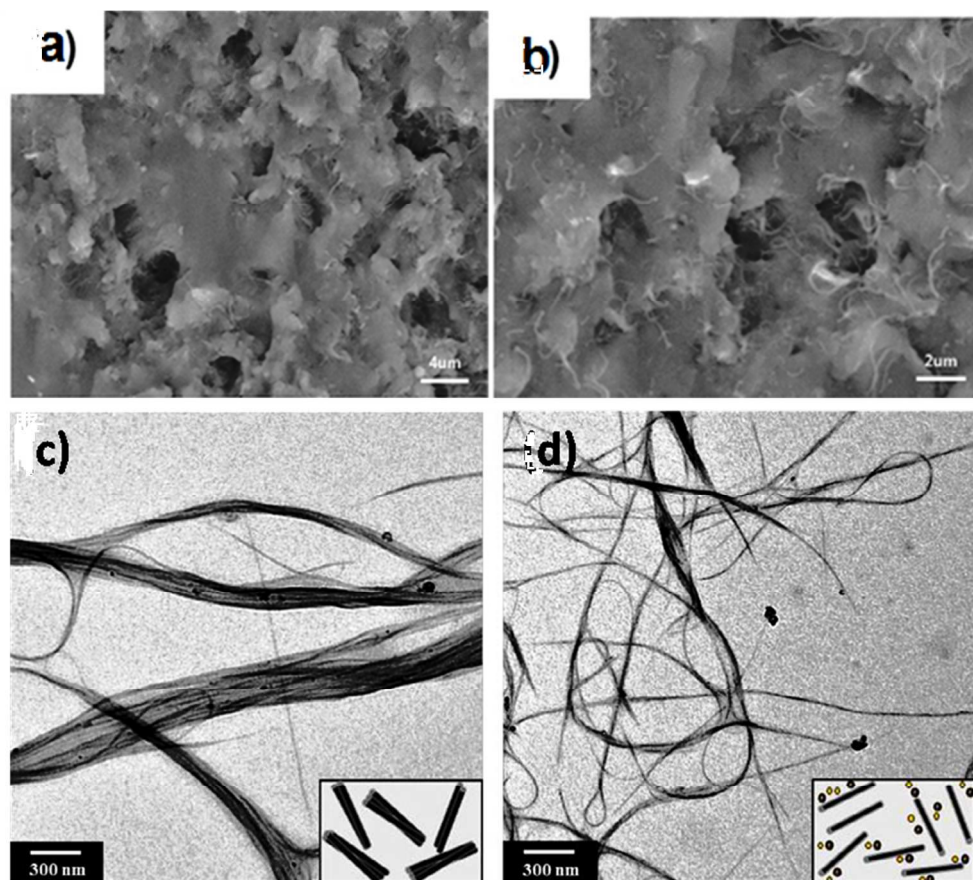
Figure 5- Cross-sectional SEM images of the cured (a) 0.2 wt% and (c) 1.4 wt% MWCNT/PDMS composites. TEM images of (c) SWCNT/PDMS and (d) IL-SWCNT/PDMS (8 wt% IL) composites containing 1.6 wt% SWCNT [Reprinted from ref 123 and 124 with permission].
926x808mm (96 x 96 DPI)
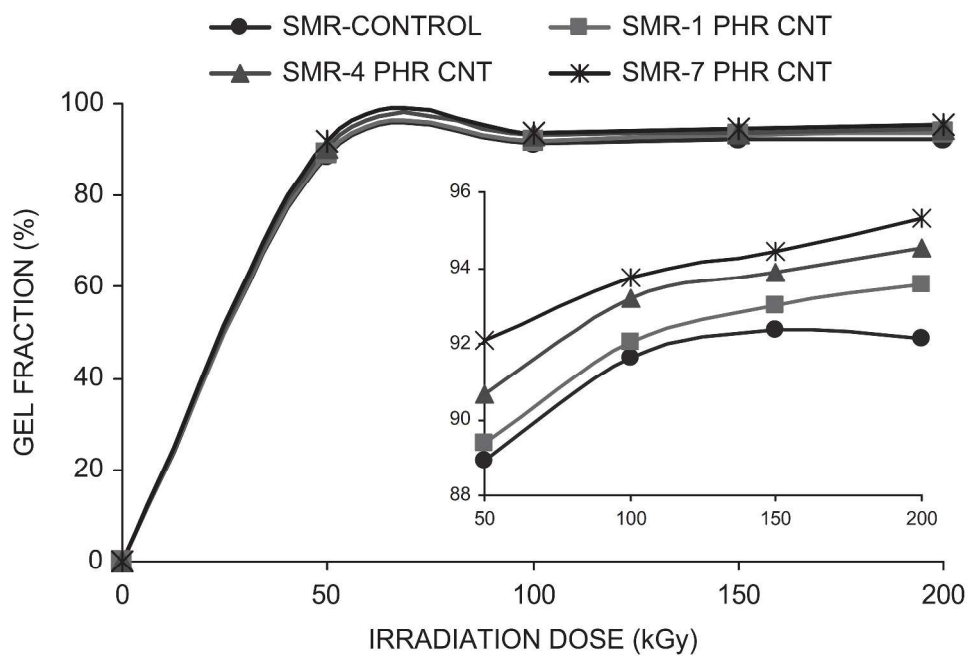
Figure 6- Effect of radiation dose on the gel fraction of rubber/CNT composites. SMR indicates Standard Malaysian Rubber. [Reprinted from ref 71 with permission]
1249x837mm (96 x 96 DPI)
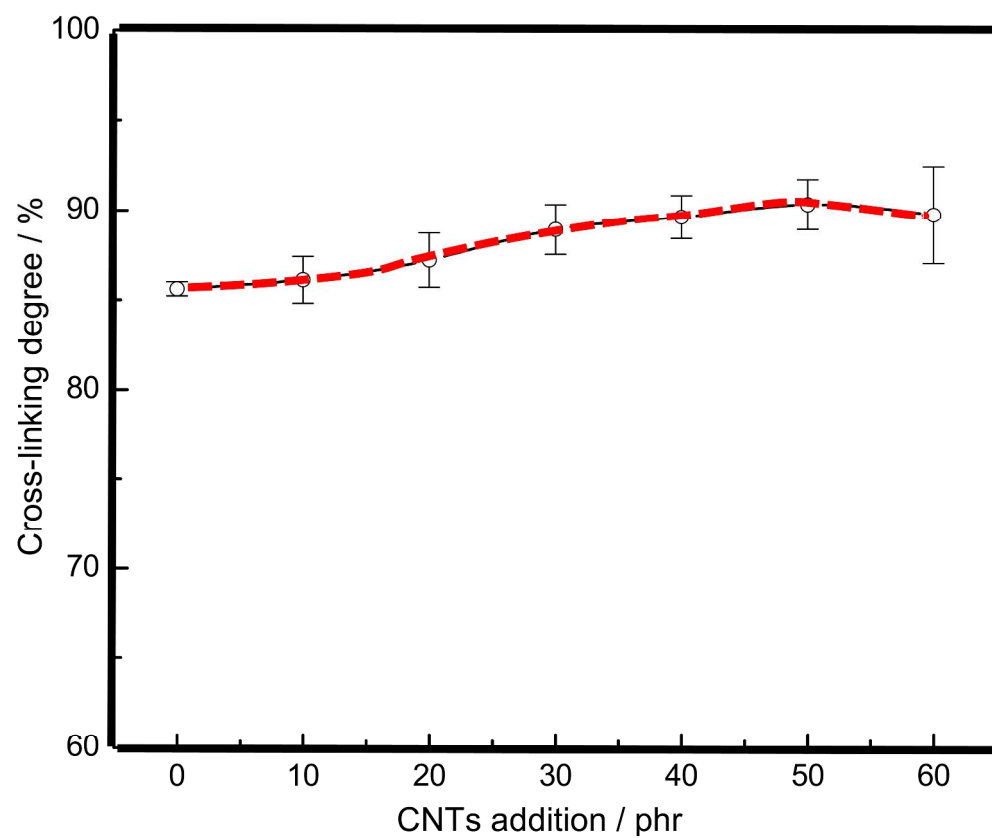
Figure 7- Cross linking degrees of the vulcanizates filled with different CNTs addition [Reprinted from ref 127 with permission]
1081x891mm (96 x 96 DPI)
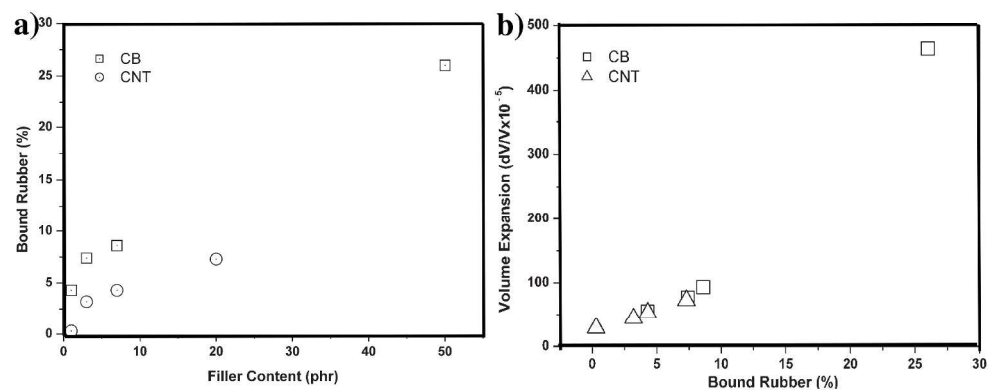
Figure 8- Variation in bound rubber content of CNT/NR and CB/NR (a) with filler loadings and (b) with volume expansion [Reprinted from ref 129 with permission].
2565x1053mm (96 x 96 DPI)
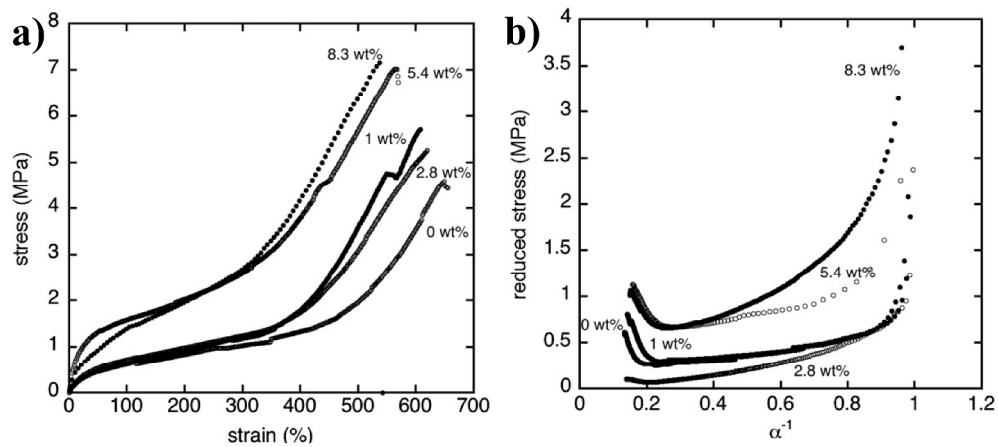
Figure 9- (a) Stress–strain curves for pure NR latex and its composites (b) variation in the value of modulus with filler volume fraction [Reprinted from ref 144 with permission]
2137x952mm (96 x 96 DPI)
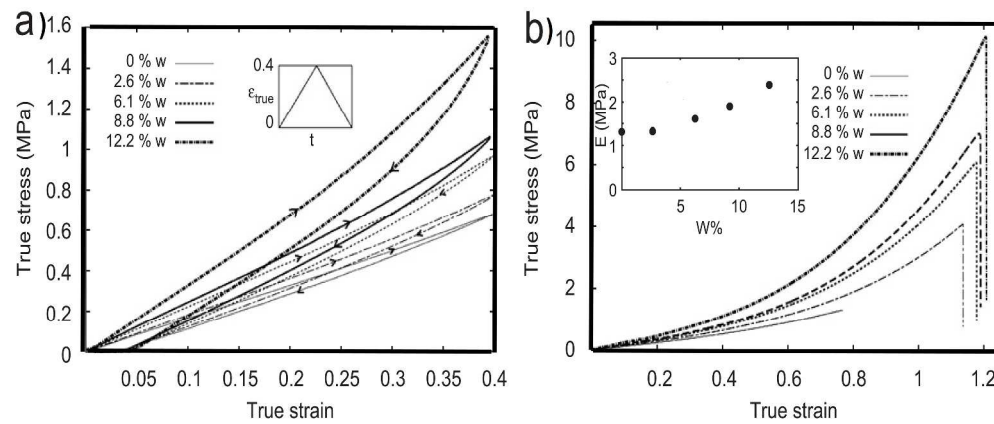
Figure 10- (a) Uniaxial tension load–unload true stress vs. true strain at a strain rate of 0.01/s to a strain of 0.4 for the elastomer and the MWCNT/elastomer composites and (b) uniaxial tension true stress vs true strain at a strain rate of 0.01/s taken to failure; the inset plot reports the initial axial modulus as a function of weight fraction MWCNT [Reprinted from ref 149 with permission]
2129x886mm (96 x 96 DPI)
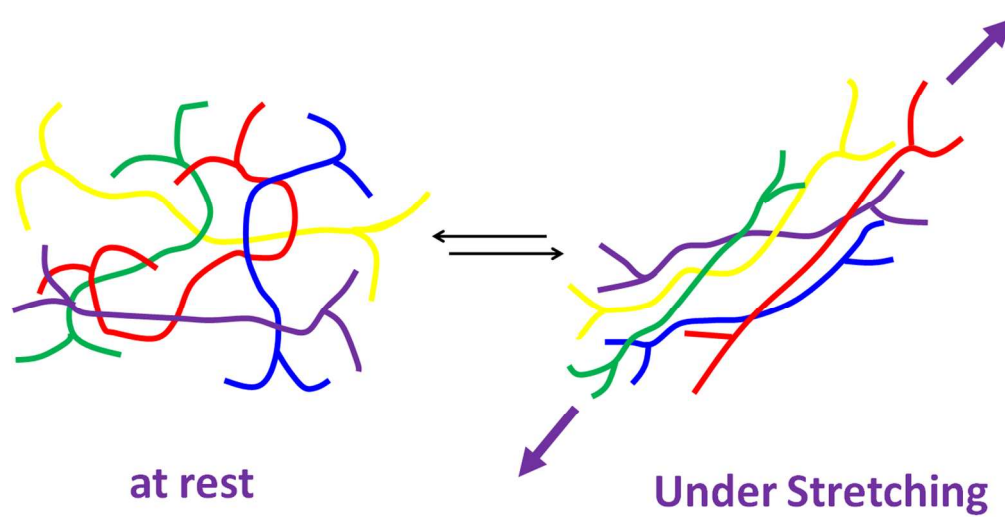
Figure 11- A model of the viscoelastic deformation of polymers in the rubber elastic state [Reprinted from ref 188 with permission]
1722x914mm (96 x 96 DPI)
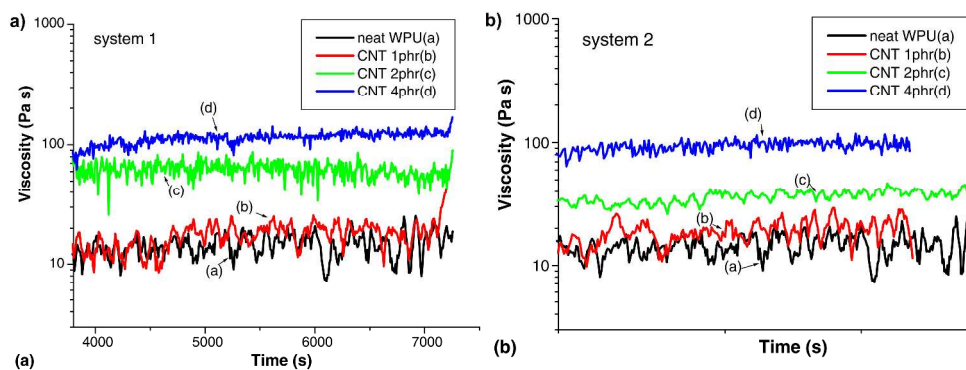
Figure 12- Viscosity of CNT/WPU composites vs time at various compositions when the processing temperature is 200°C (system 1-covalent bonding system) (a) System 2-ionic bonding system (b) [Reprinted from ref 168 with permission].
2444x914mm (96 x 96 DPI)
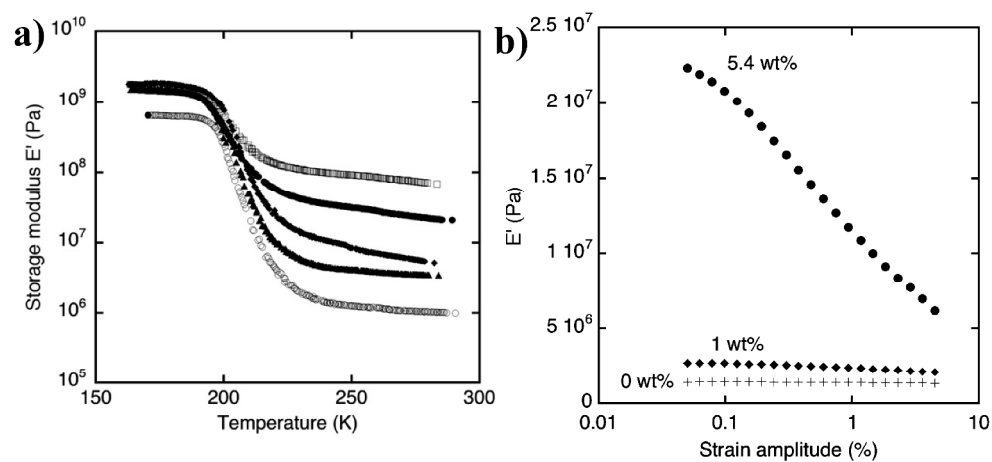
Figure 13- Variation of storage modulus (a) with temperature (b) with strain amplitude [Reprinted from ref 144 with permission].
2252x1021mm (96 x 96 DPI)
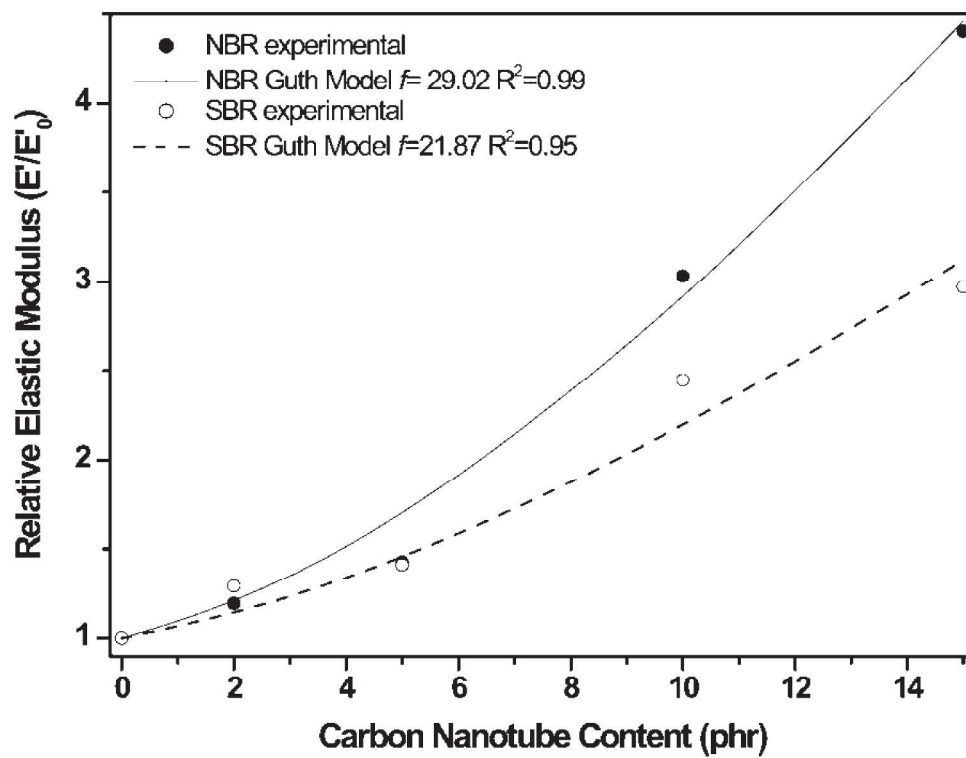
Figure 14- Elastic modulus of the NBR and SBR elastomers reinforced with the nanotubes from DMA measurements, and fitted to the Guth model [Reprinted from ref 64 with permission]
1453x1154mm (96 x 96 DPI)
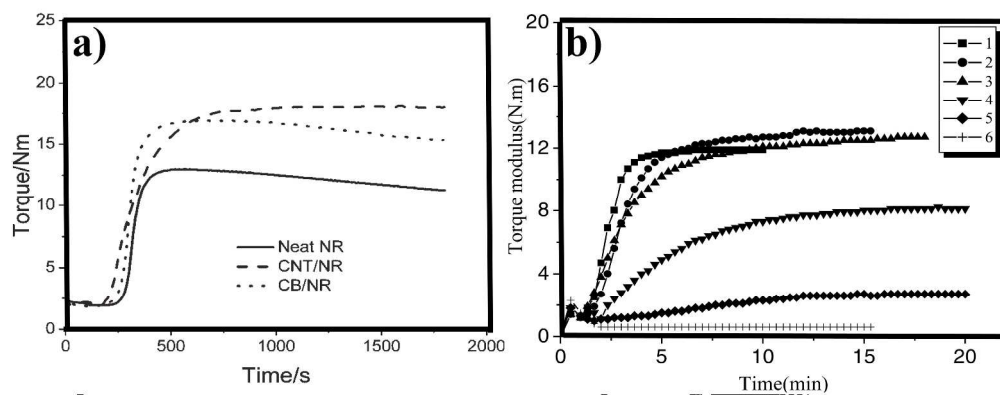
Figure 15- Vulcanizing curves of (a) neat NR and NR composites and (b) CNT/SR composite [Reprinted from ref 173 and 137 with permission].
1384x542mm (96 x 96 DPI)
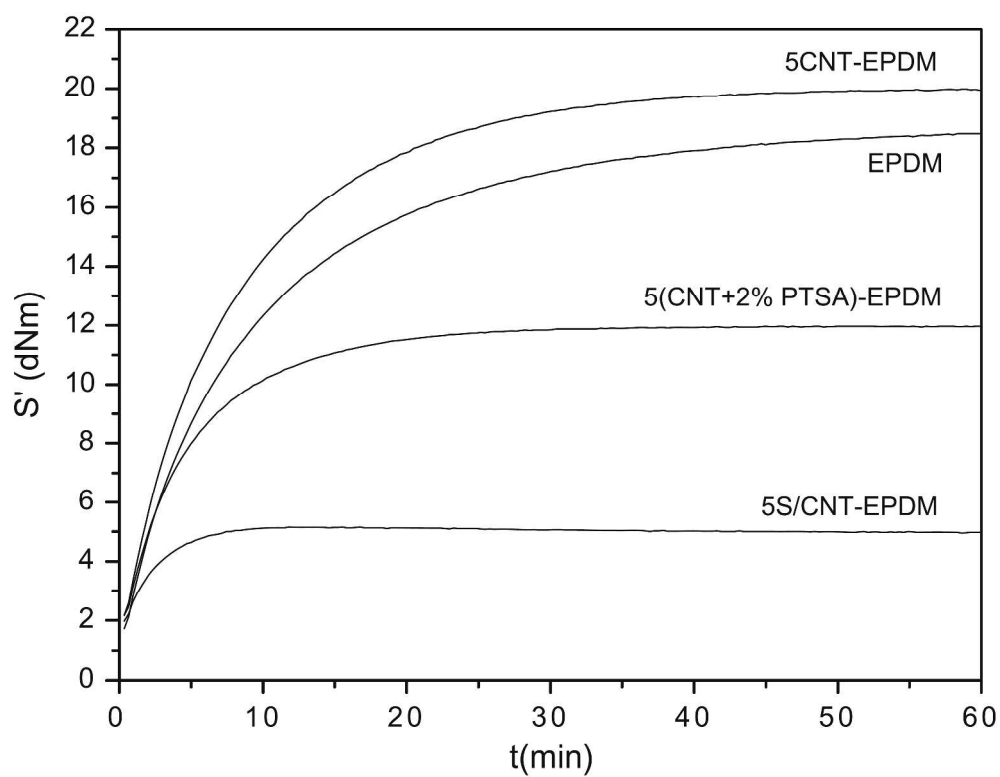
Figure 16- Depressive effect of CNTs with 2% PTSA (p-toluenesulfonic acid) on EPDM vulcanization at 160°C. Comparison of the vulcanization kinetic of EPDM, 5CNT–EPDM and 5S/CNT–EPDM [Reprinted from ref 183 with permission].
1033x819mm (96 x 96 DPI)
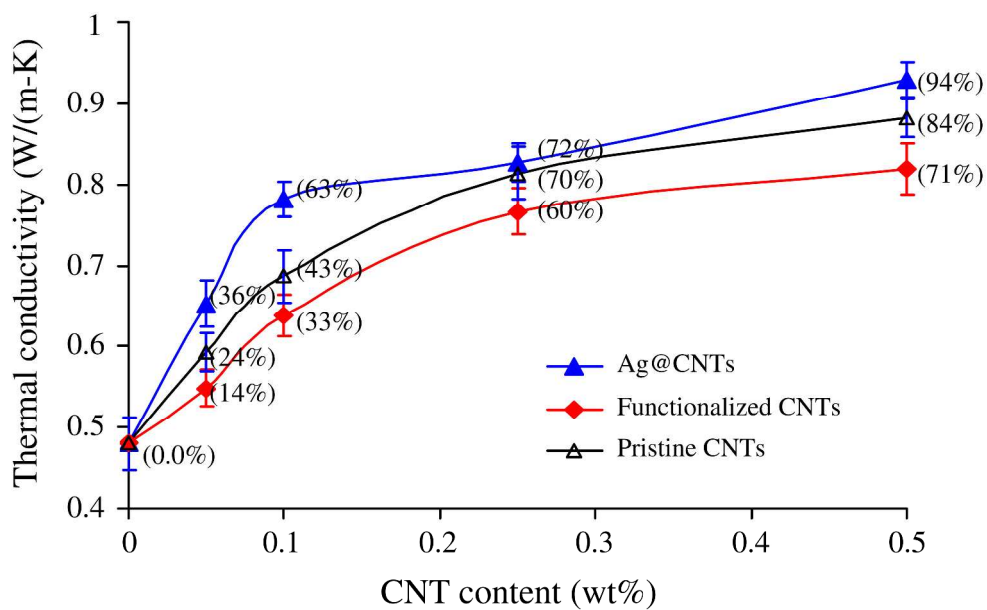
Figure 17- Comparison of thermal conductivities of composites containing CNTs with different functionalities (data in bracket indicate% increase in thermal conductivity against the polymer matrix) [Reprinted from ref 93 with permission].
1117x715mm (96 x 96 DPI)
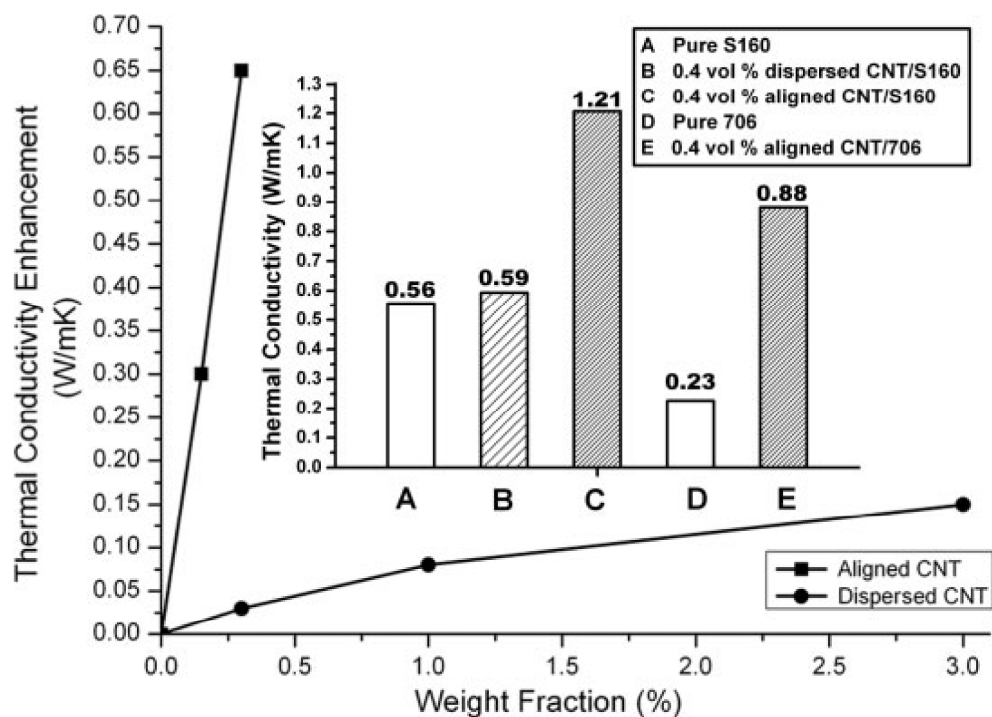
Figure 18- The enhanced values of thermal conductivity vs weight fractions of the CNTs. The inset is a comparison of measured thermal conductivity values of different samples [Reprinted from ref 191 with permission].
1616x1187mm (96 x 96 DPI)
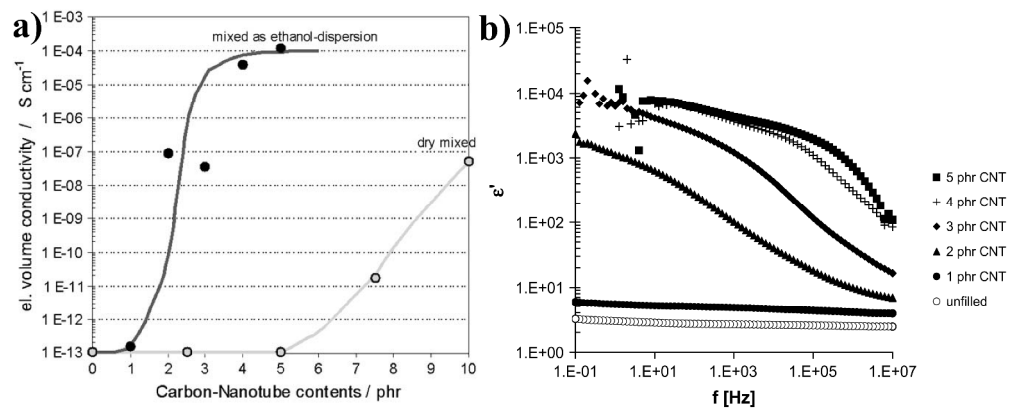
Figure 19- Variation of electrical conductivity (a) with CNT content (b) with frequency [Reprinted from ref 16 with permission].
2381x975mm (96 x 96 DPI)
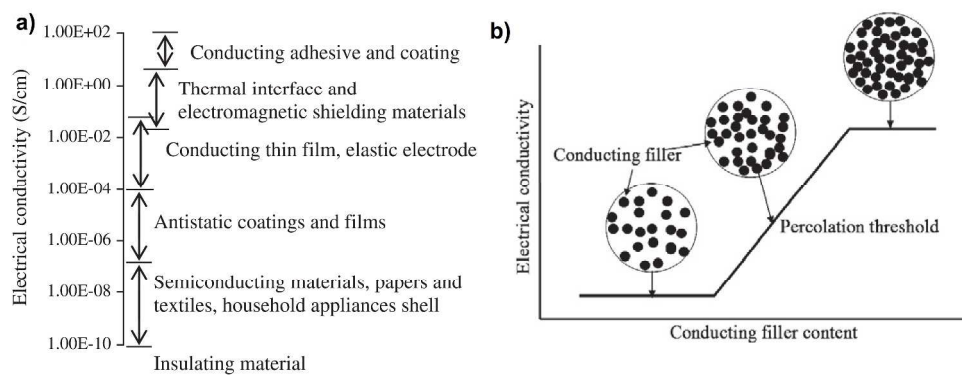
Figure 20- Typical applications of conducting composites (a) and a schematic of percolation phenomenon and conducting network in conducting composites (b) [Reprinted from ref 93 with permission]
1955x750mm (96 x 96 DPI)
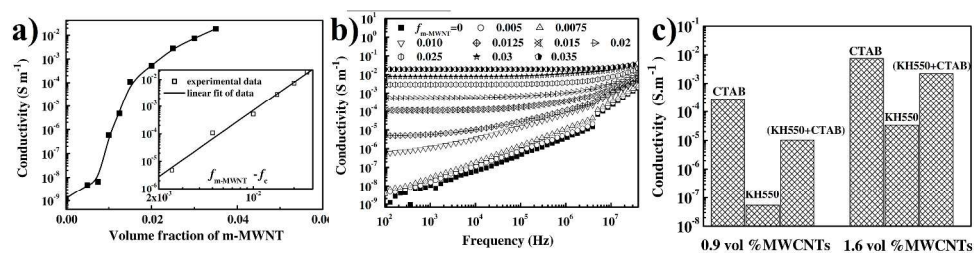
Figure 21- Dependence of the conductivity of the m-MWCNT/VMQ composites on the (a) m-MWCNT volume fraction, fm-MWCNT, at room temperature and 100 Hz and the inset shows the best fits of the conductivity to Eq. (17) (b) on frequency at room temperature [206](c) Dependence of conductivities of the MWCNT/VMQ composites with the modified MWCNTs at two concentrations (0.9 vol% and 1.6 vol%) on the modifiers at 102 Hz [Reprinted from ref 206 and 66 with permission].
2129x575mm (96 x 96 DPI)
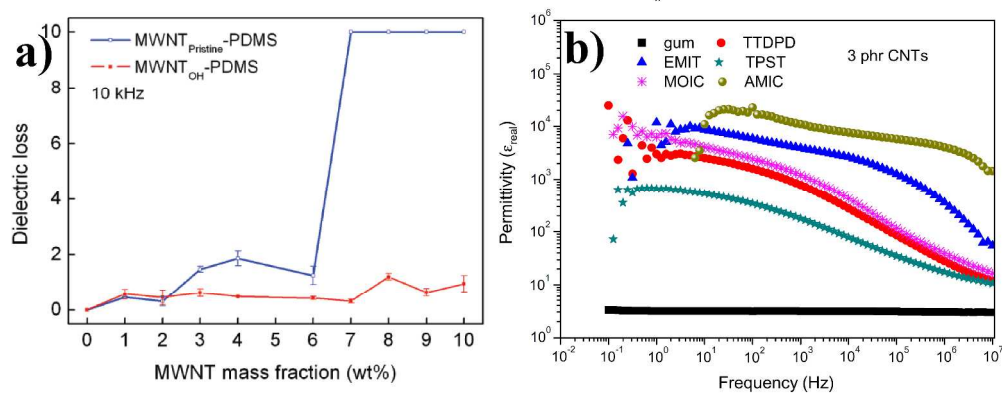
Figure 22- a) Room temperature dielectric loss of both MWCNT/PDMS composites as a function of MWCNT mass fraction (wt %) at 10 kHz [212] b) Dependence of permittivity of 3 phr CNTs loaded SSBR/BR matrix in presence of different ionic liquid measured at 20 °C [Reprinted from ref 212 and 70 with permission].
1875x768mm (96 x 96 DPI)
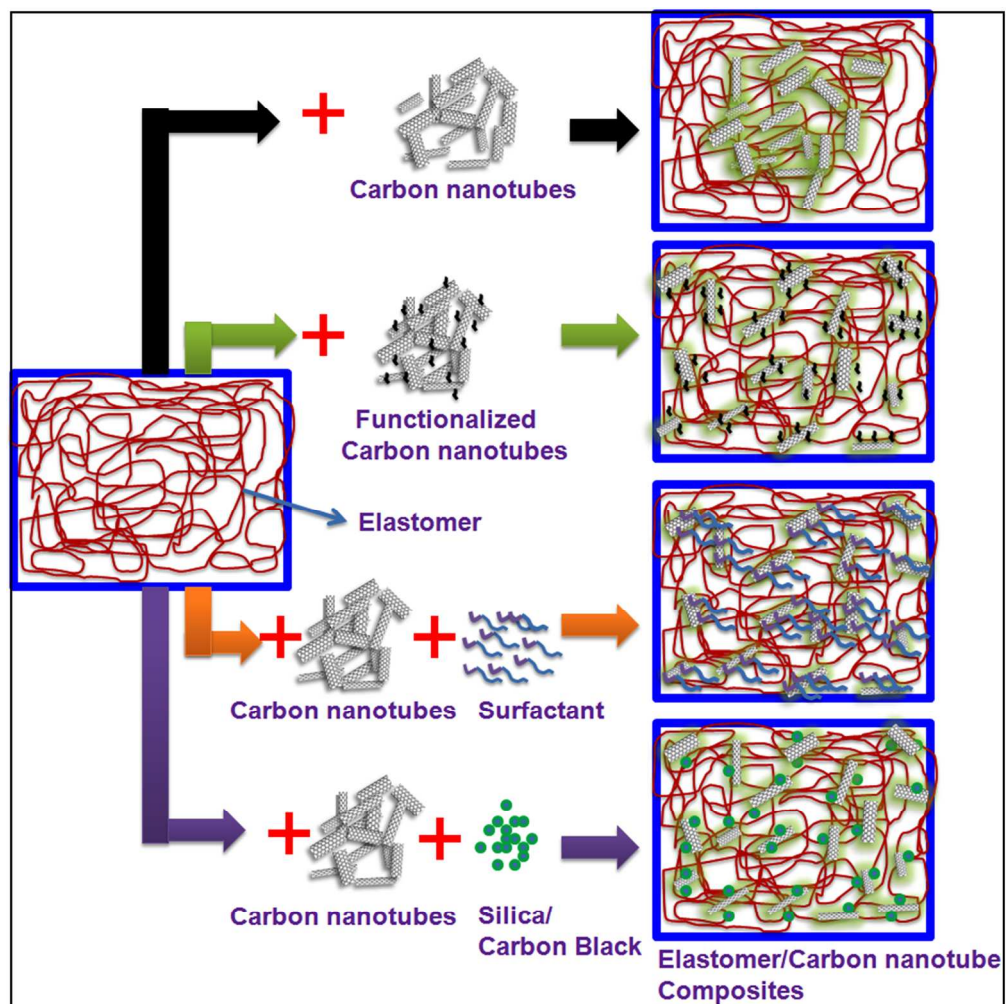
Figure 23- A schematic representation for CNT/elastomer composites.
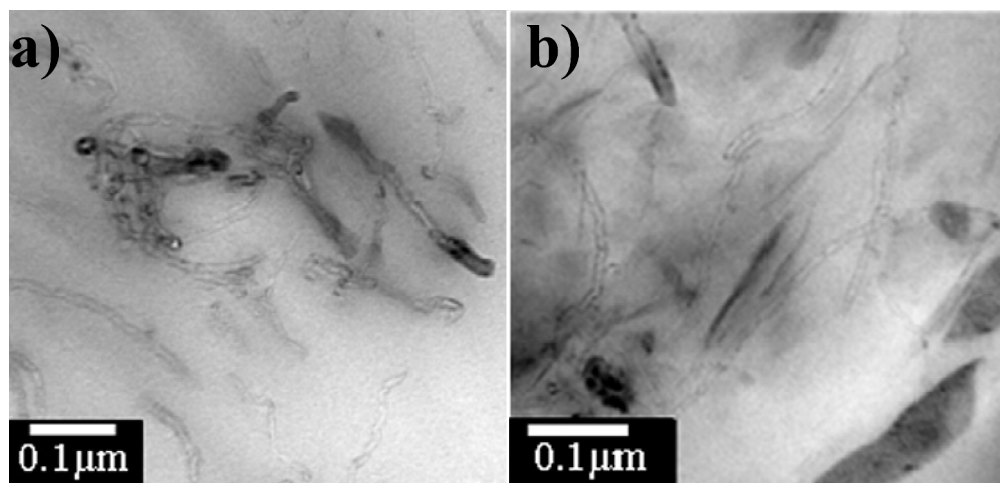700x703mm (96 x 96 DPI)

Figure 24- TEM images of the MWCNT/organo-clay/EPDM composites a)10 wt% MWCNT, b) 10 wt% MWCNT/6 wt% Cloisite 15A [Reprinted from ref 135 with permission].
1411x673mm (96 x 96 DPI)
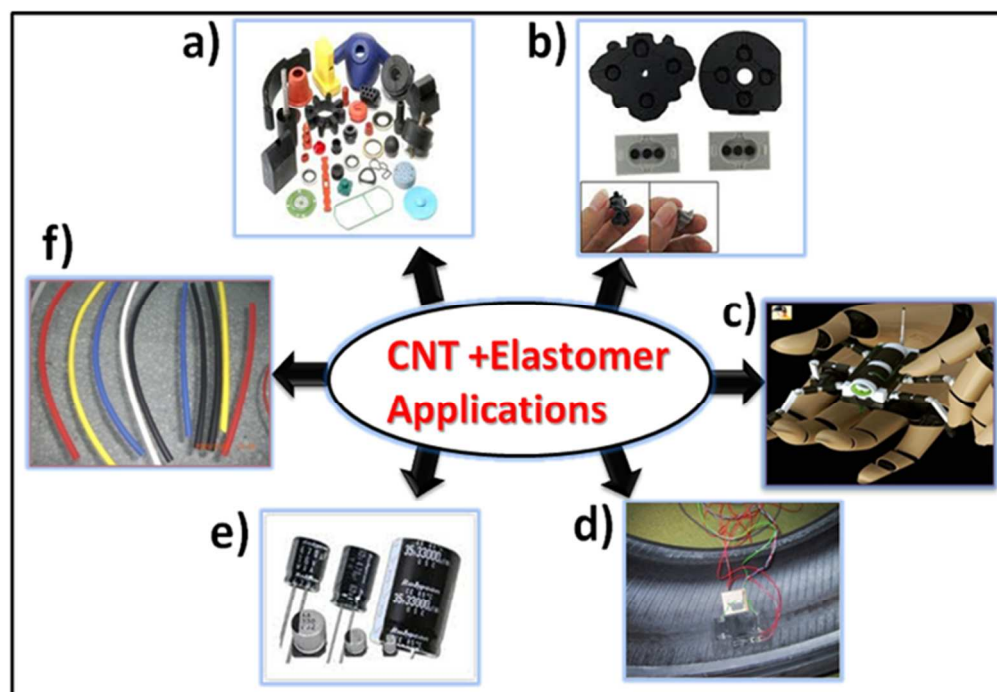
Figure 25- Major application of CNT/elastomer composites a) Home appliances b) switches c) pressure sensing skin in robotics d) strain sensor attached to tyre engineering e) energy storage application as capacitors and f) cables
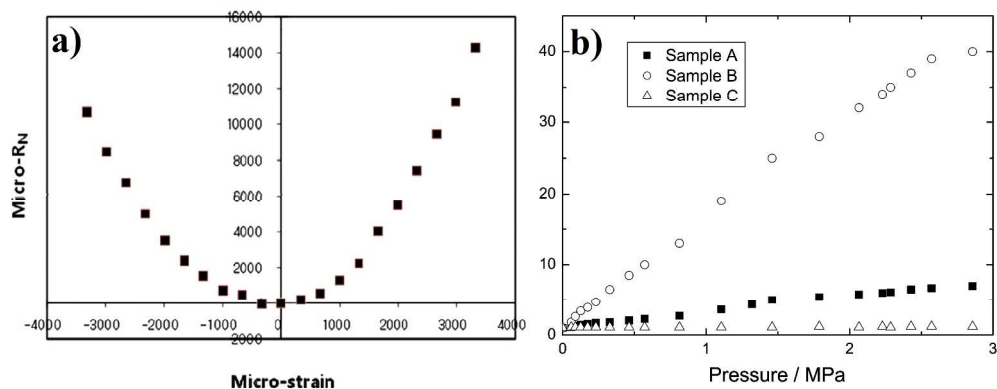601x412mm (96 x 96 DPI)

Figure 26- Strain response of the MWCNT/EPDM composite containing 20 wt % of MWCNT during compression and extension [135] (b) Changes of electrical resistance under various pressures for the samples A-C (Sample A = Uunmodified-MWCNTs, Sample B= Carboxylated-MWCNTs, Sample C=Silicon Rubber) [Reprinted from ref 135 and 170 with permission]
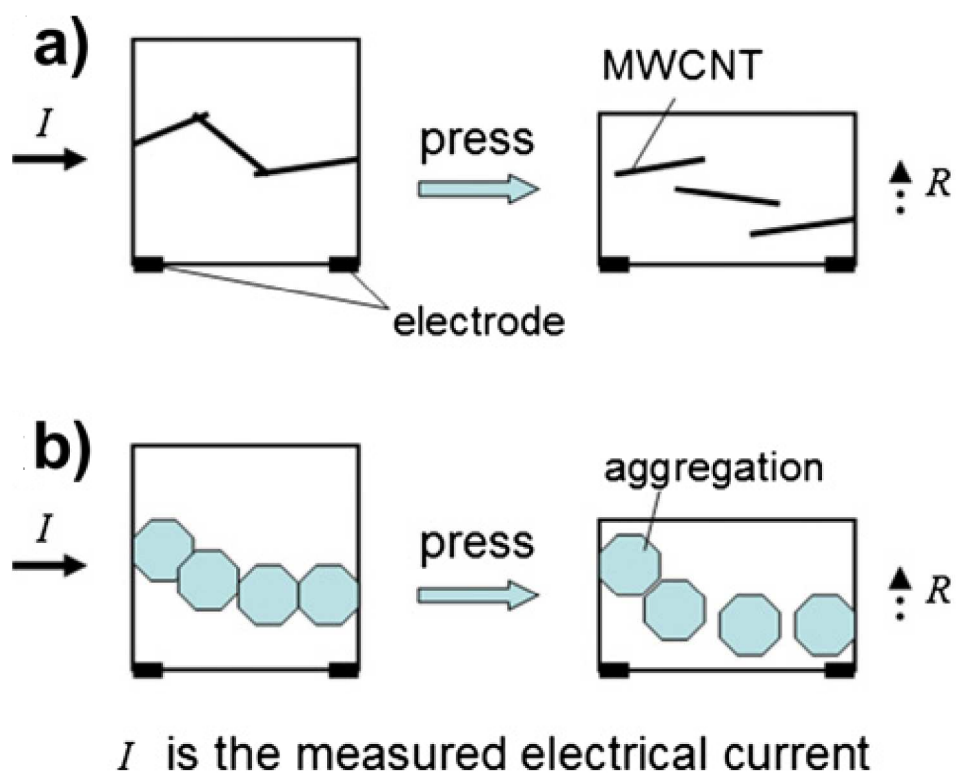1411x567mm (96 x 96 DPI)

Figure 27- A schematic representation of the deformation in homogeneous-MWCNTs and aggregated-
MWCNTs filled composites [Reprinted from ref 170 with permission].
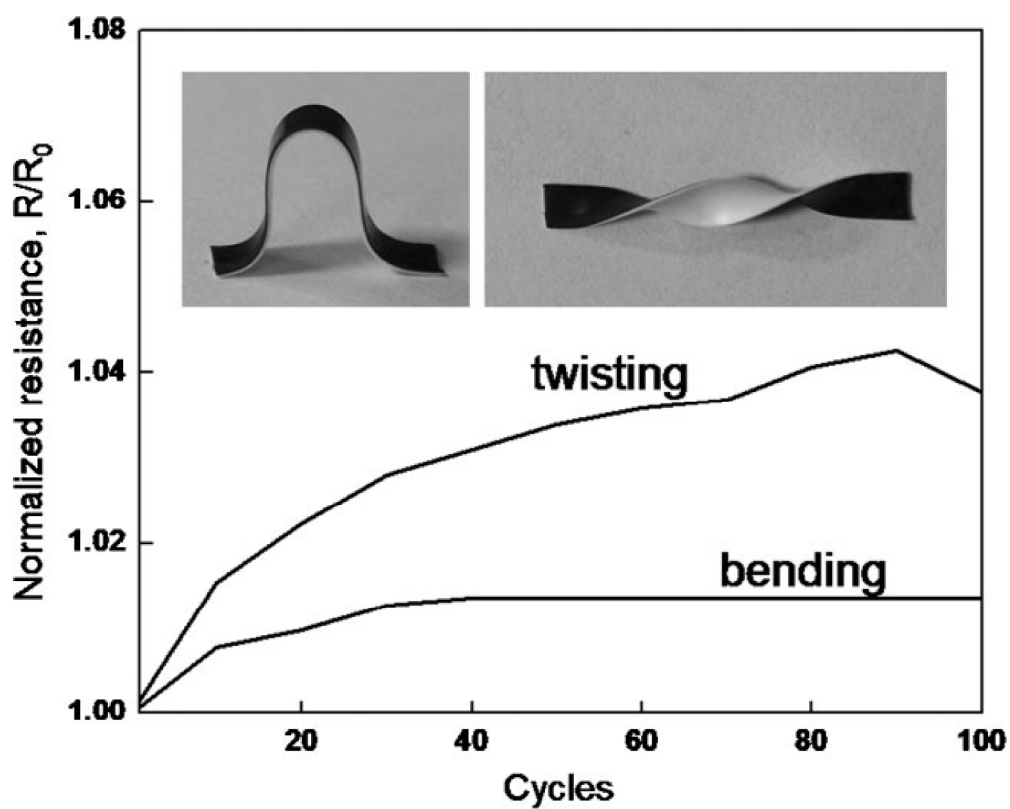883x714mm (96 x 96 DPI)

Figure 28- Dependence of zero strain resistance (R/R0) on the number of bending and twisting cycles. The sample shape induced by bending and twisting is shown in the insets [Reprinted from ref 252 with permission]
1144x938mm (96 x 96 DPI)